Design and Screening of Hypothetical Charged Metal-organic Frameworks for Carbon Dioxide Capture

Jason Wai-Ho Lo

Thesis submitted to

The Faculty of Graduate and Postdoctoral Studies

in partial fulfillment of the requirements for

the degree of Master of Science in Chemistry

Department of Chemistry and Biomolecular Science

Faculty of Science

University of Ottawa

Table of Contents

List of Tables

List of Figures

List of Equations

Legend

CCDC .....Cambridge Crystallographic Data Centre

CCS..... Carbon Dioxide Capture and Sequestration

DFT..... Density Functional Theory

DRG .....Database Representative Group

ESP.....Electrostatic Potential

FA^{3}PS.....Fully Automated Adsorption Analysis in Porous Solids

GCMC.....Grand Canonical Monte Carlo

MC ..... Monte Carlo

MEA.....Monoethanolamine

MOF..... Metal-organic Framework

SBU ..... Structural Building Unit

PAW.....Projector Augmented Wave

PSA .....Pressure Swing Adsorption

QEq..... Charge Equilibration

QM.....Quantum Mechanics

RDF..... Radial Distribution Function

TPSA..... Temperature and Pressure Swing Adsorption

TSA .....Temperature Swing Adsorption

UFF ..... Universal Force Field

VASP..... Vienna *Ab Initio* Simulation Package

Abstract

Reducing anthropogenic carbon dioxide emissions from coal-fired power plants is an important step in mitigating climate change. To implement carbon dioxide capture technologies, materials capable of removing carbon dioxide efficiently are required. Currently, liquid amine technology is used for carbon dioxide capture. However, the mechanism for carbon dioxide removal in liquid amine requires extraordinary amounts of energy input. Alternatively, solid sorbents such as metal-organic frameworks (MOFs) show promising potentials as a type of material for carbon dioxide capture. Due their varying structural properties, MOFs can be configured for specific purposes. Certain MOFs carry a net charge on their frameworks, which may allow for increased interactions with carbon dioxide molecules. In this work, charged MOFs were studied for their potential in carbon dioxide capture. Due to the massive number of MOFs available, computational methods were employed for the study.

This project includes three major components: (1) the development of novel computational methods to simulate the gas adsorption properties in charged materials, (2) a diverse database of 47,244 hypothetical charged MOFs was constructed to represent the capabilities of charged MOFs, and (3) screening of high performing charged MOFs for carbon capture application by combining the previous two portions of the project. The methods developed in this work include fitting intermolecular interaction parameters to quantum mechanical calculations in periodic systems with net charges. No methods have been reported in literature for such parameter fittings, even in well studied materials such as zeolites. Therefore, the gas adsorption estimation method for charged materials

developed in this work is proprietary. Also, databases of hypothetical MOFs with framework net charges have never been reported previously in literature.

By screening the charged MOFs in the database with the methods developed, gas adsorption capabilities were evaluated. The adsorption properties of a neutral group of hypothetical MOFs were also obtained for a baseline comparison. Between the two groups of MOFs, charged MOFs were found to outperform neutral MOFs in three key aspects. Firstly, charged MOFs were able to adsorb an average of three times as much carbon dioxide than the neutral group. Secondly, charged MOFs were capable of removing twice the amount of carbon dioxide per adsorption/desorption cycle than the neutral MOFs. Lastly, charged MOFs were able to selectively adsorb much more carbon dioxide over other gasses present in the carbon dioxide capture situations. Specific structural features that resulted in the selectiveness of adsorption in charged MOFs were identified. Also, positive correlations were found between the adsorption of carbon dioxide and the charge present in the MOFs.

As seen in the results, charges present in MOFs can greatly increase their ability to remove carbon dioxide. Charged MOFs in the hypothetical database not only outperformed neutral MOFs, certain top performers were also found to exceed the requirements for post-combustion carbon capture application. Therefore, charged MOFs were shown to be a possible material for future carbon dioxide capture. The proprietary methods developed in this work can not only be used to simulate gas adsorptions in charged MOFs, but also for other porous materials, regardless of net charges presented in

their systems. Also, the database constructed in this work can be utilized in multiple ways. Aside from carbon dioxide capture capabilities, the charged MOFs in the database can be screened for other gas separations and catalysis via high throughput screening. The database and the computational methods developed in this work pave the way for discovering the capabilities of charged materials.

Acknowledgements

The journey through graduate school is tough and I am incredibly grateful to the ones who helped me along the way. First of all, I would like to thank my supervisor Tom Woo who provided me with the guidance and freedom to research, and taught me the effective storytelling skills in the academic world. To my peers, my special thanks go to Peter Boyd and Tom Daff, whose works were the direct predecessors of my research, as well as Chris Demone, whom is carrying out the continuation of my project. I am also grateful to other members of the Woo Group: Sean Collins, Mohammad Zein Aghaji, Bianca Provost, Hana Duracova, Phil De Luna, Tom Burns, Carlos Campañá, Dr. Mykhaylo Krykunov, and Dr. Saman Alavi.

I would also like to acknowledge my dear lovely Andrea, for the moral support and being there when I need her the most. To so many of my friends and members of the University of Ottawa Outdoors Club, who help clear my mind, raise my spirit, and put me back on track. In addition, my gratitude to my family who have supported me through thick and thin: me Mum 高明惠, Da 羅華安, sister Ting, and brother-in-law Simon. They have a major influence in my love and respect towards the environment.

To the great outdoors, sanctuaries where I can be lost to find myself, described so profoundly perfect by Lord Byron in the Childe Harold's Pilgrimage:

"There is a pleasure in the pathless woods,
There is a rapture on the lonely shore,
There is society, where none intrudes,
By the deep sea, and music in its roar:
I love not man the less, but Nature more"

From summiting unnamed mountains to SCUBA diving unknown depths and interacting with unfamiliar creatures in all levels, they remind me why I am here and do the research I am doing. I believe that I can lend my efforts to help preserving what I have appreciated, even the leg-shredding vegetation on top of Mt. Owen and all the sandflies in Middle Earth. Long after I've passed, I hope you will find pleasure in the green grass, not the charred remains of Mother Nature, under your boot-soles (Song of Myself, Walt Whitman).

Lastly, to my donkeys, you and your effects on nature are a major part of the reason I decided that I need to help preserve this earth for future generations to come!

Ottawa, May 2016

Jason Wai-Ho Lo

1 Introduction

1.1 Carbon Capture

Climate change in recent history is undeniably affecting our lives on a global scale. Issues such as the shortage of food and water, the increased frequency of extreme weather, and the rising sea levels are direct results of humanity's impact on our environment[1–5]. Anthropogenic carbon dioxide (CO_2) is the main greenhouse gas emitted at ~32.3 giga tonnes per year[6] and its reduction is a valid starting point to mitigate the environmental impact made by humans[2]. Due to the low cost and abundance of coal, approximately 60% of carbon dioxide emissions are from coal-fired power plants[7]. Although renewable energy sources will be preferable long term solutions, coal-fired power plants will likely remain as our main source of electricity for the next century[5]. The short term solution is to decrease the pollution made by these power plants. This will allow for continued use of fossil fuels with reduced environmental impact and have a smoother transition to a sustainable, low-carbon energy future.

Carbon Capture and Sequestration (CCS) is a strategy to reduce CO_2 emissions, it encompasses all technologies which aim to selectively filter carbon dioxide from emissions gasses for permanent storage[8,9]. CO_2 is typically proposed to be stored in deep saline reservoirs, and depleted oil and gas fields after compression[10–12]. Alternatively, CO_2 can be used to assist in oil and gas recovery by injection into nearly depleted wells[13–

[15]. These storage methods are proven to be safe and cost efficient[16]. Therefore, the main focus of improving CCS has been to develop materials and methods for CO_2 capture[9].

The three main types of CCS consists of oxy-fuel combustion, pre-combustion capture, and post-combustion capture[9]. In oxy-fuel combustion, pure O_2 is separated from the ambient air for fuel combustions[17]. The exhaust produced is a binary gas mixture composed of H_2O and CO_2 where the water is removed by condensation[7]. This yields concentrated CO_2 that can be easily purified or stored directly after compression[7,9,18]. However, the efficiency of power production with oxy-fuel combustion will be up to 37% lower than coal-burning power plants without CO_2 capture[18]. Pre-combustion capture involves the conversion of fuel into H_2 and CO_2 via gasification with the CO_2 being captured from the mixture, leaving behind clean burning H_2 fuel[9,18]. Since pre-combustion capture requires the additional process of gasifying the fuel, it will require a power plant specifically built for pre-combustion carbon capture. In addition, the power production in such plants would be 25% lower than coal-fired power plants with carbon capture[18]. For post-combustion carbon capture, the power plant is operated as usual, up until the moment before the exhaust flue gas is vented into the atmosphere[8,16]. With this method, CO_2 is captured from the flue gas and existing power plants can be retrofitted with carbon dioxide scrubbers[9]. Post-combustion capture will also reduce the efficiency of the power plant by 25-30%[18–20].

Of the three main types of CCS, pre-combustion capture has the most efficiency[18]. However, post-combustion capture is the most suitable for economical implementation

and existing power plants can be retrofitted[16]. Instead of abolishing existing power plants, post-combusting capture technologies can be retrofitted to existing power plants and, therefore, reduce the initial costs[7,16]. This type of retrofitting is proven to be effective and economical, as demonstrated by the addition of the flue gas desulfurization technologies in the 1990s[21]. When scrubbers were added to remove SO_2 from flue gas in power plants, little or no modification was required in the original plant; 98% or more of the SO_2 was able to be removed by this method[22].

The existing post-combustion CCS technologies are capable of capturing 70-99.9% of the CO_2 using solvent separation[7,23–25]. Following the separation, the CO_2 is released from the materials by temperature differentials and stored, thereby regenerating the solvent to be reused[19,26]. Figure 1-1 shows the general process of post-combustion CCS, and different setups may be engineered for each specific usage[7]. In the figure, flue gas from power generation is fed into the system during the absorption step. The CO_2 is selectively captured by the solvent, and then the remaining exhaust with low CO_2 content is vented into the atmosphere. After the solvent has been saturated with CO_2, it enters the desorption/regeneration step to release the captured CO_2 gases[26]. The CO_2 can be stored after compression and the solvent can be reused for additional cycles of CO_2 capture[27].

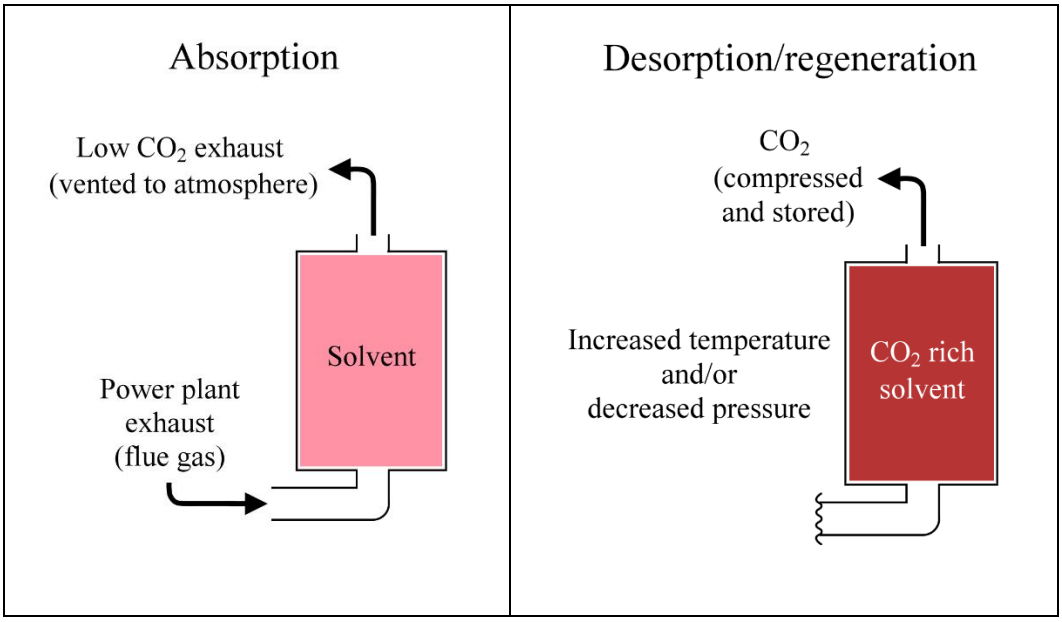

Figure 1-1. General process of post-combustion CCS showing absorption and desorption/reneration steps.

An example of solvent separation is demonstrated by aqueous amine absorption, which has been well established and used by the natural gas industry to separate CO_2 from methane over the past six decades[18]. In fact, SaskPower of Saskatchewan, Canada, has the first commercial-scale 110 megawatt power plant fitted with amine absorption post-combustion CCS[28]. The CCS technology fitted to this power plant is capable of reducing 90% of the CO_2 emission, capturing approximately one million tonnes of CO_2 per year; this is equivalent to the emission of 250,000 vehicles[28]. In the amine absorption process, 20-30% by weight monoethanolamine (MEA) is the most commonly used sorbent to selectively absorb CO_2, as shown in Equation 1-1[29].

Equation 1-1. Equilibrium of chemical absorption between MEA and CO_2.

$$C_2H_4OHNH_2 + H_2O + CO_2 \rightleftharpoons C_2H_4OHNH_3^+ + HCO_3^-$$

After the capture, MEA saturated with CO_2 can then be regenerated at high temperature for further use[27]. However, the aqueous amine solutions can be unstable when heated, limiting the regeneration temperature and reducing the lifetime of the solutions[30]. Also, the solutions tend to be corrosive towards the vessels, limiting their concentrations to below 40% by weight[26,27]. As a result, a larger quantity of solutions is required[26]. In addition, due to the high heat capacity of the solutions and the energy requirement of chemical absorption, the sorbent regeneration can use upwards of 30% of the energy generated from the power plant[20]. Although highly concentrated CO_2 (above 99%) can be separated by this method, the intense energy input required to regenerate the starting solvent render this method uneconomical[7].

Another common method of separating CO_2 is through the use of solid porous sorbents[26,31]. Two examples of sorbent materials available are zeolites and activated carbons[32]. These highly porous materials have high internal surface areas and are capable of selectively adsorbing CO_2 based on their pore sizes, shapes, and surface functional groups[26]. Since physical adsorption is due to the intermolecular forces present, the interaction is weaker compared to chemical bonding in absorption[33]. Therefore, the desorption process would require less energy and more favourable for CCS applications[7,26]. Zeolite 13X is a prime example of a solid sorbent studied for CO_2 capture by physical adsorption, it is capable of capturing CO_2 with 90% or higher purity[34]. However, the presence of water in post-combustions CCS conditions reduces the capacity of CO_2 uptake[35]. Another type of solid porous sorbent is activated carbon[32]. Activated carbons are amorphous forms of carbon that are highly porous; their hydrophobic nature

can prevent decomposition due to the presence of water, unlike zeolites[36]. Activated carbons can have even higher surface areas, upwards of 3,000 m^2/g[37–39], where zeolite 13X only has 756 m^2/g[40]. The higher surface area allows for additional interaction surface and greater adsorption of CO_2 at high pressures[26]. However, the relatively uniform electric potential on its surface reduces favourable intermolecular interactions, hence a lower CO_2 adsorption at low pressures in post-combustion CCS conditions[41].

For a direct comparison between different types of CCS technologies, the costs associated are used in this study. The costs of CCS can be broken down into the CO_2 capture cost and the storage cost. Storing CO_2 underground is cost efficient and estimated at USD$3-10 per tonne of CO_2 stored[9]. However, the cost of capturing CO_2 is much higher, estimated at between USD$49-57 per tonne of CO_2 using the current materials and methods[20]. In order to widely implement CCS technologies, it must be economically viable for power companies. Currently, the major financial cost of emitting CO_2 for power companies is the carbon tax, where industries are taxed by the government based on the amount of CO_2 emitted. The rates of carbon tax for electricity generation, range from a few dollars to CDN$30 per tonne of CO_2 in British Columbia and Alberta, Canada[42–44]. Even at the highest rate of CDN$30 per tonne of CO_2, it will still be more economical for power companies to emit the CO_2 and pay the carbon tax than to implement CCS. In order to decrease the amount of CO_2 pollution by power generation, reducing the cost of CCS has thus become the main concern. Studies done by Ho *et al.*[20] show that the cost of CCS can be lowered to approximately USD$30 per tonne of CO_2 if a sorbent material can be made to meet the following conditions: (1) the sorbent material

has to be able to selectively adsorb CO_2 over N_2 at a ratio of above 150, and (2) it must be capable of removing more than 4 mmol of CO_2 per gram of material per adsorption/desorption cycle[20]. The current material commonly used to separate CO_2 from natural gas, zeolite 13X[18], can only remove 2.2 mmol of CO_2 per gram of material per cycle at selectivity of 54[20,34,45]. To allow for economical and effective implementations of post-combustion CCS, new materials have to be discovered or designed.

1.2 Finding the Ideal Materials for CCS Applications

The ideal materials for post-combustion CCS applications must be able to selectively adsorb CO_2 and capable of removing large amounts of CO_2 per adsorption/desorption cycle[20]. To satisfy the first requirement, the sorbent have to selectively separate CO_2 from a mixture of gasses present in the exhaust gas of power plants[46]. Typical post-combustion flue gas is composed of many different types of gases, as listed in Table 1-1. Gases such as SO_x and NO_x are removed after desulfurization[21], leaving a gaseous mixture of N_2, CO_2, and H_2O[26]. While most of the H_2O can be removed via condensation, as practiced in oxy-combustions[7], trace water vapour may still be present in the gas mixture[47–49]. Therefore, the ideal materials for post-combustion CCS are require to separate the CO_2 from the remaining N_2/CO_2 mixture in humid conditions.

Table 1-1. Typical post-combustion flue gas composition[20,26].

Molecule	Concentration (by volume)
N_2	73-77%
CO_2	13-16%
H_2O	5-7%
O_2	3-5%
SO_x	200-800 ppm
NO_x	50-500 ppm

The preferential adsorption of CO_2 from the N_2/CO_2 mixture is defined by a normalized ratio between the uptake of CO_2 and N_2; this is called the selectivity[26,50]. The gas adsorption selectivity factor is calculated by Equation 1-2, where the ratio of gas uptake between CO_2 and N_2 is normalized with their respective partial pressures[26,50]. As the selectivity factor represents the ratio of gas uptakes, therefore it is unitless. For efficient post-combustion CCS applications, the selectivity of a material for CO_2 over N_2 would have to be above 150 to satisfy the first requirement of ideal materials used in post-combustion CCS[20].

Equation 1-2. Gas adsorption selectivity factor normalized with partial pressures.

$$S = \frac{x_{CO_2}/x_{N_2}}{p_{CO_2}/p_{N_2}}$$

The second requirement of ideal materials used in post-combustion CCS in this study is their ability to remove at least 4 mmol/g of CO_2 per adsorption/desorption cycle. The quantity of CO_2 captured and released per each cycle is called the working capacity[26]. The working capacity can be determined experimentally by the amount of CO_2 captured

and released in a adsorption/desorption cycle, typically measured in mmol/g, mol/kg, or weight percent[26,51]. Working capacities can also be calculated by subtracting the uptake of CO_2 during adsorption by the amount of CO_2 retained during desorption in simulations[26].

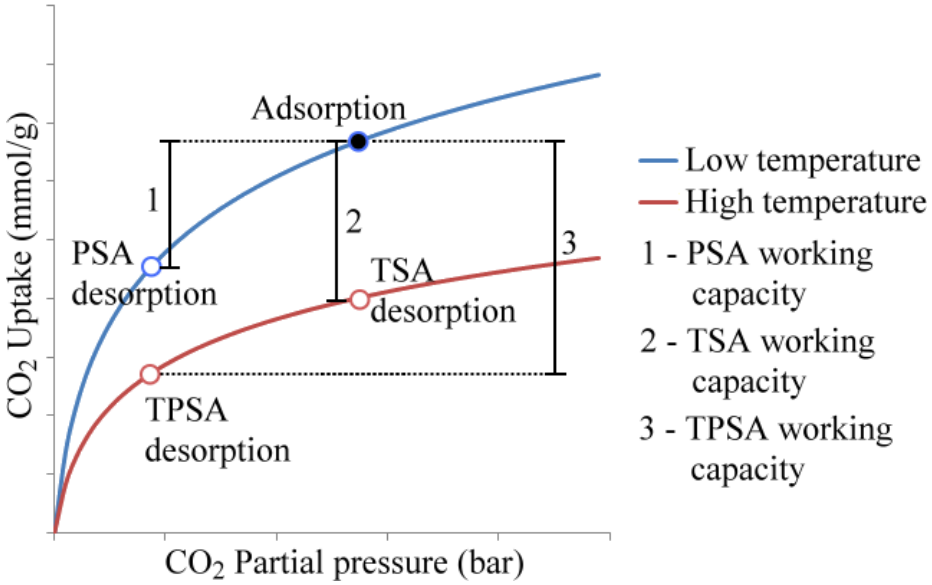

Figure 1-2. Calculation of working capacity from adsorption isotherms[26].

Figure 1-2 depicts adsorption isotherms which shows the quantity of gas adsorbed at different pressures and a given temperature. In Figure 1-2, different adsorption and desorption conditions are shown on the two isotherms at different temperatures[52]. The adsorption condition is marked with a solid circle and the desorption conditions are marked with empty circles. Using different temperature and/or pressure between adsorption and desorption conditions, schemes such as Temperature Swing Adsorption

(TSA), Pressure Swing Adsorption (PSA), and Temperature and Pressure Swing Adsorption (TPSA) can be achieved[26]. The difference in CO_2 uptake between adsorption and desorption is calculated as the working capacity. Working capacity can span a wide range depending on the conditions in which the adsorption and desorption processes are carried out. Generally, the lower the temperature and the higher the pressure, the more CO_2 that can be adsorbed onto the material[26]. Therefore, adsorptions would ideally be carried out in low temperature and high pressure environment, with the opposite being true for desorptions[51].

When designing new materials, it is important to aim for high selectivities and working capacities, as these are the two main criteria for economical implementation of CCS. High selectivity allows for the capture of purer CO_2 and reduces the cost of purification and compression prior to storage, hence the reduction of cost[26]. High working capacity reduces the number of cycles required to capture the same quantity of CO_2, therefore reducing the cost as well[20].

1.3 Metal-organic Frameworks (MOFs)

Metal-organic frameworks (MOFs) are a relatively new type of porous material that only came into the researchers' focus recently. However, as many as 20,000 different MOFs were reported and studied in the past decade alone[53]. Figure 1-3 shows six MOFs structures with different shapes, sizes, and chemical compositions reported to the Cambridge Crystallographic Data Centre[54–59].

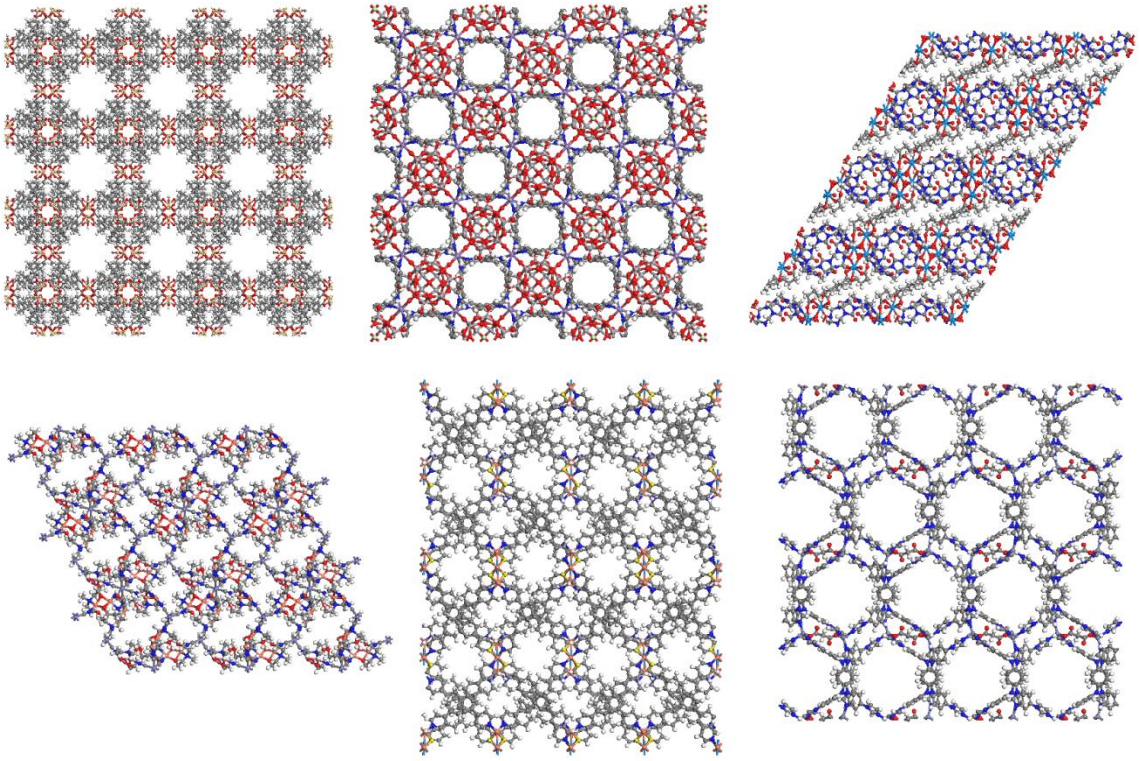

Figure 1-3. A varity of MOFs reported to the Cambridge Crystallographic Data Centre, each with different structural properties.

MOFs are structures formed by linking organic and inorganic building units into different topological networks[60,61]. These building units are named secondary building units (SBUs), similar to the description of protein secondary structures[26]. Figure 1-4 and Figure 1-5 show examples of SBUs of MOFs, the inorganic SBUs are defined as the building blocks containing metal atoms (Figure 1-5), whereas organic SBUs do not have metal atoms (Figure 1-4)[26]. By varying the structures of the individual SBUs, the overall structures and properties of the MOF can be finely tuned to suit each specific application[62–64]. In addition to their tunability, MOFs have extraordinary surface areas

and the capability to be scaled up for industrial use, this make them highly attractive to researchers for CO_2 capture applications[65,66].

Figure 1-4. An organic SBU which contains no metal atoms.

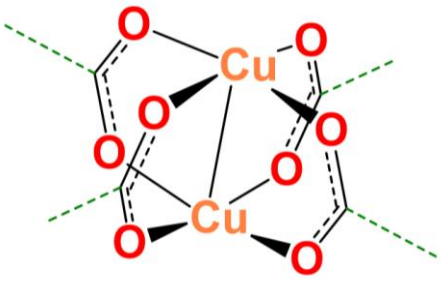

Figure 1-5. A metal SBU containing copper atoms.

In post-combustion CCS applications, CO_2 is to be separated from N_2[26]. Though neither CO_2 nor N_2 are formally charged or have a dipole moment, CO_2 molecules have a larger quadrupole moment than N_2 molecules[67]. The intermolecular interactions between the gas and the MOF framework may be exploited for the gas capture and separation. However, if the interactions are too strong, the energy penalty for desorption may be too high; if too weak, the selectivity and CO_2 uptake may be lowered[68]. Therefore, selecting the materials for CO_2 capture must take the energy penalty into consideration, in addition to having the highest possible selectivity and working capacity.

MOFs are not always neutral, certain MOF carry a net charge on its framework balanced by extra-framework counter ions. As an example, Wang *et al.*[69] has synthesized a MOF with an inorganic SBU consisting of an In(III) atom chelated by four carboxylate groups, as shown in Figure 1-6. The presence of the four carboxylate groups, each with a -1 charge, along with the +3 charge of the In(III) result in an overall -1 charge in the

inorganic SBU, hence the net charge on the framework. Conversely, organic SBUs can also be charged by the addition of charged functional groups. Goesten *et al.*[70] has shown that poly-aromatic organic SBUs can be functionalized with sulfate groups (Figure 1-7), which can result in a -1 charge.

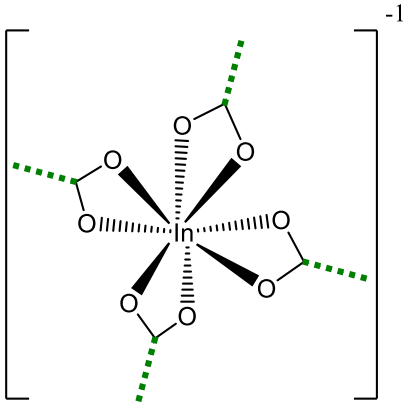

Figure 1-6. Inorganic SBU of MOF synthesized by Wang *et al.*[69], where the In(III) is chelated by four carboxylate groups, resulting in a -1 charge in the SBU.

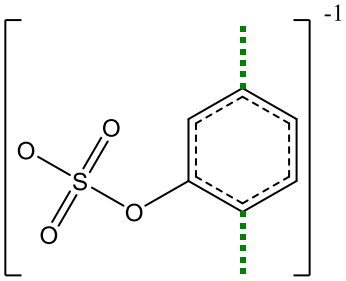

Figure 1-7. Organic SBU of MOF synthesized by Goesten *et al.*[70], where the benzene has a sulfate functional group, resulting in a -1 charge in the SBU.

Since MOFs have such vast diversity in structural properties, it is hard to intuitively design the ideal material for post-combustion CCS directly. Alternatively, high performing candidates can be selected from a diverse database of MOFs. As hypothetical MOFs can be constructed by matching organic and inorganic SBUs to different topologies[71], there is virtually no limit in terms of the number of MOF structures.

1.4 Computer Simulation

Owing to the near infinite combinations of SBUs and topologies for building MOFs, it is impractical to experimentally determine the performance of each individual MOF. Fortunately, advances in computational simulation allow us to not only accurately estimate the experimental results, but also to predict the properties of MOFs that have yet to be synthesized.

1.4.1 Determination of Gas Adsorption Properties with Monte Carlo Simulations

As the selectivities and working capacities of MOFs are calculated from the uptake of gasses, it is important to understand their adsorption properties. To determine the gas adsorption properties, statistical mechanics methods such as Monte Carlo (MC) algorithms may be employed[72]. As the Monte Carlo algorithms are based on probability and chance, they are named after the Monaco district on the French Riviera prominent for its casinos. Such algorithms generate ensembles, which are copies of the system of interest each with different configurations of the atoms[73]. By evaluating the energy of the systems due to intermolecular interactions, the probability of guest adsorptions at equilibrium can be predicted[72]. In canonical ensembles, variables such as temperature, volume, and the number of guest molecules remain constant[74]. Canonical ensembles can be useful when simulating extra-framework counter ions, as the number of ions is kept fixed to neutralize the charged frameworks. On the other hand, Grand Canonical Monte Carlo (GCMC) ensemble allows the number of guest molecules to fluctuate, effectively simulating the uptake of guest molecules by the MOF framework[74].

The adsorption data obtained from GCMC simulations can also be used to derive thermodynamic properties such as adsorption isotherms and heats of adsorptions[75]. With the gas uptake at different pressures, adsorption isotherms can be plotted. This allows for the visualization of the pressure dependency of gas uptakes. Also, the isosteric heats of adsorption can be used as an indicator of the MOF's affinity towards a guest molecule[76]. Finally, the guest locations can be plotted with a Radial Distribution Function (RDF), which helps visualize the density of guests at different distances surrounding a given origin[77]. By identifying the binding locations of guests, specific structural features for guest binding can be determined. With the thermodynamic properties and structural features, they can be correlated with one another for more intuitive design and screening.

As MOFs are crystalline materials made up of infinitely repeating images of identical structures, simulations cannot be effectively performed on the whole system. Instead, simulations are performed on a single image of the structure to represent the entire system[78]. Periodic boundary conditions are imposed during the simulations such that when a guest molecule leaves the simulation cell and enters the neighbouring cell, it re-enters the opposite end of the same cell[73]. In Figure 1-8, a simulation cell in the centre and two neighbouring cells are shown with dots on the left and right. In the simulation cell, the empty circles depict the original location of the molecule, their path of travel is shown by the black arrow to their new location. As the molecule leaves the simulation cell and enters the neighbouring cell to the left, the molecule from the cell to the right enters the simulation cell. To account for the intermolecular interactions in the simulation, interactions between molecules within half the cell length are considered.

Typically, a minimum cell length of 12.5 Å is used for to ensure that the same interactions would not be counted more than once. As shown in Figure 1-8, the orange dotted line represents the interaction between the closest molecules, which is located in the periodic image to the right. With the periodic boundary conditions, the simulation of the whole system can be effectively represented by only one unit cell in the middle.

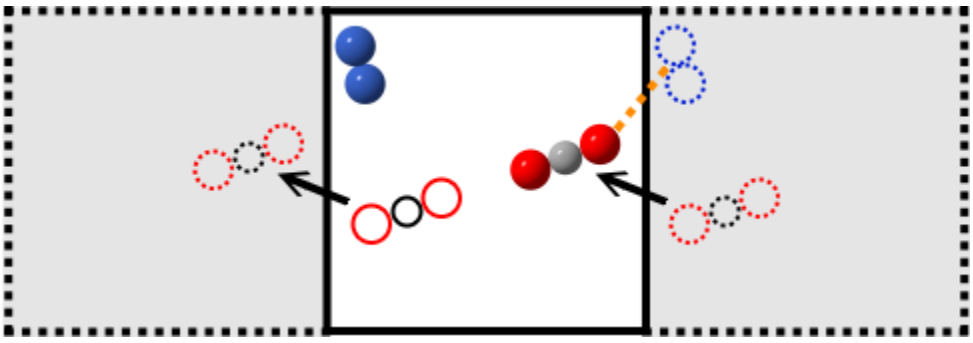

Figure 1-8. A depiction of simulation cells with periodic boundary conditions. As a molecule moves to a neighbouring cell, it re-enters the opposite side of the same simulation cell. The dotted molecules represent the original location of the molecule and they follow the path of the black arrow and arrive at their new locations. The interactions between molecules at the minimum distance is shown by the orange dotted line.

1.4.2 Partial Atomic Charge Derivation

To represent the intermolecular interactions in GCMC simulations, accurate representations of the electrostatics are required. Quantum Mechanical (QM) methods such as Density Function Theory (DFT) are often used for their ability to precisely describe the electronic structures in periodic systems[79]. In addition, DFT calculations can determine the ground state properties using only the density of electrons, therefore it requires less computational effort than traditional wave function methods[80]. The electrostatic potentials (ESPs) obtained from DFT calculations are located on fine grid

points around the atoms in the simulations. The ESP at a point is defined as the work done to bring a unit of positive charge from infinitely far away to this point[73]. The ESP reflects the electrostatics of both the nuclei and the electrons and is used to rationalize the guest-host interactions, for which electrostatic forces are the primary contributor to the long-range interactions[73,81]. As a high number of fine grid points are used to represent the ESPs as a continuous electronic distribution, simulating the interactions using the ESP at all grid point results in high computational costs[82]. To reduce the computational efforts, partial atomic charges are fitted to atomic centres to reproduce the quantum mechanical ESPs.

Partial atomic charge derivation has a long history since accurate determination of electronic wave functions became available. The CHELP method proposed by Chirlian and Francl[83] in 1987 is a basic example of this method: first, the ESP is determined at a select set of grid points around the system of interest. Then, a least square fit utilizing a Lagrangian multiplier, with the total molecular charge as the constraint, is used to solve for the charges at each atomic centre that gives the best representation of the quantum mechanical ESP at each point[83]. Over the years, similar methods have been proposed by updating the choices of the ESP point selection in CHELPG[84] and adding restraints to account for buried atoms in RESP[85]. Although the parameters of charge fitting have evolved over the years, the basic principles of fitting charges to the ESP have remained largely unchanged. However, these methods were only available for non-periodic molecular systems.

Since MOF simulations use infinitely repeating periodic cells, accurate charge derivation in periodic simulations are required. As the absolute energy of atoms in infinite periodic systems is not an intrinsic property, the reference ESP in such systems is ill-defined[79]. The baseline ESP resulting from quantum mechanical calculations for periodic systems are arbitrary; therefore, the methods designed for molecular systems are not valid for periodic calculations[79,86]. This problem was overcome by Woo and co-workers[79] in 2009 with the introduction of the REPEAT method, which utilizes a new error functional that treats the relative differences in the ESP instead of the absolute values. By considering only the relative differences in the potential, it ensures that the quality of the fit is entirely independent of the ill-defined references state of the ESP[79]. This approach allows for charge derivation from the ESP in periodic crystalline solids as well as molecular systems. REPEAT was proven effective by Chen *et al.*[86] and Manz and Sholl[87] in 2010. In addition, the REPEAT method has been shown to accurately reproduce the electronic structures in studies by Vaidhyanathan *et al.* in 2010 in the journal Science[88].

As seen previously, some MOFs have net charges on their frameworks, methods used to derive the partial atomic charge for these MOFs must take the framework net charge into consideration. The current REPEAT method can only fit partial atomic charges to systems without an overall charge. No charge fitting methods have been reported in literature for systems with a net charge. To accurately represent the electrostatic interactions and obtain gas adsorption data in charged MOFs, it is necessary to develop methods to derive partial atomic charges for systems with a net charge.

1.5 Research Goals and Outline

The goal of this research project is to investigate how net charges on MOFs' frameworks can affect their ability in CO_2 uptake, selectivity, and working capacity. In addition, this project can point experimentalists towards specific synthetic targets, thereby drastically reducing the number of MOFs needed to be synthesized. In order to accomplish these goals, methods to simulate gas uptake properties of charged porous materials were developed. In addition to simulating the CO_2 uptake for this project, the methods developed can also be used to understand properties in other charged materials. A database of vastly diverse charged hypothetical MOFs was built and the CO_2 uptake properties of the charged MOFs were simulated. The development and validation of the methods will be discussed in Chapter 2, and the database construction will be discussed in Chapter 3. Chapter 4 will consist of the results and discussions in screening the database as well as the effects of charges on CCS. The conclusions will be drawn in Chapter 5 and followed by the future direction of this project.

1.6 References

1. Hansen, J., Sato, M., Ruedy, R., Kharecha, P., Lacis, A., Miller, R., Nazarenko, L., Lo, K., Schmidt, G., and Russell, G. Dangerous Human-made Interference with Climate: A GISS Model E study. *Atmos. Chem. Phys.* **7,** 21 (2006).

2. Solomon, S., Plattner, G.-K., Knutti, R., and Friedlingstein, P. Irreversible Climate Change due to Carbon Dioxide Emissions. *Proc. Natl. Acad. Sci. U. S. A.* **106,** 1704–1709 (2009).

3. IPCC. *Climate Change 2007: Impacts, Adaptation and Vulnerability*. *International Journal of Climatology* (2007). doi:10.2134/jeq2008.0015br

4. Ramanathan, V. and Feng, Y. On Avoiding Dangerous Anthropogenic Interference with the Climate System: Formidable Challenges Ahead. *Proc. Natl. Acad. Sci. U. S. A.* **105,** 14245–14250 (2008).

5. Aalst, van M., Adger, N., Arent, D., Barnett, J., Betts, R., Bilir, E., Birkmann, J., Carmin, J., Chadee, D., and Challinor, A. *Climate Change 2014: Impacts, Adaptation, and Vulnerability*. *Assessment Report 5* (2014).

6. International Energy Statistics - EIA. *International Energy Statistics – EIA* (2016). Available at: https://www.eia.gov/cfapps/ipdbproject/iedindex3.cfm?tid=90. (Accessed: 18th August 2016)

7. Verma, M., Palacios, J., Pélletier, F., Godbout, S., Brar, S., Tyagi, R., and Surampalli, R. in *Carbon Capture and Storage* 37–64 (American Society of Civil Engineers, 2015). doi:10.1061/9780784413678.ch03

8. Haszeldine, R. S. Carbon Capture and Storage: How Green can Black be? *Science* **325,** 1647–1652 (2009).

9. Gurjar, B., Ojha, C., Surampalli, R., Zhang, T., and Walvekar, P. in *Carbon Capture and Storage* 7–35 (2015).

10. Secure Geologic Storage of CO2. *Global Carbon Capture and Storage Institute* (2015). Available at: https://www.globalccsinstitute.com/publications/secure-geologic-storage-co2. (Accessed: 8th July 2015)

11. Benson, S. M. and Surles, T. Carbon Dioxide Capture and Storage: An Overview With Emphasis on Capture and Storage in Deep Geological Formations. *Proc. IEEE* **94,** 1795–1805 (2006).

12. Aydin, G., Karakurt, I., and Aydiner, K. Evaluation of Geologic Storage Options of CO2: Applicability, Cost, Storage Capacity and Safety. *Energy Policy* **38,** 5072–5080 (2010).

13. Carbon Capture and Storage, Full-Scale Demonstration Progress Update. Available at: https://www.iea.org/publications/freepublications/publication/ccs_g8july09.pdf. (Accessed: 13th May 2016)

14. Alvarado, V. and Manrique, E. Enhanced Oil Recovery: An Update Review. *Energies* **3,** 1529–1575 (2010).

15. Khoo, H. H. and Tan, R. B. H. Environmental Impact Evaluation of Conventional Fossil Fuel Production (Oil and Natural Gas) and Enhanced Resource Recovery with Potential CO 2 Sequestration. *Energy & Fuels* **20,** 1914–1924 (2006).

16. Metz, B., Davidson, O., De Coninck, H., Loos, M., and Meyer, L. Carbon Dioxide Capture and Storage. (2005).

17. IPCC. *IPCC Special Report on Carbon Dioxide Capture and Storage*. *IPCC Special Report on Carbon Dioxide Capture and Storage* **2,** (2005).

18. Yang, H., Xu, Z., Fan, M., Gupta, R., Slimane, R., Bland, A., and Wright, I. Progress in Carbon Dioxide Separation and Capture: A Review. *J. Environ. Sci.* **20,** 14–27 (2008).

19. Duan, L., Zhao, M., and Yang, Y. Integration and Optimization Study on the Coal-fired Power Plant with CO2 Capture Using MEA. *Energy* **45,** 107–116 (2012).

20. Ho, M. T., Allinson, G. W., and Wiley, D. E. Reducing the Cost of CO2 Capture from Flue Gases Using Pressure Swing Adsorption. *Ind. Eng. Chem. Res.* **47,** 4883–4890 (2008).

21. Lonsdale, C. R., Stevens, R., Brock, C., Makar, P., Knipping, E., and Pierce, J. The

Effect of Coal-fired Power-plant SO2 and NOx Control Technologies on Aerosol Nucleation in the Source Plumes. *Atmos. Chem. Phys.* **12,** 11519–11531 (2012).

22. Rubin, E. S., Rao, A. B., and Chen, C. in *Greenhouse Gas Control Technologies 7* 285–293 (2005). doi:10.1016/B978-008044704-9/50029-X

23. Clarens, F., Espí, J. J., Giraldi, M. R., Rovira, M., and Vega, L. F. Life Cycle Assessment of CaO Looping Versus Amine-based Absorption for Capturing CO2 in a Subcritical coal Power Plant. *Int. J. Greenh. Gas Control* **46,** 18–27 (2016).

24. Korre, A., Nie, Z., and Durucan, S. Life Cycle Modelling of Fossil Fuel Power Generation with post Combustion CO2 Capture. *Energy Procedia* **1,** 3771–3778 (2009).

25. Desideri, U. and Paolucci, A. Performance Modelling of a Carbon Dioxide Removal System for Power Plants. *Energy Convers. Manag.* **40,** 1899–1915 (1999).

26. Sumida, K., Rogow, D., Mason, J., McDonald, T., Bloch, E., Herm, Z., Bae, T., and Long J. Carbon Dioxide Capture in Metal-Organic Frameworks. *Chem. Rev. (Washington, DC, United States)* **112,** 724–781 (2012).

27. Yu, C. H., Huang, C. H., and Tan, C. S. A Review of CO2 Capture by Absorption and Adsorption. *Aerosol and Air Quality Research* **12,** 745–769 (2012).

28. Capturing Carbon and the World's Attention - SaskPower. *SaskPower* (2015). Available at: http://www.saskpower.com/our-power-future/innovating-today-to-power-tomorrow/capturing-carbon-and-the-worlds-attention/?linkid=slider_innovating_today_power_tomorrow. (Accessed: 7th July 2015)

29. da Silva, E. F. Theoretical Study of the Equilibrium Constants for Solvents for CO2 Capture. *Energy Procedia* **4,** 164–170 (2011).

30. Davis, J. and Rochelle, G. Thermal Degradation of Monoethanolamine at Stripper Conditions. in *Energy Procedia* **1,** 327–333 (2009).

31. Meisen, A. and Shuai, X. Research and Development Issues in CO2 Capture.

Energy Convers. Manag. **38,** S37–S42 (1997).

32. Choi, S., Drese, J. H., and Jones, C. W. Adsorbent Materials for Carbon Dioxide Capture from Large Anthropogenic Point Sources. *ChemSusChem* **2,** 796–854 (2009).

33. Berger, A. H. and Bhown, A. S. Comparing Physisorption and Chemisorption Solid Sorbents for use Separating CO2 from flue as Using Temperature Swing Adsorption. in *Energy Procedia* **4,** 562–567 (2011).

34. Su, F. and Lu, C. CO2 Capture from gas Stream by Zeolite 13X Using a Dual-column Temperature/Vacuum Swing Adsorption. *Energy & Environmental Science* **5,** 9021 (2012).

35. Li, G., Xiao, P., Webley, P. A., Zhang, J., and Singh, R. Competition of CO2/H2O in Adsorption Based CO2 Capture. in *Energy Procedia* **1,** 1123–1130 (2009).

36. Plaza, M. G., García, S., Rubiera, F., Pis, J. J., and Pevida, C. Post-combustion CO2 Capture with a Commercial Activated Carbon: Comparison of Different Regeneration Strategies. *Chem. Eng. J.* **163,** 41–47 (2010).

37. Yang, K., Peng, J., Srinivasakannan, C., Zhang, L., Xia, H., and Duan, X. Preparation of high Surface area Activated Carbon from Coconut Shells Using Microwave Heating. *Bioresour. Technol.* **101,** 6163–6169 (2010).

38. Kaneko, K., Ishii, C., Ruike, M., and Kuwabara, H. Origin of Superhigh Surface area and Microcrystalline Graphitic Structures of Activated Carbons. *Carbon N. Y.* **30,** 1075–1088 (1992).

39. Nakayama, A., Suzuki, K., Enoki, T., Koga, K., Endo, M., and Shindo, N. Electronic and Magnetic Properties of Activated Carbon Fibers. *Bull. Chem. Soc. Jpn.* **69,** 333–339 (1996).

40. Vyas, R. K., Kumar, S., and Kumar, S. Determination of Micropore Volume and Surface area of Zeolite Molecular Sieves by D-R and D-A equations: A Comparative Study. *Indian J. Chem. Technol.* **11,** 704–709 (2004).

41. Martín, C. F., Plaza, M. G., Pis, J. J., Rubiera, F., Pevida, C., and Centeno, T. A.

On the Limits of CO2 Capture Capacity of Carbons. *Sep. Purif. Technol.* **74,** 225–229 (2010).

42. Province of British Columbia: How the Carbon Tax Works. (2015). Available at: http://www.fin.gov.bc.ca/tbs/tp/climate/A4.htm. (Accessed: 13th July 2015)

43. Carbon Tax Center: Where Carbon Is Taxed. (2014). Available at: http://www.carbontax.org/where-carbon-is-taxed/. (Accessed: 13th July 2015)

44. Carbon levy and rebates | Climate Leadership Plan | Climate Leadership. Available at: http://www.alberta.ca/climate-carbon-pricing.cfm. (Accessed: 12th May 2016)

45. Bae, Y.-S., Farha, O. K., Hupp, J. T., and Snurr, R. Q. Enhancement of CO2/N2 Selectivity in a Metal-organic Framework by Cavity Modification. *J. Mater. Chem.* **19,** 2131 (2009).

46. Flue gas Treatment for CO2 Capture. Available at: http://www.iea-coal.org/documents/82357/7542/Flue-gas-treatment-for-CO2-capture-(CCC/169). (Accessed: 13th May 2016)

47. Lee, K. B. and Sircar, S. Removal and Recovery of Compressed CO 2 from flue gas by a Novel Thermal Swing Chemisorption Process. *AIChE J.* **54,** 2293–2302 (2008).

48. Granite, E. J. and Pennline, H. W. Photochemical Removal of Mercury from Flue Gas. *Ind. Eng. Chem. Res.* **41,** 5470–5476 (2002).

49. Flue gas Processing: Strategies for Water Management. Water Removal and Moisture Control via dew Point Modelling. Available at: https://www.eventspro.net/iea/viewpdf.esp?id=1090060&file=%5C%5Cdata%5Cmo%24%5CEventwin%5CPool%5COffice109%5Cdocs%5Cpdf%5Cocc3Abstract00011.pdf. (Accessed: 26th May 2016)

50. D'Alessandro, D. M., Smit, B., and Long, J. R. Carbon Dioxide Capture: Prospects for new Materials. *Angewandte Chemie - International Edition* **49,** 6058–6082 (2010).

51. Mason, J. A., Sumida, K., Herm, Z. R., Krishna, R., and Long, J. R. Evaluating

Metal–organic Frameworks for Post-combustion Carbon Dioxide Capture via Temperature Swing Adsorption. *Energy & Environmental Science* **4,** 3030 (2011).

52. Foo, K. Y. and Hameed, B. H. Insights into the Modeling of Adsorption Isotherm Systems. *Chemical Engineering Journal* **156,** 2–10 (2010).

53. Furukawa, H., Cordova, K. E., O'Keeffe, M., and Yaghi, O. M. The Chemistry and Applications of Metal-organic Frameworks. *Science* **341,** 1230444 (2013).

54. Yao, X. Q., Zhang, M., Hu, J., Li, Y., Guo, Z., and Zheng, H. Two Porous zinc Coordination Polymers with (10,3) Topological Features Based on a N-centered Tripodal Ligand and the Conversion of a (10,3)-d Subnet to a (10,3)-a Subnet. *Cryst. Growth Des.* **11,** 3039–3044 (2011).

55. Thuéry, P. Uranyl ion Complexation by Aliphatic Dicarboxylic Acids in the Presence of Cucurbiturils as Additional Ligands or Structure-directing Agents. *Cryst. Growth Des.* **11,** 2606–2620 (2011).

56. Lu, Z.-Z., Zhang, R., Li, Y.-Z., Guo, Z.-J., and Zheng, H.-G. [WS(4)Cu(3)I(2)](-) and [WS(4)Cu(4)](2+) Secondary Building Units Formed a Metal-organic Framework: Large Tubes in a Highly Interpenetrated System. *Chem. Commun. (Camb).* **47,** 2919–21 (2011).

57. Das, S., Kim, H., and Kim, O. Metathesis in Single Crystal: Complete and Reversible Exchange of Metal ions Constituting the Frameworks of Metal-organic Frameworks. *J. Am. Chem. Soc.* **131,** 3814–3815 (2009).

58. Karabach, Y. Y., Guedes da Silva, M. F., Kopylovich, M. N., Gil-Hernández, B., Sanchiz. J., Kirillov. A. M., and Pombeiro, A. J. Self-assembled 3D Heterometallic CuII/FeII Coordination Polymers with Octahedral net Skeletons: Structural Features, Molecular Magnetism, Thermal and Oxidation Catalytic Properties. *Inorg. Chem.* **49,** 11096–11105 (2010).

59. Zhang, C. D., Liu, S., Gao, B., Sun, C., Xie, L., Yu, M., and Peng, J. Hybrid Materials Based on Metal-organic Coordination Complexes and Cage-like Polyoxovanadate Clusters: Synthesis, Characterization and Magnetic Properties. *Polyhedron* **26,** 1514–1522 (2007).

60. Tranchemontagne, D. J., Mendoza-Cortés, J. L., O'Keeffe, M., and Yaghi, O. M. Secondary Building Units, nets and Bonding in the Chemistry of Metal-organic Frameworks. *Chem. Soc. Rev.* **38,** 1257–1283 (2009).

61. Eddaoudi, M., Moler, D. B., Li, H., Chen, B., Reineke, T. M., and O'Keeffe, M. Modular Chemistry: Secondary Building Units as a Basis for the Design of Highly Porous and Robust Metal−Organic Carboxylate Frameworks. *Acc. Chem. Res.* **34,** 319–330 (2001).

62. Li, J. R., Sculley, J., and Zhou, H. C. Metal-organic Frameworks for Separations. *Chemical Reviews* **112,** 869–932 (2012).

63. Wang, Z. and Cohen, S. M. Postsynthetic Modification of Metal-organic Frameworks. *Chem Soc Rev* **38,** 1315–1329 (2009).

64. Du, L., Lu, Z., Zheng, K., Wang, J., Zheng, X., Pan, Y., You, X., and Bai, J. Fine-tuning pore size by Shifting Coordination Sites of Ligands and Surface Polarization of Metal-organic Frameworks to Sharply Enhance the Selectivity for CO2. *J. Am. Chem. Soc.* **135,** 562–565 (2013).

65. Czaja, A. U., Trukhan, N., and Müller, U. Industrial Applications of Metal-organic Frameworks. *Chem. Soc. Rev.* **38,** 1284–93 (2009).

66. Zhou, H.-C., Long, J. R., and Yaghi, O. M. Introduction to Metal-organic Frameworks. *Chem. Rev.* **112,** 673–4 (2012).

67. Buckingham, A. D., Disch, R. L., and Dunmur, D. A. Quadrupole Moments of some Simple Molecules. *J. Am. Chem. Soc.* **90,** 3104–3107 (1968).

68. Lin, L.-C. C., Berger, A., Martin, R., Kim, J., Swisher, J., Jariwala, K., Rycroft, C., Bhown, A., Deem, M., Haranczyk, M., and Smit, B. In Silico Screening of Carbon-capture Materials. *Nat. Mater.* **11,** 633–641 (2012).

69. Wang, L., Song, T., Huang, L., Xu, J., Li, C., Ji, C., Shan, L., and Wang, L. A Porous Chiral In-MOF with Anionic-type Diamond Network: Synthesis, Structure and Nitrogen gas Adsorption. *CrystEngComm* **13,** 4005 (2011).

70. Goesten, M. G., Juan-Alcañiz, J., Ramos-Fernandez, E., Sai Sankar Gupta, K.,

Stavitski, E., van Bekkum, H., Gascon, J., and Kapteijn, F. Sulfation of Metal-organic Frameworks: Opportunities for acid Catalysis and Proton Conductivity. *J. Catal.* **281,** 177–187 (2011).

71. Wilmer, C. E., Farha, O. K., Bae, Y.-S., Hupp, J. T., and Snurr, R. Q. Structure–Property Relationships of Porous Materials for Carbon Dioxide Separation and Capture. *Energy Environ. Sci.* **5,** 9849 (2012).

72. Yazaydin, A., Snurr, R., Park, T., Koh, K., Liu, J., Levan, M., Benin, A., Jakubczak, P., Lanuza, M., Galloway, D., Low, J., and Willis, R. Screening of Metal-organic Frameworks for Carbon Dioxide Capture from flue gas Using a Combined Experimental and Modeling Approach. *J. Am. Chem. Soc.* **131,** 18198–18199 (2009).

73. Leach, A. R. *Molecular Modelling: Principles and Applications*. *Prentice Hall Harlow UK* **2nd,** (2001).

74. Chesnut, D. A. and Salsburg, Z. W. Monte Carlo Procedure for Statistical Mechanical Calculations in a Grand Canonical Ensemble of Lattice Systems. *J. Chem. Phys.* **38,** 2861 (1963).

75. Düren, T., Bae, Y.-S., and Snurr, R. Q. Using Molecular Simulation to Characterise Metal-organic Frameworks for Adsorption Applications. *Chem. Soc. Rev.* **38,** 1237–1247 (2009).

76. Pan, H., Ritter, J. A., and Balbuena, P. B. Examination of the Approximations Used in Determining the Isosteric Heat of Adsorption from the Clausius−Clapeyron Equation. *Langmuir* **14,** 6323–6327 (1998).

77. Alder, B. J., Frankel, S. P., and Lewinson, V. A. Radial Distribution Function Calculated by the Monte-Carlo Method for a Hard Sphere Fluid. *J. Chem. Phys.* **21,** 417–419 (1955).

78. Thompson, S. Use of Neighbor Lists in Molecular Dynamics.

79. Campañá, C., Mussard, B., and Woo, T. K. Electrostatic Potential Derived Atomic Charges for Periodic Systems Using a Modified Error Functional. *J. Chem. Theory Comput.* **5,** 2866–2878 (2009).

80. Becke, A. D. Perspective: Fifty Years of Density-functional Theory in Chemical Physics. *J. Chem. Phys.* **140,** 18A301 (2014).

81. Sigfridsson, E. and Ryde, U. Comparison of Methods for Deriving Atomic Charges from the Electrostatic Potential and Moments. *J. Comput. Chem.* **19,** 377–395 (1998).

82. Watanabe, T., Manz, T. A., and Sholl, D. S. Accurate Treatment of Electrostatics during Molecular Adsorption in Nanoporous Crystals without Assigning Point Charges to Framework Atoms. *J. Phys. Chem. C* **115,** 4824–4836 (2011).

83. Chirlian, L. E. and Francl, M. M. Atomic Charges Derived from Electrostatic Potentials: A Detailed study. *J. Comput. Chem.* **8,** 894–905 (1987).

84. Breneman, C. M. and Wiberg, K. B. Determining Atom-centered Monopoles from Molecular Electrostatic Potentials. The need for high Sampling Density in Formamide Conformational Analysis. *J. Comput. Chem.* **11,** 361–373 (1990).

85. Bayly, C. C. I., Cieplak, P., Cornell, W. D., and Kollman, P. A. A Well-behaved Electrostatic Potential Based Method Using Charge Restraints for Deriving Atomic Charges: the RESP Model. *J. Phys. …* **97,** 10269–10280 (1993).

86. Chen, D. L., Stern, A. C., Space, B., and Johnson, J. K. Atomic Charges Derived from Electrostatic Potentials for Molecular and Periodic Systems. *J. Phys. Chem. A* **114,** 10225–10233 (2010).

87. Manz, T. A. and Sholl, D. S. Chemically Meaningful Atomic Charges that Reproduce the Electrostatic Potential in Periodic and Nonperiodic Materials. *J. Chem. Theory Comput.* **6,** 2455–2468 (2010).

88. Vaidhyanathan, R., Iremonger, S., Shimizu, G., Boyd, P., Alavi, S., and Woo, T. Direct Observation and Quantification of CO_2 Binding Within an Amine-functionalized Nanoporous Solid. *Science* **330,** 650–653 (2010).

2 Computational Property Evaluations of Charged MOFs

Abstract

A novel computational method was developed for the determination of gas adsorption properties in charged periodic systems such as MOFs. The automated series of programs use partial atomic charges to simulate the electrostatic interactions between the MOF host framework and gas molecules as guests. The REPEAT method[1] was incorporated to derive the partial atomic charges, which reproduces the ESPs of QM calculations. In systems with net charges in their simulation cells, the periodic ESPs are calculated with DFT while a constant neutralizing background charge is applied. REPEAT is then used to derive partial atomic charges for the periodic systems with net charges. The whole charge derivation process is performed without the use of ions to render the system neutral. Though REPEAT has been proven to derive quality charges in neutral systems, using counter ions may cause polarization of the framework atoms and produce inaccurate charges. Following the charge determination, GCMC simulations are performed to obtain gas adsorption isotherms for the systems.

We found that the REPEAT charges fitted to periodic ESPs from QM calculations performed on a charged framework were in excellent agreement with those neutralized with counter ions. Furthermore, REPEAT charges were derived for a benzene-tris-tetrazolate MOF synthesized by Dincă *et al.* which has a net charge of -3 in its unit cell and contains Mn^{+2} counter ions[2]. By running a MC simulation with the REPEAT charges, the positions of the Mn^{+2} counter ions were determined and were in agreement with

experimental X-ray crystallography results. By reproducing the counter ion locations, the method developed in this work was shown to accurately reproduce the electrostatic environment of charged MOFs, allowing the evaluation of gas uptake in charged periodic systems.

2.1 Introduction

Computer simulations of neutral MOFs have been well established, as described in the previous chapter. However, as the study of MOFs with a net charge is a relatively new field, simulation methods for such charged systems have not yet matured. For example, De Toni *et al.*[3] attempted to derive partial atomic charges of a periodic system with cluster QM calculation, whereas the study done by Getman *et al.*[4] resorted to force field parameters similar to those used for zeolites. Zeolites have relatively low atomic diversity, consisting of only Al, Si, and O atoms which abides the Löwenstein's rule[5,6]. Empirically derived partial atomic charges are commonly used to represent the electrostatic interactions in gas uptakes simulations[7–9]. Although some sets of these generic charges have shown transferability for different zeolite topologies[10], they are mostly limited to specific topologies and or compositions[9–11]. In 2013, Fischer and Bell[12] attempted to develop generic charges semi-empirically, and they minimized the error of interaction energy between ones obtained with force field parameters and with DFT calculation. However, their generic charges underestimate the interactions between the framework and guest molecules when compared to the results obtained with REPEAT

charges[1], the underestimation were close to 30% in numerous cases[5,12]. They concluded that it is important to use system-specific charges to produce the most accurate representation of electrostatic interactions[12]. Charged systems, such as MOFs, have higher atomic diversity than zeolites[12,13]. Therefore, they require system-specific calculations to accurately determine their partial atomic charges[12].

A series of modules to evaluate MOF properties have been developed in the Woo Lab. However, these modules have only been applied to systems with an overall neutral charge. Fortunately, the series of steps taken to evaluate MOF properties are similar for both neutral and charged systems. First, the ESPs for each MOF are calculated quantum mechanically using DFT at the PBE level of theory[14]. Then, partial atomic charges are assigned with the REPEAT method to reproduce the quantum mechanically determined ESPs[1]. Next, appropriate Lennard-Jones and Coulomb potentials are chosen for the framework and guest molecules. The force field parameters dictate the intermolecular forces present during gas adsorption simulations which are performed using Grand Canonical Monte Carlo (GCMC). Lastly, structural properties such as dimensions, pore sizes, and void spaces are calculated. To investigate MOFs with net charges in this study, considerable modifications were required for each individual module outlined above.

2.2 Partial Atomic Charge Derivations of Periodic Structures with Net Charges

In order to evaluate the properties of charged MOFs, the electronic distribution is required to accurately model the intermolecular interactions. As discussed in Chapter 1.4,

ESPs can accurately represent the electronic distribution of the system[1,15]. However, ESPs on a high number of fine grid points were used to represent the continuous electronic distribution[1], simulating the interactions with ESPs at all grid points would result in immense computational costs[16]. To reduce the computational load, partial atomic charges fitted to reproduce the quantum mechanical ESPs of the system are used to represent the intermolecular interactions[1,17].

In this work, the REPEAT method[1] was used to derive partial atomic charges fitted to reproduce the QM ESPs. However, when performing periodic QM calculations in charged systems, the net charge in each of the infinite number of periodic images results in unphysical infinite charge and infinite energy[15]. One could perform calculations on a neutral system where counter ions are incorporated to balance the framework charge. However, the interactions between the counter ions and the framework may affect the charge distribution and the charges produced may be polarized[15]. Therefore, the QM calculations for the framework ESPs were performed with a compensating background charge was used[18–20]. The calculations were performed with the Vienna *Ab Initio* Simulation Package (VASP) with projector augmented wave (PAW) method and plane wave basis sets[19,21]. The net charge of the framework was inputted by adjusting the total number of valence electrons (NELECT) in VASP[22]. The ESPs obtained can then be used to derive partial atomic charges using the REPEAT method[1].

The REPEAT method uses a Lagrange multiplier to impose a constraint so the sum of the partial atomic charges on the atoms equal to the net framework charge[1]. In neutral periodic systems, the Lagrange multiplier ensures the sum of the partial atomic charges equals zero. In charged systems, the sum of the partial atomic charges would equal the net charge of the periodic simulation cell, as well as the background charge

used in the DFT calculation[1,23]. Thereby, the partial atomic charges in periodic systems with net charges can be derived.

2.3 GCMC Gas Uptake Simulations in Charged Frameworks

With partial atomic charges fit to reproduce the ESPs of systems with net charges, the electrostatic interactions between the framework and guests could be mimicked for gas uptake assessment. As discussed in Chapter 1.4, GCMC simulations are able to accurately reproduce the gas uptake in neutral MOFs by relating the interaction energies to uptake[4,15,23].

FastMC is a program developed in the Woo Lab for simulating gas uptake in systems with GCMC[15]. In the simulations, the frameworks are immobile while gas molecules can be introduced as a guest. The simulations proceed in a stepwise fashion where an individual step includes moving a guest molecule and the evaluation of the resulting potential energy of the system. FastMC is capable of applying moves such as translational movement, and rotation, to a randomly selected guest in canonical MC ensembles. In GCMC ensembles, two additional moves, insertion and deletion are allowed. Following each move set, the energy of the entire system is evaluated.

The energy evaluation is dependant of the ensemble of the simulation. In canonical MC ensemble, if the energy of the new configuration is lower than it was prior to the move, the new configuration is accepted. If the new energy is higher, the new configuration would be accepted or rejected based on the probability of the Boltzmann

distribution function[15]. Equation 2-1 shows the probability of acceptance depending on the change in energy (ΔE) and the thermal energy of the system (kT), where k is the Boltzmann constant and T is the temperature.

Equation 2-1. Boltzmann distribution function for acceptance probability.

$$P = e^{-\left(\frac{\Delta E}{kT}\right)}$$

In GCMC ensembles, since guests can be inserted or deleted, the partial pressures of the guests are taken into consideration in the chemical potential (μ). The energy evaluation in GCMC ensemble would take the chemical potential as well as the potential energy into account. When a step is accepted, the new configuration is recorded for the ensemble average. Also, the new configuration is used as a starting point for the next step. When a step is rejected, the original configuration prior to the move is recorded and used to start the following step. After the target number of MC steps has been reached, an average of all the accepted steps is taken and properties such as average number of guest molecules are determined. In order to sample the ensemble effectively, two stages are used. During the first stage, steps are run until equilibration is achieved. Equilibration steps are not used for the average of the gas adsorption results. In the second stage, production steps are used to generate the results for the gas adsorption data.

In gas uptake simulations, the potential energy of the systems can be calculated by the non-bonded interactions between the guests and the framework atoms, as well as between guest molecules. In FastMC, these non-bonded interactions are evaluated with the Lennard-Jones and Coulomb interactions[4]. The framework atoms use the Universal

Force Field for the Lennard-Jones parameters and the REPEAT partial atomic charges as the Coulomb potentials[1,24]. As for the CO_2 guest molecules, the TraPPE force field, designed for evaluating carbon dioxide adsorption in zeolites, is used[10].

As periodic systems are described with infinitely repeating simulation cells, systems with net charges are unphysical[23]. The infinite number of periodic images with each having a net charge would result in an unbounded amount of energy in the system. Therefore, counter ions are used to balance the charges on the framework prior to the evaluation of gas uptakes.

2.3.1 Counter Ion Insertion

To balance the net charge on the framework, extra-framework counter ions are inserted into the simulation cells. To insert counter ions, many different attempts were made. Initially, the counter ions were fixed in locations where the lowest energy was achieved. Incorporating the counter ions into the framework was desirable, since a set number of counter ions can be used to balance the charge on the framework. However, as the counter ion was shown to be mobile in a multitude of cases[3,7,25–27], fixing the locations of the counter ions may produce invalid results.

In order to incorporate mobile counter ions, FastMC was modified so it is capable of performing GCMC where the positions of the counter ions were also sampled. While the guest molecules are allowed move sets such as insertions and deletions in the GCMC ensemble, counter ions have fixed numbers in the canonical MC ensemble. By setting

the number of counter ions, it ensures the system remain charge neutral. To calculate the interactions between the counter ions and other atoms in the system, Universal Force Field parameters are used for the counter ions[28].

In this scheme, the mobile counter ions are first introduced in random locations in the simulation cell. Following each insertion, an overlap check is performed in case the counter ion comes into proximity of any framework atoms or other ions. The overlap check is necessary to avoid an infinite energy that halts the simulation. The total number of ions used depends on the individual ion's charge, as well as the overall charge on the framework; the net charge of the system must be zero with the counter ions included.

2.3.2 Optimizing GCMC/MC move sets and sampling:

While sampling the counter ion locations in an experimental benzene-tris-tetrazolate MOF[2], not all of the binding locations were identified in one simulation. A simplified two dimensional system was used to illustrate the problem. In the hypothetical two dimensional simulation box (Figure 2-1), there are two counter ions (shown in red) with four equally probable binding locations (A, B, C, and D). For the sake of simplicity, the framework is not shown. FastMC often acquires only two of the four binding locations within one simulation; the two sets of locations are shown in Figure 2-2 and Figure 2-3. It is theorized that the counter ions repel each other due to long range electrostatic interactions[15]. Because of the charge repulsion forces, the counter ions should optimally be positioned as far apart as possible. In this case, the counter ions

should be placed in the equivalent binding sites A and D (Figure 2-2), or B and C (Figure 2-3). As the binding sites are equivalent, the energy of the system for either set of locations is equal. Due to the nature of FastMC, where the energy of the system is evaluated after each move, it is difficult for all of the locations to be discovered in one simulation. When one set of binding locations are found (Figure 2-2), both counter ions need to be moved at once in order to find the other locations (Figure 2-3) without drastically increasing the energy in the system. As the previously implemented program performs an energy evaluation immediately following a move, the energy of the intermediate system (Figure 2-4) would always be higher and therefore the move would not likely be accepted.

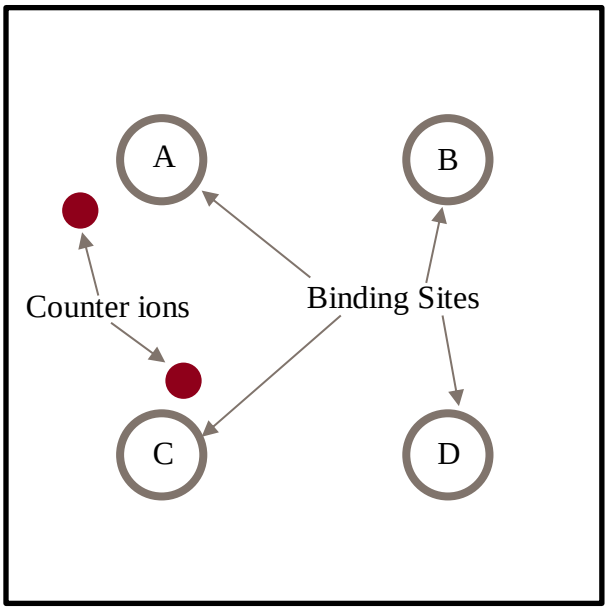

Figure 2-1. A simple 2D hypothetical simulation box with two counter ions and four binding sites. The framework is not shown.

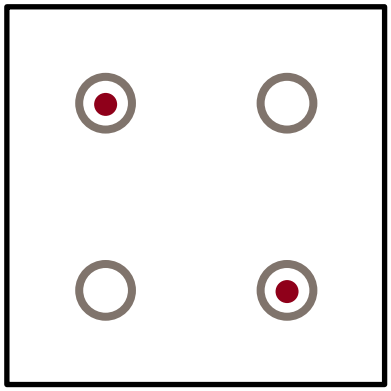

Figure 2-2. Counter ions located in two out of four binding locations, A and D.

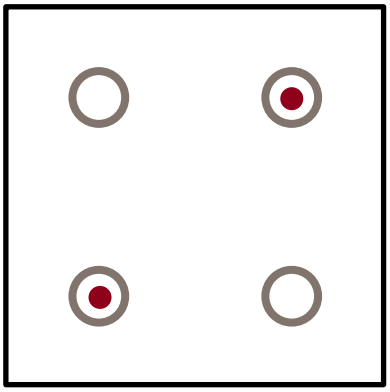

Figure 2-3. Counter ions located in the other two out of four binding locations, B and C.

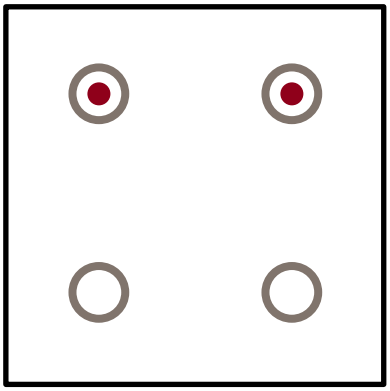

Figure 2-4. Counter ions located in binding locations A and B. As the ions are closer to each other than in **Figure 2-2** or **Figure 2-3**, the energy in this simulation cell is higher.

In order to find all four binding locations, a special MC move was introduced to ensure proper sampling of the counter ion locations. The double jump move was implemented such that two jump moves of two randomly selected counter ions were performed before the energy of the system is evaluated. In this new scheme, the probabilities of the move sets are 25% for displacement, 45% for the jump move, and 30% for the double jump move. With the double jump move set implemented, all of the correct counter ion binding locations in the experimental benzene-tris-tetrazolate MOF[2] were found. In addition to counter ions, the double jump move set can also be applied to other guests when many equivalent binding sites are available.

2.4 Determination of Structural Properties

In order to associate structural properties with the gas uptakes of the MOFs, the Zeo++ software package was used to calculate the MOFs' physical properties[29]. The Zeo++ software can compute the surface areas and void volumes with specified probe sizes. The Universal Force Field parameters were used for the van der Waals atomic radii of the framework atoms[24]. Additional properties such as the number of channels, pore sizes, and charges within the simulation cell can be calculated with an in-house developed program. The methods of determining the channels and pore sizes are similar to the Zeo++ methods[29]. As the volume of simulation cells differ from one to another, charges per volume were used for the comparisons. The charges within a specific volume is used to maintain consistency.

2.5 Fully Automated Adsorption Analysis in Porous Solids

To simulate the properties of MOFs, the modules described above are required to be run one after another. In order to rapidly screen a large number of MOFs, an in-house program named Fully Automated Adsorption Analysis in Porous Solids (FA^3PS) was used. It is capable of performing calculations for each individual module, as well as collecting and organizing the results from the modules following the calculations. The automated program creates input files for individual modules and passes results to subsequent modules' input files. Parameters such as the number of GCMC simulation steps or the adsorption guest molecule type can be specified. In addition, FA^3PS is

capable of performing the calculations with default values for unspecified parameters. With FA^{3}PS, the analysis of adsorption properties of porous materials can be done computationally, even by individuals with little knowledge on the methods.

As FA^{3}PS was originally developed for neutral systems, significant amounts of modifications were made to allow for simulations of charged systems. In order to perform calculations in FA^{3}PS, the crystallographic information files (cif) of the structures in question are used as inputs. In addition to the framework atom locations, the net charge on the framework is read from the input. The ESPs of the framework were then determined with a QM calculation. As charged systems are analyzed in this work, FA^{3}PS calculates the number of valence electrons with the framework net charge taken into consideration. When the QM ESP calculation is completed, FA^{3}PS collects the result and creates the input files for the partial atomic charge derivation. Since the ESPs were calculated with the framework's net charge taken into consideration, the partial atomic charge is fitted such that the sum of the partial atomic charges is equal to the overall net charge.

The partial atomic charges derived are used to mimic the intermolecular electrostatic interactions that occur in gas adsorption. In charged systems, FA^{3}PS inserts mobile counter ions to balance the framework net charge. For each ion inserted, FA^{3}PS performs an overlap check between the newly inserted ion with the framework atoms and other ions. If a counter ion is inserted within 1.6 Å of another atom in the simulation cell, it is discarded and another ion will be inserted. FA^{3}PS will continue to perform insertion

and overlap check cycles until the correct number of ions is in the cell to balance the framework net charge. Following the counter ion insertion, the GCMC and MC simulations are performed. FA^{3}PS includes the partial atomic charges derived in previous steps in the input files. To maintain the neutral net charge within the simulation cell, FA^{3}PS specifies the canonical MC ensemble for the mobile counter ions in the input files. Unlike the counter ions, the other guests can adapt the GCMC ensemble.

After the gas adsorption analysis, FA^{3}PS performs the property calculations for the framework structure. With the results from all of the modules, FA^{3}PS then organizes and saves them into a log file for user analysis. With FA^{3}PS as the automated rapid screening method, a large number of adsorption analysis calculations can be carried out simultaneously. The number of calculations that can be performed simultaneously is only limited by the computational resources available. In the Woo Lab, upwards of 600 MOFs can be analyzed at one time per user.

2.6 Validation of the Property Evaluation Methods

In order to validate the screening methods, modules such as partial atomic charge derivation as well as the gas uptake GCMC and MC simulations should be examined. To show that the REPEAT charges fitted to periodic ESPs calculated with a background charge is valid, REPEAT ESP charges derived in systems with and without a net charge were examined. First, the ESP fitted charges were derived in a neutral MOF with a large pore, IRMOF-16[30,31]. Then, the ESP charges were revaluated with cobalt ions placed

within the centre of the pores of IRMOF-16. Different oxidation states of the Co ions were used to introduce net charges of +3, +1, -1, and -3 into the simulation cell. IRMOF-16 was chosen for its large pore so the ions were ~14 Å to the nearest framework atom of the MOF, the distances were sufficient to minimize charge polarizations to the framework.

Table 2-1 lists the mean absolute deviation and maximum deviation between the two sets of REPEAT ESP charges. The mean absolute deviations in the charges were less than 0.031e and the maximum deviation at around 0.092e, indicating that the sets of REPEAT charges were nearly identical regardless of the net charge. The REPEAT ESP charges derived with different net charges in its simulation cells were also plotted the neutral REPEAT charges in Figure 2-5 to Figure 2-8. The agreements for the sets of REPEAT charges were excellent in all cases.

Table 2-1. Comparison of ESP fitted charges derived the neutral IRMOF-16 to ones calculated with ions inserted.

net charge	ion inserted	Mean absolute deviation (e)	Max deviation (e)
-3	Co^{-3}	0.031	0.092
-1	Co^{-}	0.018	0.065
+1	Co^{+}	0.014	0.056
+3	Co^{+3}	0.027	0.069

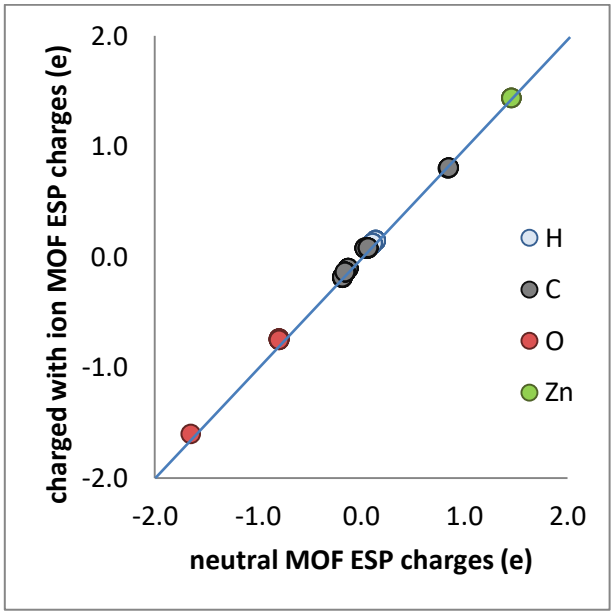

Figure 2-5. ESP charges of IRMOF-16 derived from a neutral framework compared to the ESP charges with a Co^{+3} ion inserted into the centre of the pore of IRMOF-16.

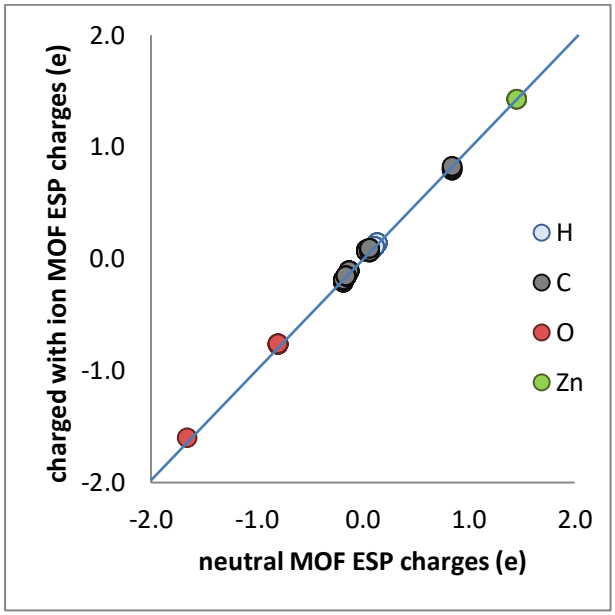

Figure 2-6. ESP charges of IRMOF-16 derived from a neutral framework compared to the ESP charges with a Co^{+} ion inserted into the centre of the pore of IRMOF-16.

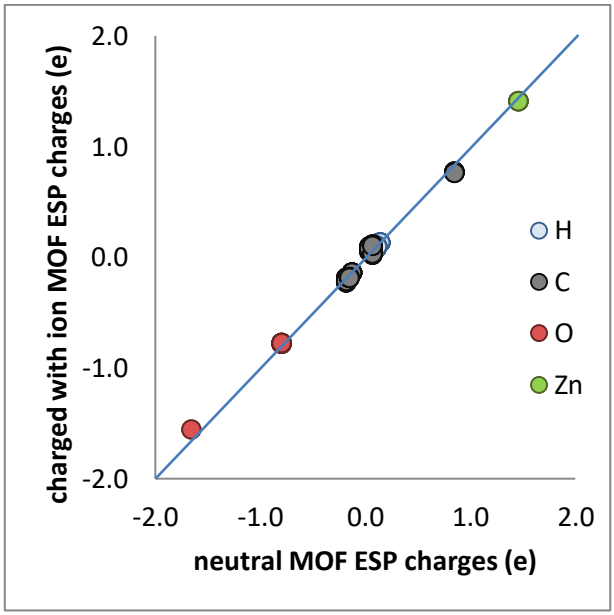

Figure 2-7. ESP charges of IRMOF-16 derived from a neutral framework compared to the ESP charges with a Co^{-} ion inserted into the centre of the pore of IRMOF-16.

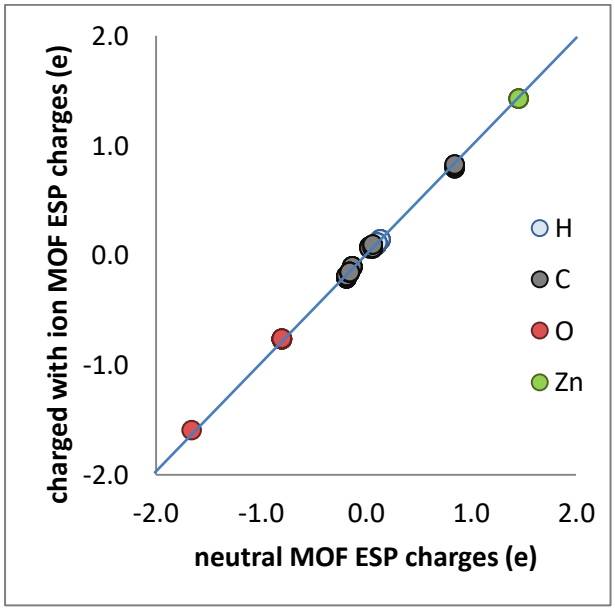

Figure 2-8. ESP charges of IRMOF-16 derived from a neutral framework compared to the ESP charges with a Co^{-3} ion inserted into the centre of the pore of IRMOF-16.

Another comparison was made between the REPEAT ESP charges derived from a charged framework and ones derived from the same framework with an ion to counter balance the net charge. The charged MOF in question was POST-1 developed by Seo *et al.*[32] which has large triangular pores with ~13.4 Å sides and a -4e net charge in its simulation cell. In the MOF where the net charge was neutralized, a Ti^{4+} ion was inserted into the centre of the pore. The differences between the two sets of ESP charges were minute where the mean absolute deviation was 0.027e and the maximum deviation was 0.155e. Figure 2-9 shows the REPEAT charges derived with and without the counter ions. Once again, the agreement between the two sets of charges was superb.

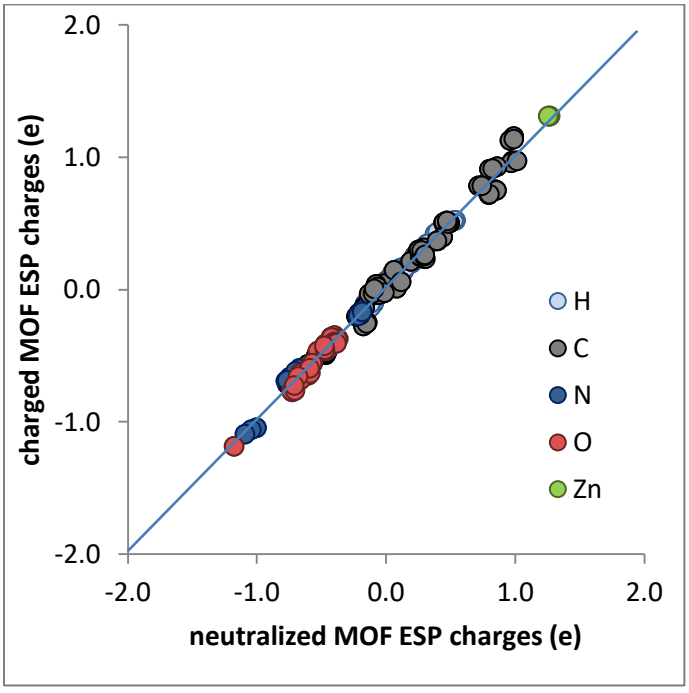

Figure 2-9. ESP charges of POST-1 derived from its charged framework plotted against the ESP charges derived from POST-1 neutralized with a Ti^{+4} ion in the centre of its pore.

As partial atomic charges are not physically observable, they cannot be measured and compared experimentally. Fortunately, the counter ion binding locations can sometimes be determined experimentally[1]. Since these locations are strongly dependent on electrostatic interactions within the framework of the charged MOF, counter ion locations found in simulations strongly reflect the electronic structure of the framework. By comparing the simulated counter ion locations with the experimentally determined locations, the module used to evaluate gas uptake as well as the charge fitting module can be validated. This comparison serves as a good indicator of the accuracy of REPEAT charges and FastMC's gas uptake simulations in systems with net charges.

The benzene-tris-tetrazolate MOF, **1**, is a charged MOF experimentally synthesized by Dincă *et al.*[2]. In the reported X-ray crystal structure (Figure 2-10), each periodic unit cell contains a -3 charge on the framework and 24 binding sites for the counter ions (orange). Due to symmetry, only 16 of the 24 probable locations in the unit cell are visible. There are four binding sites in each of the six faces of the cube. As shown in Figure 2-10, the four sites circled in red are in the a-b plane of the unit cell. The sites indicated by the green circles are located in the perpendicular planes. Since the extra-framework counter ions used by the experimentalists were manganese(II) ions, two simulation cells were required to accommodate three Mn^{2+} ions whereas only one cell is shown in the figures.

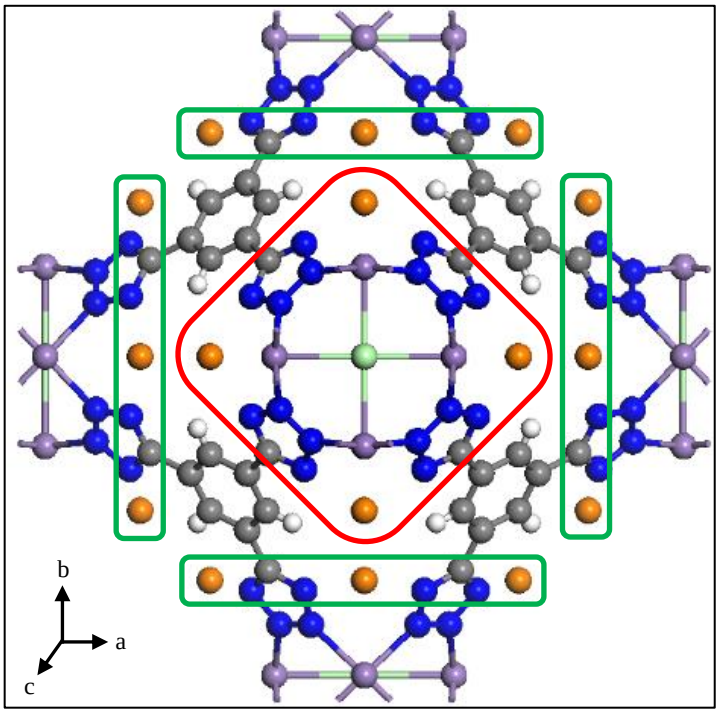

Figure 2-10. One unit cell of **1** where the experimental counter ion binding locations are shown in orange. The red circles indicates the binding locations close to each face of the cube.

In this method validation, the extra-framework counter ions' binding locations in **1** were determined and compared with experimental locations. First, the REPEAT charges of the experimental structure were derived to reproduce the VASP ESPs with a background charge applied. The sum of the REPEAT charges for all of the atoms on the framework was calculated and was found to be equal to the framework's charge of -3. After obtaining the ESP-derived REPEAT charges for **1**, a Monte Carlo simulation was performed with FastMC to obtain a probability distribution of the counter ion locations. In the simulations, a super cell formed by two simulation cells was used in conjunction with three Mn^{2+} counter ions. The resulting counter ion binding locations (orange) for **1** were shown in Figure 2-11. In addition to the counter ion locations determined with

REPEAT charges, binding locations were also simulated with charges derived with the charge equilibration (QEq) method[33] (Figure 2-12).

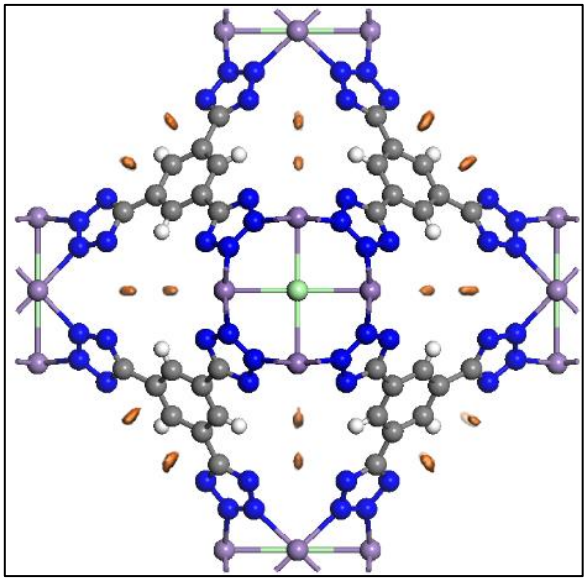

Figure 2-11. Counter ion locations (orange) found with REPEAT charges in FastMC simulations.

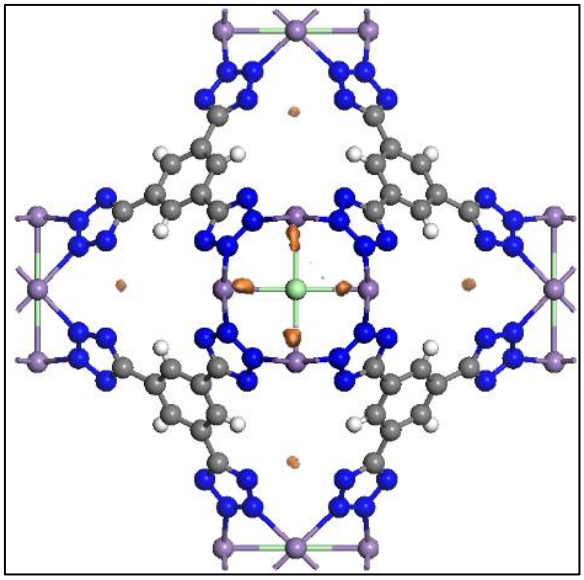

Figure 2-12. Counter ion locations (orange) found with QEq charges in FastMC simulations

As shown in Figure 2-11, the binding locations found with REPEAT and FastMC matched the experimental findings shown in Figure 2-10. On the other hand, FastMC employing QEq charges (Figure 2-12) was not able to find the correct counter ion binding locations. Since the counter ions carry a charge, their binding locations depend heavily on the framework's ESPs. Finding the correct binding locations with REPEAT and FastMC proves the accuracy of REPEAT charges in representing the electronic

distribution in a charged periodic system. Therefore, this method is capable of modelling guest binding locations in charged periodic systems.

In addition to the counter ion locations, properties of **1** were calculated and compared with experimental findings. Table 2-2 lists the properties reported by Dincă *et al.*[2], as well as ones calculated using the methods listed above. Aside from the surface area, properties such as the cell dimensions, cell volume, and pore diameter are near identical. The difference in surface areas was minute and could be attributed to the sampling methods. The experimental setup cannot guarantee a complete evacuation of the solvents and adsorbed gases in the MOF. As a result, the surface area measured experimentally may be less than the actual surface area.

Table 2-2. Property comparisons between experimental MOF, **1**, by Dincă *et al.*[2] and calculated properties of **1**.

Properties	Reported	Calculated
Cell dimensions (Å)	a = 19.009 b = 19.009 c = 19.009	a = 19.0086 b = 19.0086 c = 19.0086
Cell volume ($Å^3$)	6,868.3	6,868.32
Pore diameter (Å)	10	10.27
Surface area (m^2/g)	2,100	2,293

2.7 Summary

The development of novel methods to derive partial atomic charges and to evaluate gas adsorption uptake in charged periodic systems were outlined in this chapter. The ESPs of charged MOFs were calculated with VASP with a neutralizing background charge; partial atomic charges were then calculated with REPEAT to reproduce the QM

ESPs in systems with net charges. Using the REPEAT charges, FastMC was able to mimic the intermolecular interactions for gas adsorption simulations. FastMC was also modified to accommodate the addition of counter ions in charged systems. The sampling of FastMC was subsequently improved with the addition of the special MC double jump move set. To enable rapid screening of a large number of charged systems, FA^3PS was modified to include all of the modules listed above.

To validate the methods, REPEAT derived ESP fitted charges with and without a net charge in the simulation cell were compared. In all cases, the REPEAT charges have excellent agreement regardless of the net charge in the system. In addition, calculated properties of an experimentally synthesized charged MOF, **1**, were compared with the reported figures. The counter ion locations of **1** were successfully replicated with FA^3PS, using the charge derivation and gas uptake simulation methods described above for charged systems. In addition, structural properties were calculated and compared with the experimentally reported values. The calculated and experimental properties were nearly identical to each other. This proves the ability of FA^3PS and its individual modules to correctly simulate guest uptake as well as the calculation of other physical properties for charged MOFs.

2.8 References

1. Campañá, C., Mussard, B., and Woo, T. K. Electrostatic Potential Derived Atomic Charges for Periodic Systems Using a Modified Error Functional. *J. Chem. Theory Comput.* **5,** 2866–2878 (2009).

2. Dinča, M., Dailly, A., Liu, Y., Brown, C., Neumann, D., and Long, J. Hydrogen Storage in a Microporous Metal-organic Framework with Exposed Mn2+ Coordination Sites. *J. Am. Chem. Soc.* **128,** 16876–16883 (2006).

3. De Toni, M., Coudert, F., Paranthaman, S., Pullumbi, P., Boutin, A., and Fuchs, A. Molecular Simulation of a Zn-triazamacrocyle Metal-organic Frameworks Family with Extraframework Anions. *J. Phys. Chem. C* **116,** 2952–2959 (2012).

4. Getman, R. B., Bae, Y.-S., Wilmer, C. E., and Snurr, R. Q. Review and Analysis of Molecular Simulations of Methane, Hydrogen, and Acetylene Storage in Metal-organic Frameworks. *Chem. Rev.* **112,** 703–23 (2012).

5. Van Speybroeck, V., Hemelsoet, K., Joos, L., Waroquier, M., Bell, R., and Catlow, C. Advances in Theory and Their Application Within the Field of Zeolite Chemistry. *Chem. Soc. Rev.* (2015). doi:10.1039/c5cs00029g

6. Loewenstein, W. The Distribution of Aluminum in the Tetrahedra of Silicates and Aluminates. *Am. Mineral.* **39,** 92–96 (1954).

7. Beerdsen, E., Dubbeldam, D., Smit, B., Vlugt, T. J. H., and Calero, S. Simulating the Effect of Nonframework Cations on the Adsorption of Alkanes in MFI-type Zeolites. *J. Phys. Chem. B* **107,** 12088–12096 (2003).

8. Beerdsen, E., Smit, B., and Calero, S. The Influence of Non-framework Sodium Cations on the Adsorption of Alkanes in MFI- and MOR-Type Zeolites. *J. Phys. Chem. B* **106,** 10659–10667 (2002).

9. Jaramillo, E. and Auerbach, S. M. New Force Field for Na Cations in Faujasite-Type Zeolites. *J. Phys. Chem. B* **103,** 9589–9594 (1999).

10. García-Sánchez, A., Ania, C., Parra, J., Dubbeldam, D., Vlugt, T., Krishna, R., and Calero, S. Transferable Force Field for Carbon Dioxide Adsorption in Zeolites. *J.*

Phys. Chem. C **113,** 8814–8820 (2009).

11. Hirotani, A., Mizukami, K., Miura, R., Takaba, H., Miya, T., Fahmi, A., Stirling, A., Kubo, M., and Miyamoto, A. Grand Canonical Monte Carlo Simulation of the Adsorption of CO2 on Silicalite and NaZSM-5. *Appl. Surf. Sci.* **120,** 81–84 (1997).

12. Fischer, M. and Bell, R. G. Modeling CO2 Adsorption in Zeolites Using DFT-derived Charges: Comparing System-specific and Generic Models. *J. Phys. Chem. C* **117,** 24446–24454 (2013).

13. Sumida, K., Rogow, D., Mason, J., McDonald, T., Bloch, E., Herm, Z., Bae, T., and Long J. Carbon Dioxide Capture in Metal-Organic Frameworks. *Chem. Rev. (Washington, DC, United States)* **112,** 724–781 (2012).

14. Perdew, J. P., Burke, K., and Ernzerhof, M. Generalized Gradient Approximation Made Simple. *Phys. Rev. Lett.* **77,** 3865–3868 (1996).

15. Leach, A. R. *Molecular Modelling: Principles and Applications*. *Prentice Hall Harlow UK* **2nd,** (2001).

16. Watanabe, T., Manz, T. A., and Sholl, D. S. Accurate Treatment of Electrostatics during Molecular Adsorption in Nanoporous Crystals without Assigning Point Charges to Framework Atoms. *J. Phys. Chem. C* **115,** 4824–4836 (2011).

17. Sigfridsson, E. and Ryde, U. Comparison of Methods for Deriving Atomic Charges from the Electrostatic Potential and Moments. *J. Comput. Chem.* **19,** 377–395 (1998).

18. Bruneval, F., Crocombette, J., Gonze, X., Dorado, B., Torrent, M., and Jollet, F. Consistent Treatment of Charged Systems Within Periodic Boundary Conditions: The Projector Augmented-wave and Pseudopotential Methods Revisited. *Phys. Rev. B - Condens. Matter Mater. Phys.* **89,** (2014).

19. Hafner, J. Ab-initio Simulations of Materials Using VASP: Density-functional Theory and Beyond. *J. Comput. Chem.* **29,** 2044–2078 (2008).

20. Paier, J., Hirschl, R., Marsman, M., and Kresse, G. The Perdew-Burke-Ernzerhof Exchange-correlation Functional Applied to the G2-1 test set Using a Plane-wave

Basis set. *J. Chem. Phys.* **122,** 234102 (2005).

21. Blöchl, P. E. Projector Augmented-wave Method. *Phys. Rev. B* **50,** 17953–17979 (1994).

22. Kresse, G. and Furthmuller, J. VASP the Guide. *Comput. Physics, Fac. Physics, Univ. ...* (2012).

23. Yang, Q., Liu, D., Zhong, C., and Li, J.-R. Development of Computational Methodologies for Metal-organic Frameworks and Their Application in gas Separations. *Chem. Rev.* **113,** 8261–323 (2013).

24. Rappe, A. K., Casewit, C. J., Colwell, K. S., Goddard III, W. A., and Skiff, W. M. UFF, a full Periodic Table Force Field for Molecular Mechanics and Molecular Dynamics Simulations. *J. Am. Chem. Soc.* **114,** 10024–10035 (1992).

25. Herrero, C. P. and Ramhez, R. Cation Ordering in the Faujasite Framework: Monte Carlo Simulations. 2246–2253 (1992).

26. Dubbeldam, D., Krishna, R., Smit, B., Vlugt, T., Denayer, J., Martens, J., Maesen, T., Ingenieurstechniek, C., Uni, V., Brussel, V., Brussel, B., Centrum, V., and Opper, V. Understanding the Role of Sodium during Adsorption: A Force Field for Alkanes in Sodium-Exchanged Faujasites. 11377–11386 (2004).

27. Zhao, X., Bu, X., Wu, T., Zheng, S., Wang, L., and Feng, P. Selective Anion Exchange with Nanogated Isoreticular Positive Metal-organic Frameworks. *Nat. Commun.* **4,** 2344 (2013).

28. Casewit, C. J., Colwell, K. S., and Rappe, A. K. Application of a Universal Force Field to Organic Molecules. *J. Am. Chem. Soc.* **114,** 10035–10046 (1992).

29. Willems, T. F., Rycroft, C. H., Kazi, M., Meza, J. C., and Haranczyk, M. Algorithms and Tools for High-throughput Geometry-based Analysis of Crystalline Porous Materials. *Microporous Mesoporous Mater.* **149,** 134–141 (2012).

30. Eddaoudi, M., Kim, J., Rosi, N., Vodak, D., Wachter, J., O'Keeffe, M., and Yaghi, O. M.. Systematic Design of pore size and Functionality in Isoreticular MOFs and

Their Application in Methane Storage. *Science* **295,** 469–72 (2002).

31. Li, H., Eddaoudi, M., O'Keeffe, M., and Yaghi, O. M. Design and Synthesis of an Exceptionally Stable and Highly Porous Metal-organic Framework. **402,** 276–279 (1999).

32. Seo, J., Whang, D., Lee, H., Jun, S. I., Oh, J., and Jeon, Y. J. A Homochiral Metal-organic Porous Material for Enantioselective Separation and Catalysis. *Nature* **404,** 982–6 (2000).

33. Rappé, A. K. and Goddard III, W. A. Charge Equilibration for Molecular Dynamics Simulations. *J. Phys. Chem.* **95,** 3358–3363 (1991).

3 Hypothetical Charged MOFs Database Construction

Abstract

To explore the capability of charged MOFs, a diverse database of hypothetical charged MOFs was constructed. In this study, 158 experimental MOFs were investigated to obtain 200 organic SBUs and 54 inorganic SBUs[1]. TOBASCCO[2], a computer program previously developed in the Woo Lab was adapted to generate over 183,000 charged structures. The generated structures were then geometrically optimized using the GROMACS package[3] and universal force field parameters[4]. Stringent constraints were used to exclude unreasonable structures following optimization. The structural generation and optimization methods were validated by successfully reproducing a porous chiral In-MOF experimentally synthesized by Wang *et al.*[5]. The resulting database contains 47,244 charged hypothetical structures diverse in topology, charge, pore structures, and surface area, all generated using SBUs obtained from experimentally synthesized MOFs[1].

3.1 Introduction

There have been as many as 20,000 different MOFs reported and studied in the past decade alone[6]. The various SBUs forming the MOFs give rise to a wide variety of pore sizes, shapes, and functional groups[6–8]. Given the vast diversity of MOFs and their degrees of freedom, one cannot intuitively correlate the SBUs with the various structural properties effectively. Therefore, constructing the ideal material for CCS applications by rational design would be difficult[9,10]. Considering all of the possible combinations of SBUs that can form MOFs, the

number of MOFs experimentally synthesized and tested is quite limited[6,7,9]. Potential high performing MOFs can be determined by sampling a database of assorted hypothetical MOFs including those with charged frameworks. Such databases already exist for some MOFs[1,10,11], however, there has not been a diverse MOF database dedicated specifically for the study of charged MOFs. The database by Wilmer and co-workers[9,10] only encompasses 6 of the network topologies and the database by Martin *et al.*[11] only has 1, whereas over 2,000 nets are found experimentally[12]. Also, the CoRE database by Chung *et al.*[1] only includes 4,764 experimental structures found in the CCDC, in which, only 501 contain a net charge. Fortunately, the large number of existing MOFs can be used as template of which our hypothetical charged MOFs can based upon for the construction of our charged MOF database[1,7,10,13]. It is worth noting that a diverse database is desirable in order to discover a larger number of potential materials for a variety of applications.

As MOFs can be constructed by linking organic and inorganic SBUs to recreate different network topologies, a nearly unlimited number of hypothetical MOFs can be constructed. For example, a vast number of combinations could be demonstrated using only one organic SBU and one inorganic SBU, as shown in Figure 3-1. When the two SBUs are combined in all available topologies, approximately 200 unique structures can be generated. When additional organic and inorganic SBUs are used, the potential number of MOFs generated increases exponentially.

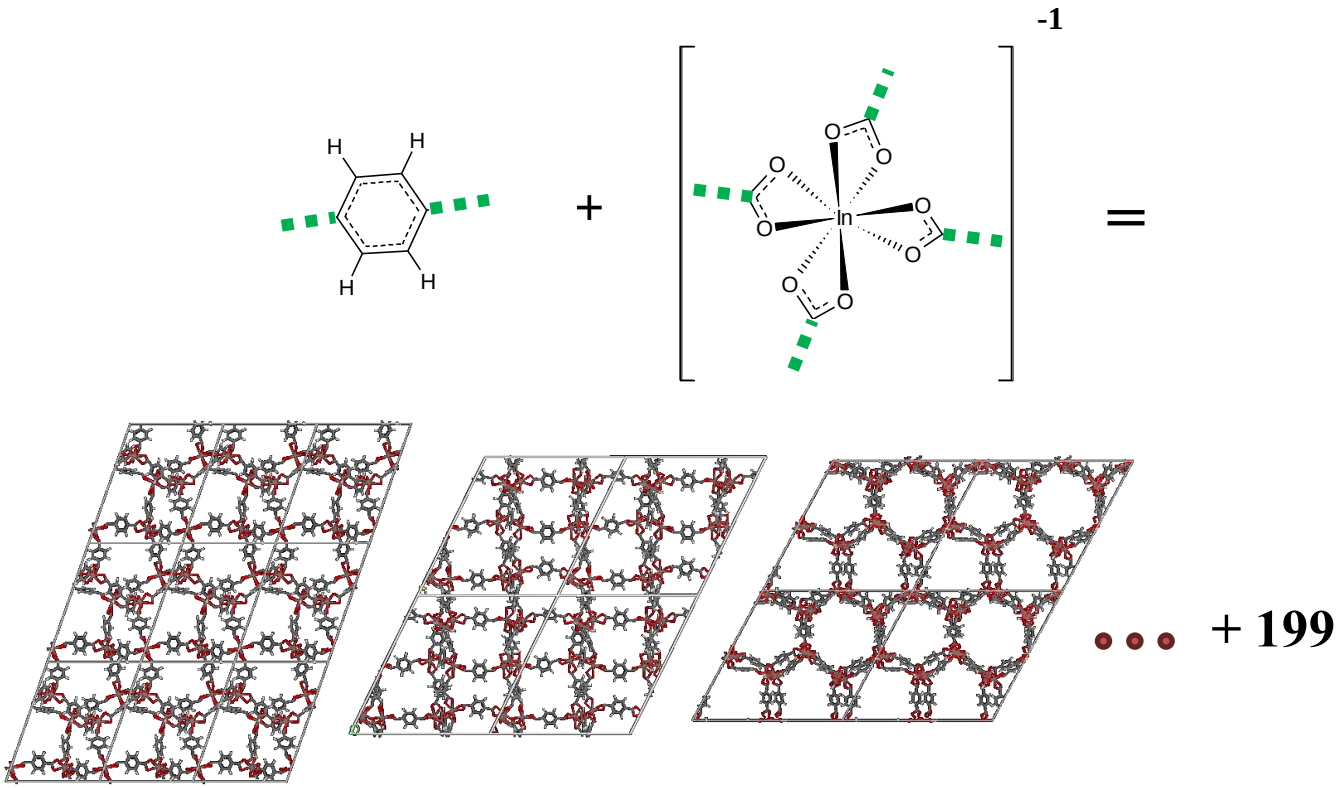

Figure 3-1. An abundance of MOFs can be constructed with only two SBUs while accounting for a large number of network topologies. With additional SBUs, virtually infinite number of MOFs can be created.

3.2 Selecting Charged MOFs and SBUs

Neutral MOFs have been studied in the Woo Lab for some time and there have been 200 neutral SBUs recorded from those MOFs, 173 organic and 27 inorganic. To construct charged MOFs for this database, charged SBUs must be added to the existing set of neutral SBUs. 158 experimental charged MOFs[1,14–18] were investigated and their charged SBUs were used. As

shown in Figure 3-2, the connectivities of all SBUs were recorded so they can be used in the construction of charged hypothetical structures. Although the method used to construct MOFs was different, the process of selecting SBUs was similar to the method used by Wilmer *et al.*[10]. Such techniques in SBU selections have been proven effective in generating valid structures[10]. In 2013, Woo Lab members Kadantsev *et al.*[19] used approximately 1,000 hypothetical structures generated to study the charge equilibration method of generating MOF-optimized atomic charges.

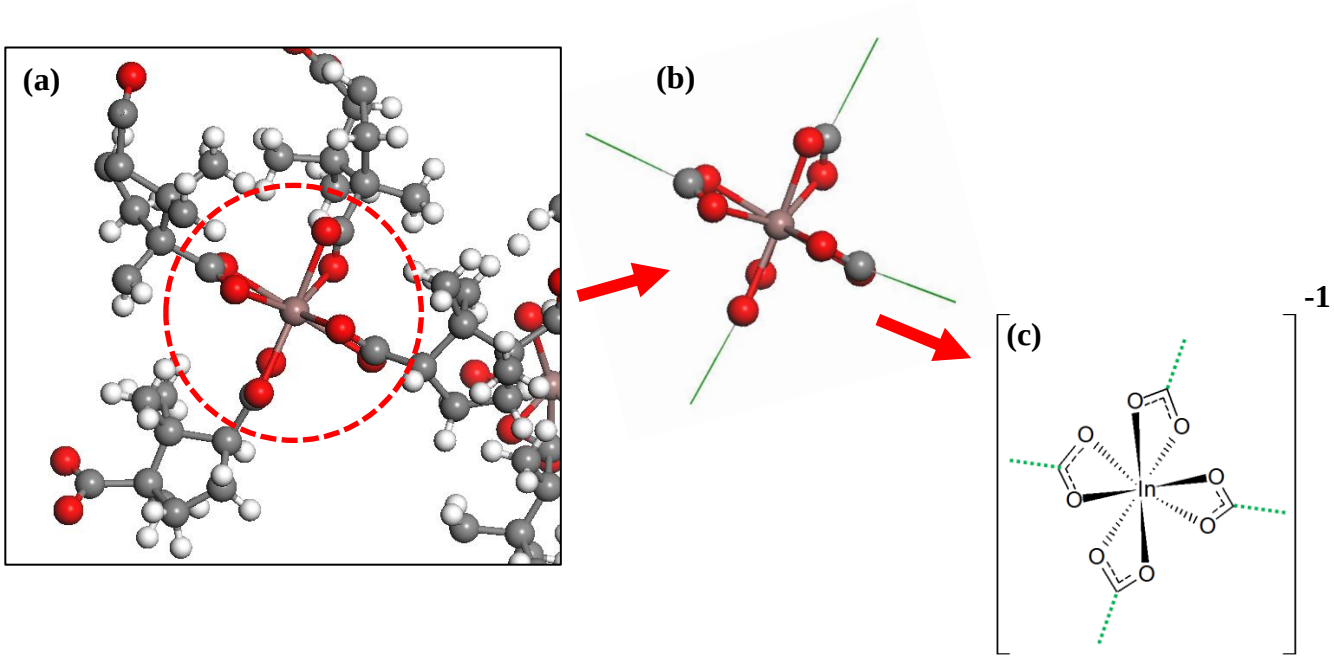

Figure 3-2. Recording SBU connectivities from MOFs. (a) Original MOF, (b) and (c) Parameterized SBUs.

Figure 3-3 to Figure 3-11 show all of the organic and inorganic SBUs used for structure generation with labels given to each SBU. Neutral organic SBUs **o1** to **o173** and inorganic (metal containing) SBUs **m1** to **m27** were previously parameterized by Woo Lab members and charged SBUs **o195** to **o200** and **m28** to **m54** were recorded in this work. Furthermore, neutral

SBUs **o174** to **o194** were also added to the group of existing neutral SBUs. Of the charged SBUs parameterized, 11 are positively charged and 22 carry a negative charge. For the purpose of this study, only the SBUs contained in experimental MOFs were chosen for parameterization as opposed to designing hypothetical SBUs.

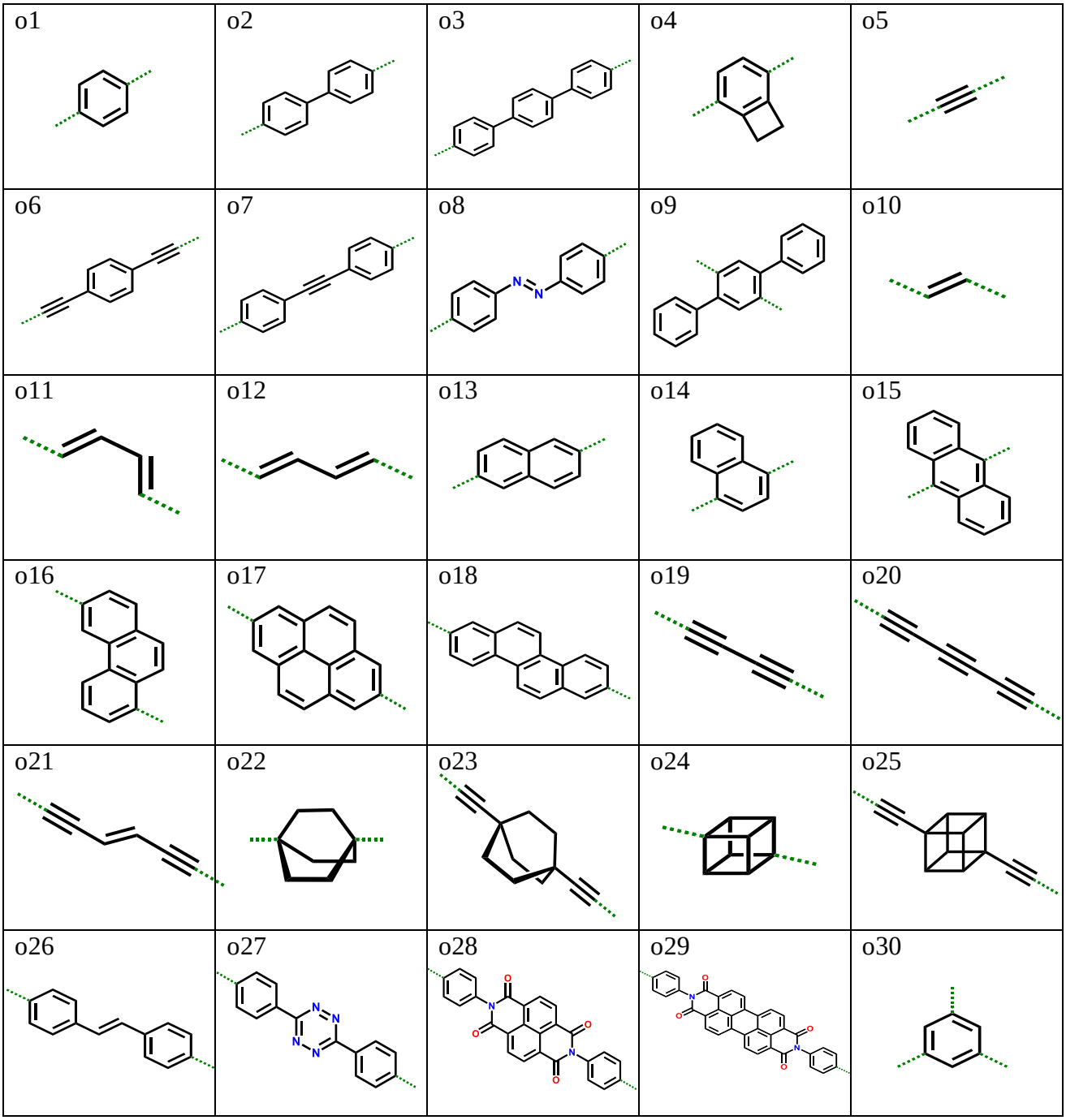

Figure 3-3. Organic SBUs used for structure generation (**o1** to **o30**).

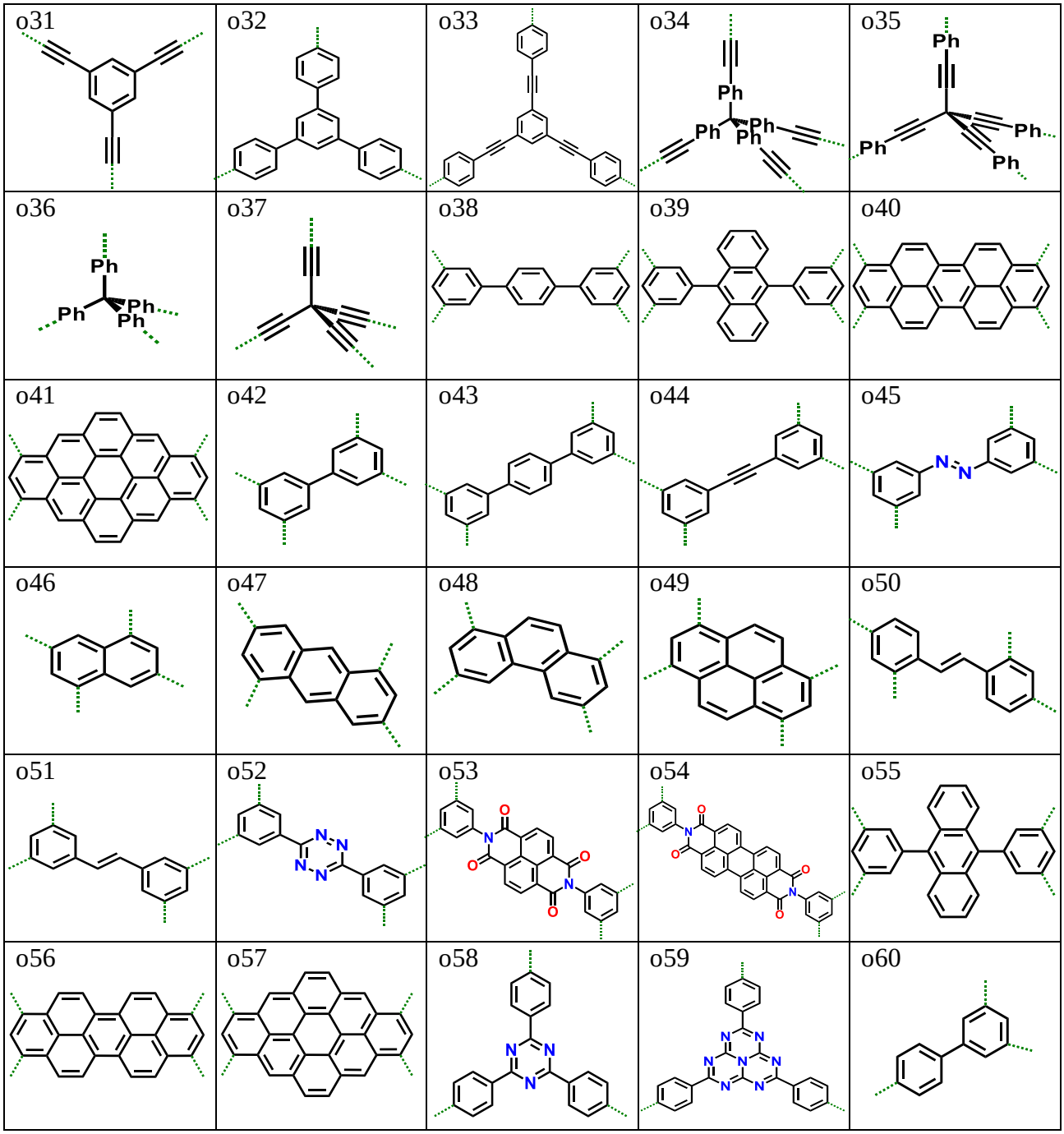

Figure 3-4. Organic SBUs used for structure generation (**o31** to **o60**).

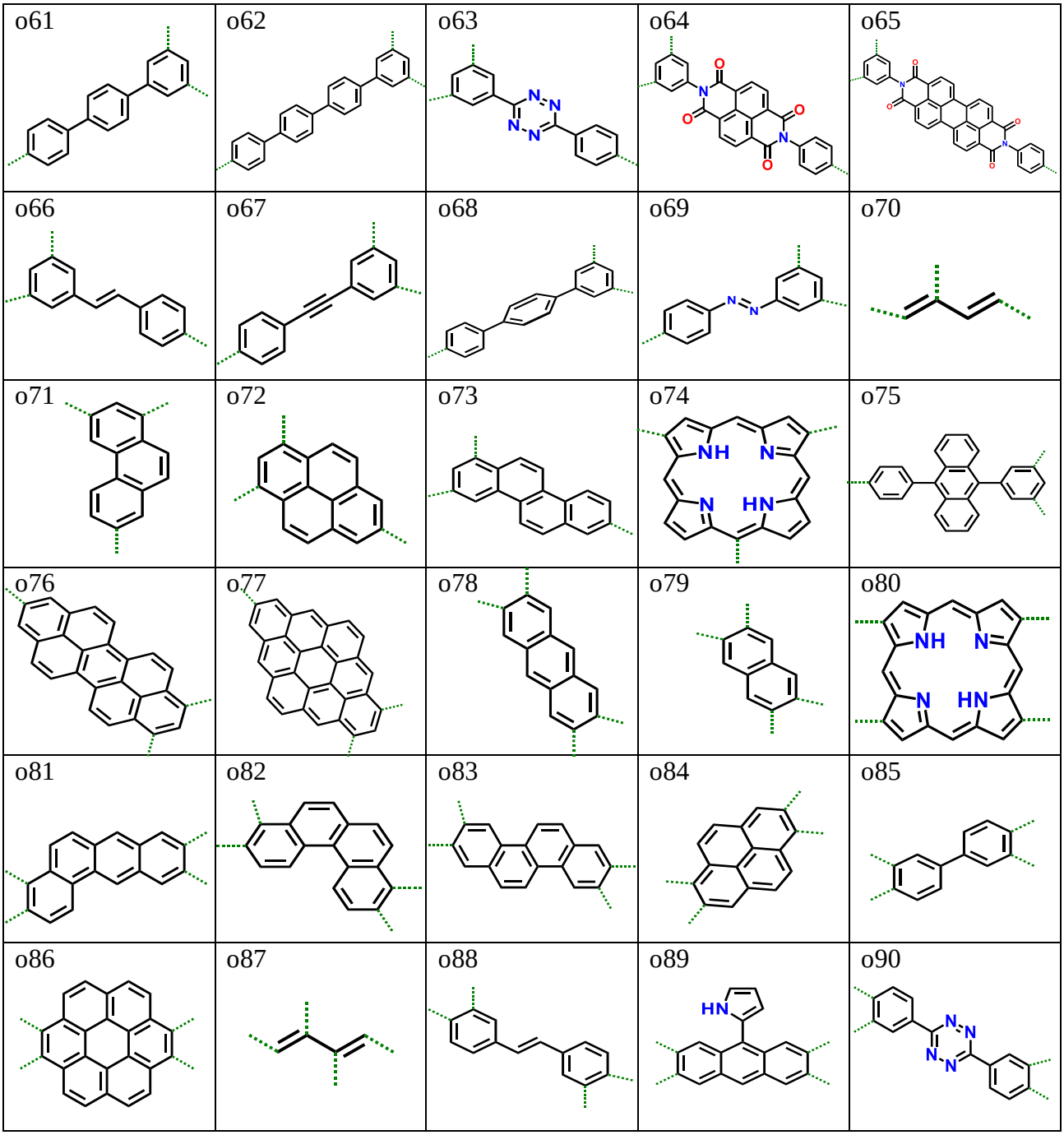

Figure 3-5. Organic SBUs used for structure generation (**o61** to **o90**).

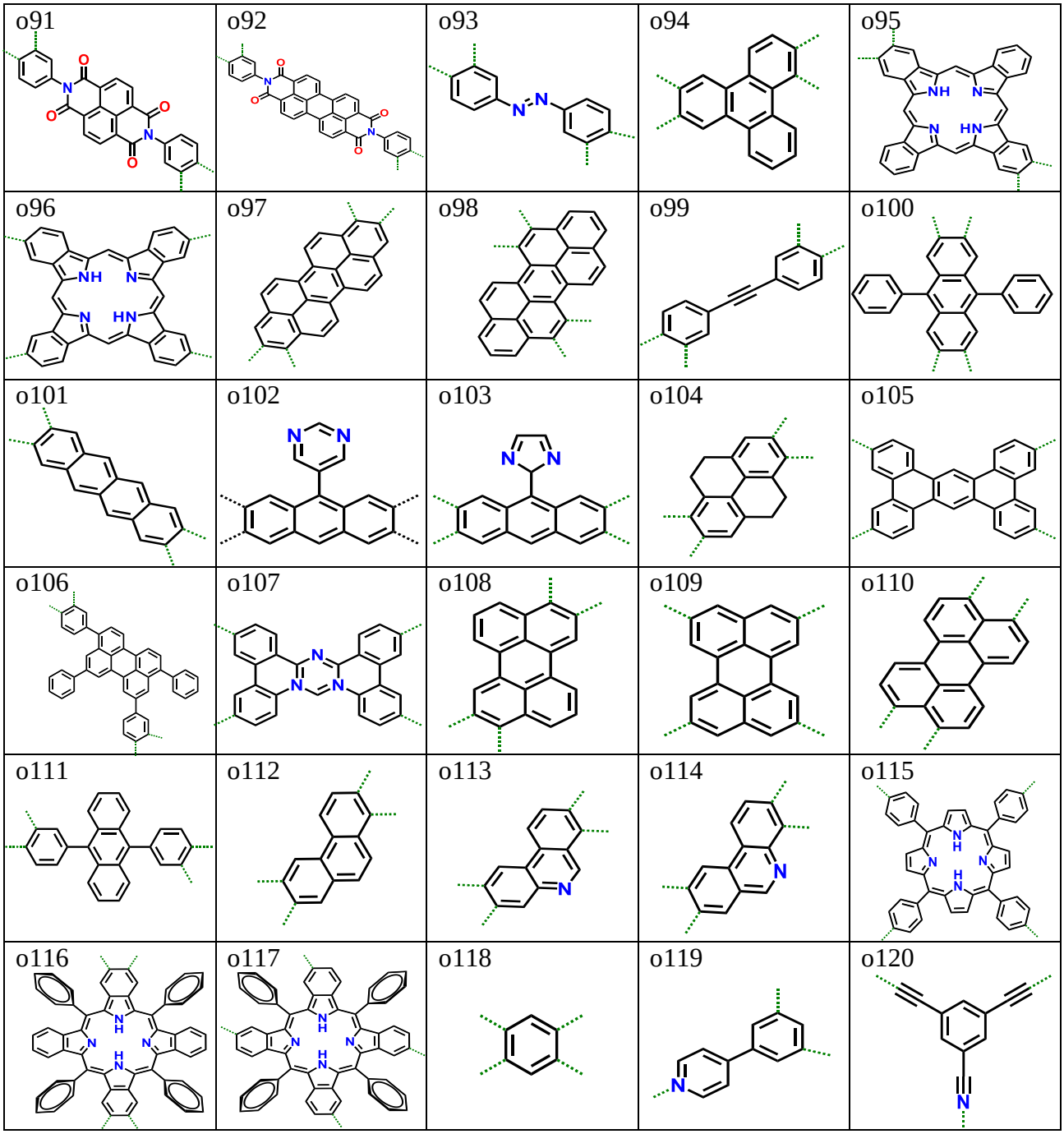

Figure 3-6. Organic SBUs used for structure generation (**o91** to **o120**).

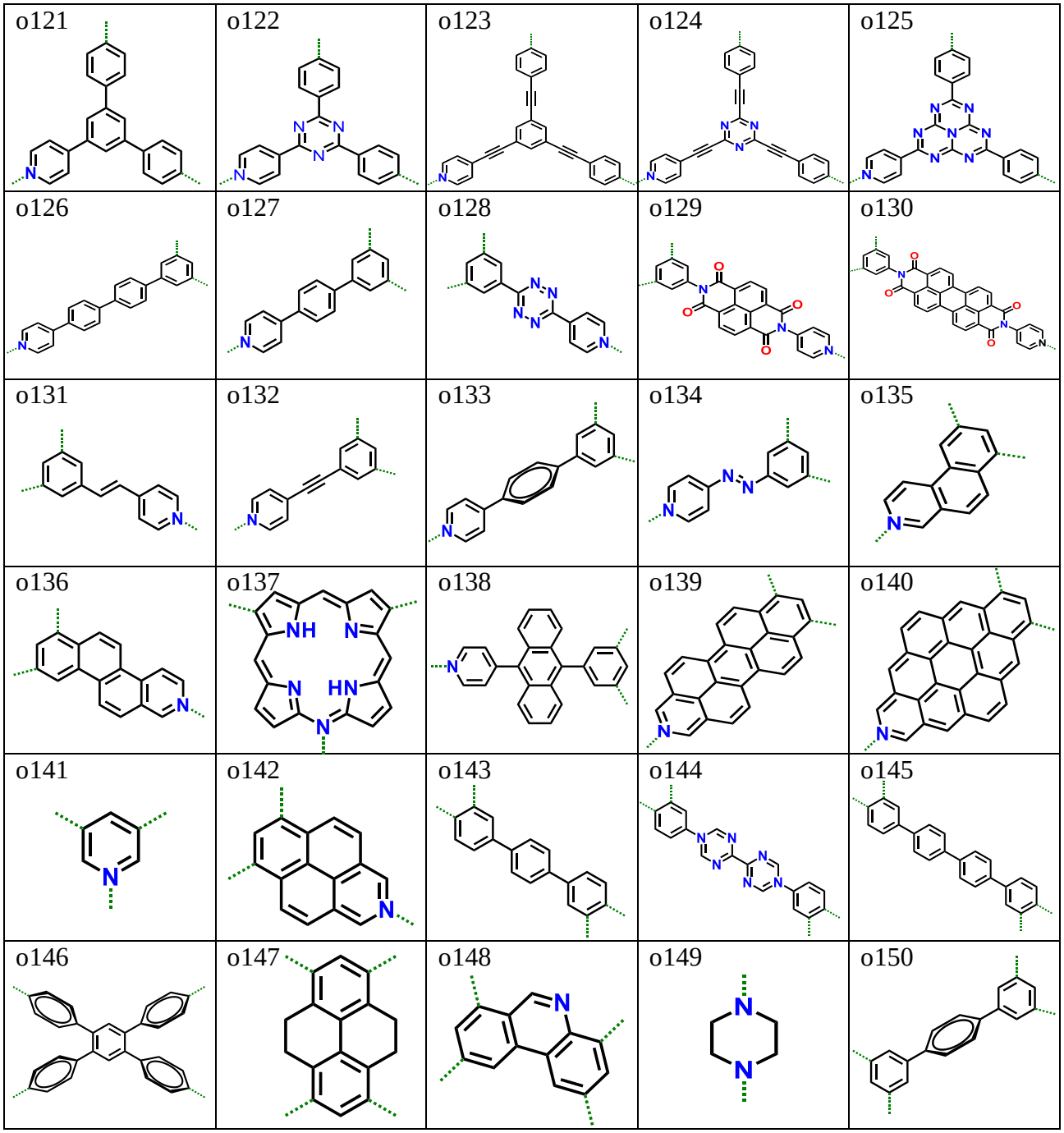

Figure 3-7. Organic SBUs used for structure generation (**o121** to **o150**).

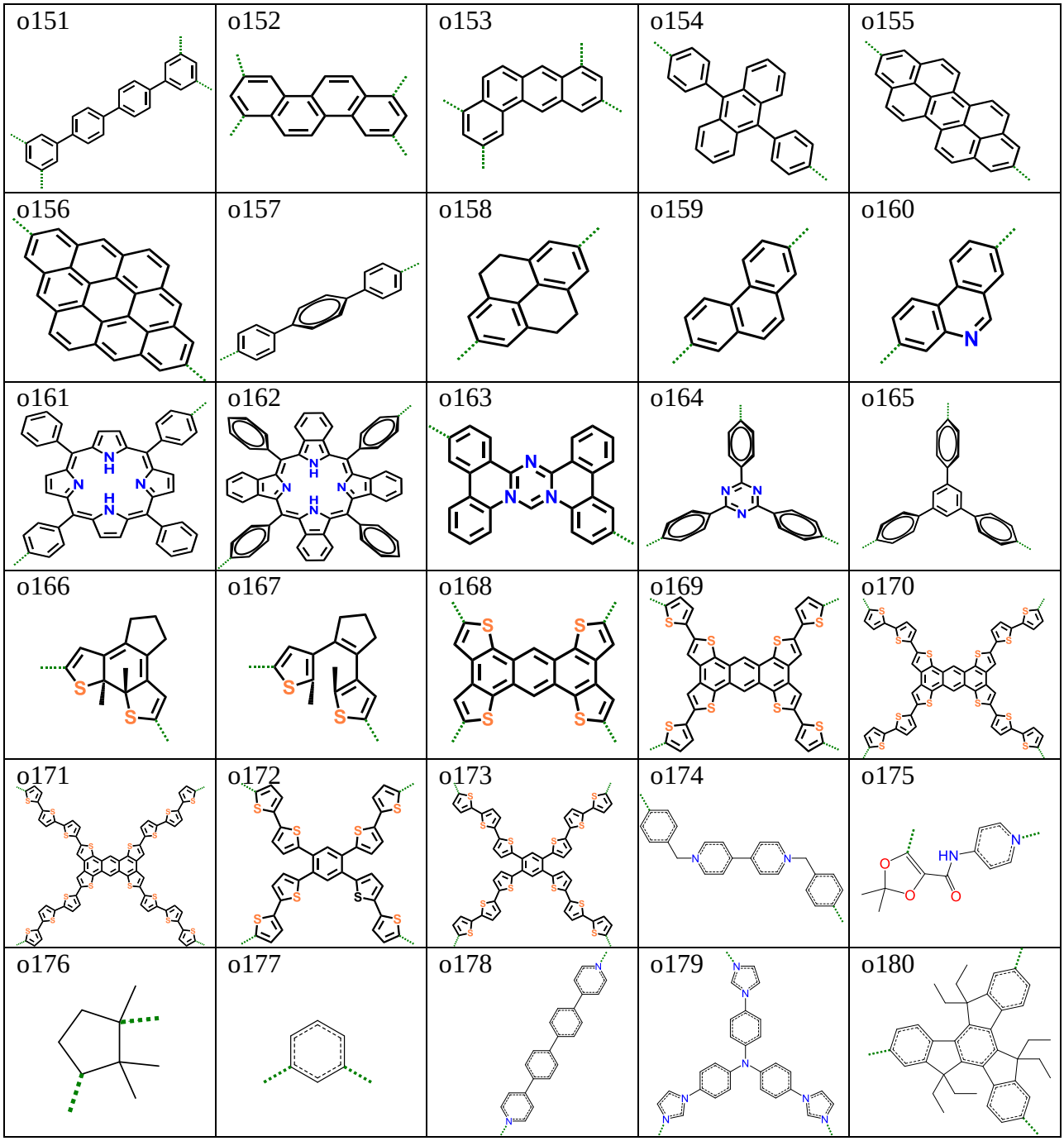

Figure 3-8. Organic SBUs used for structure generation (**o151** to **o180**).

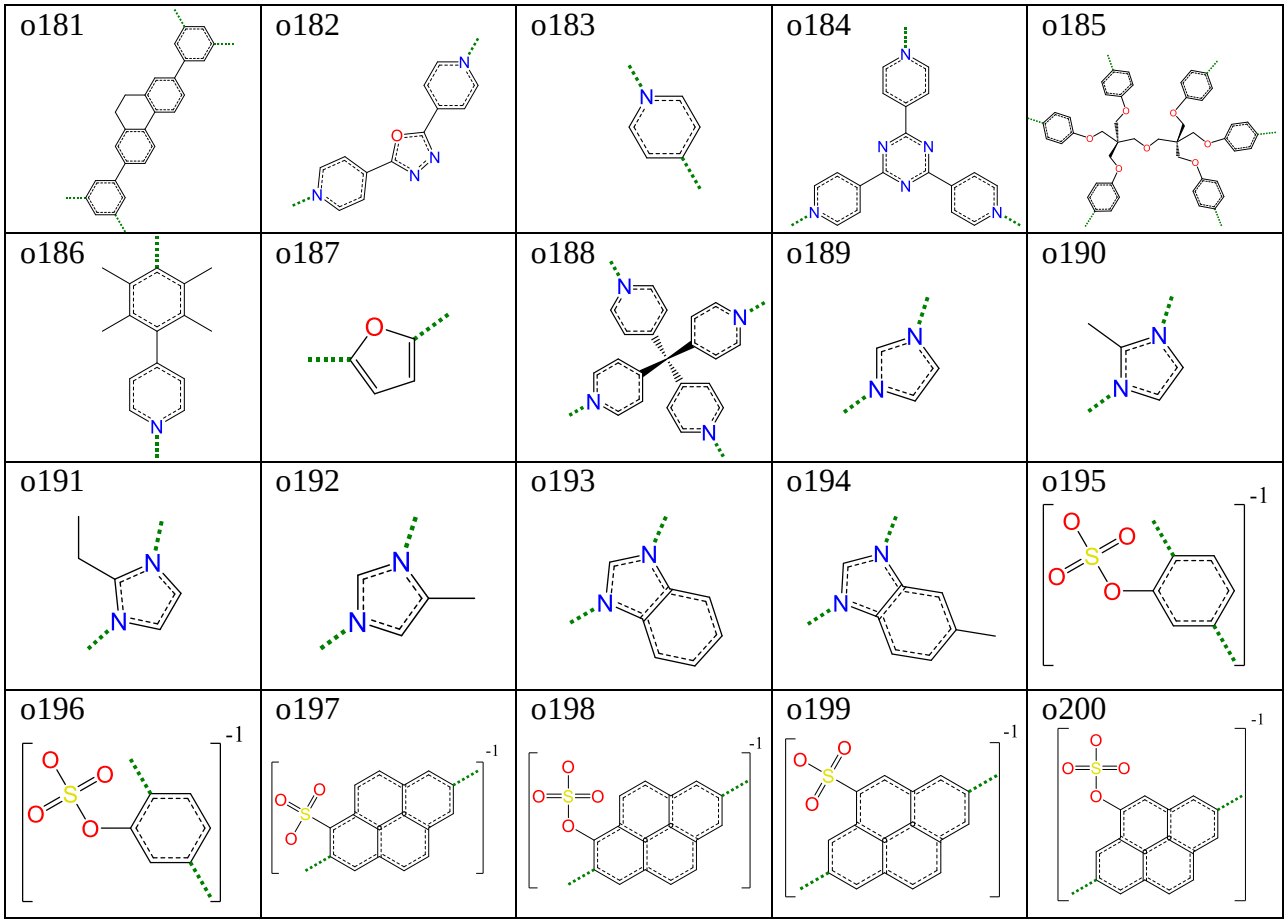

Figure 3-9. Organic SBUs used for structure generation (**o181** to **o200**).

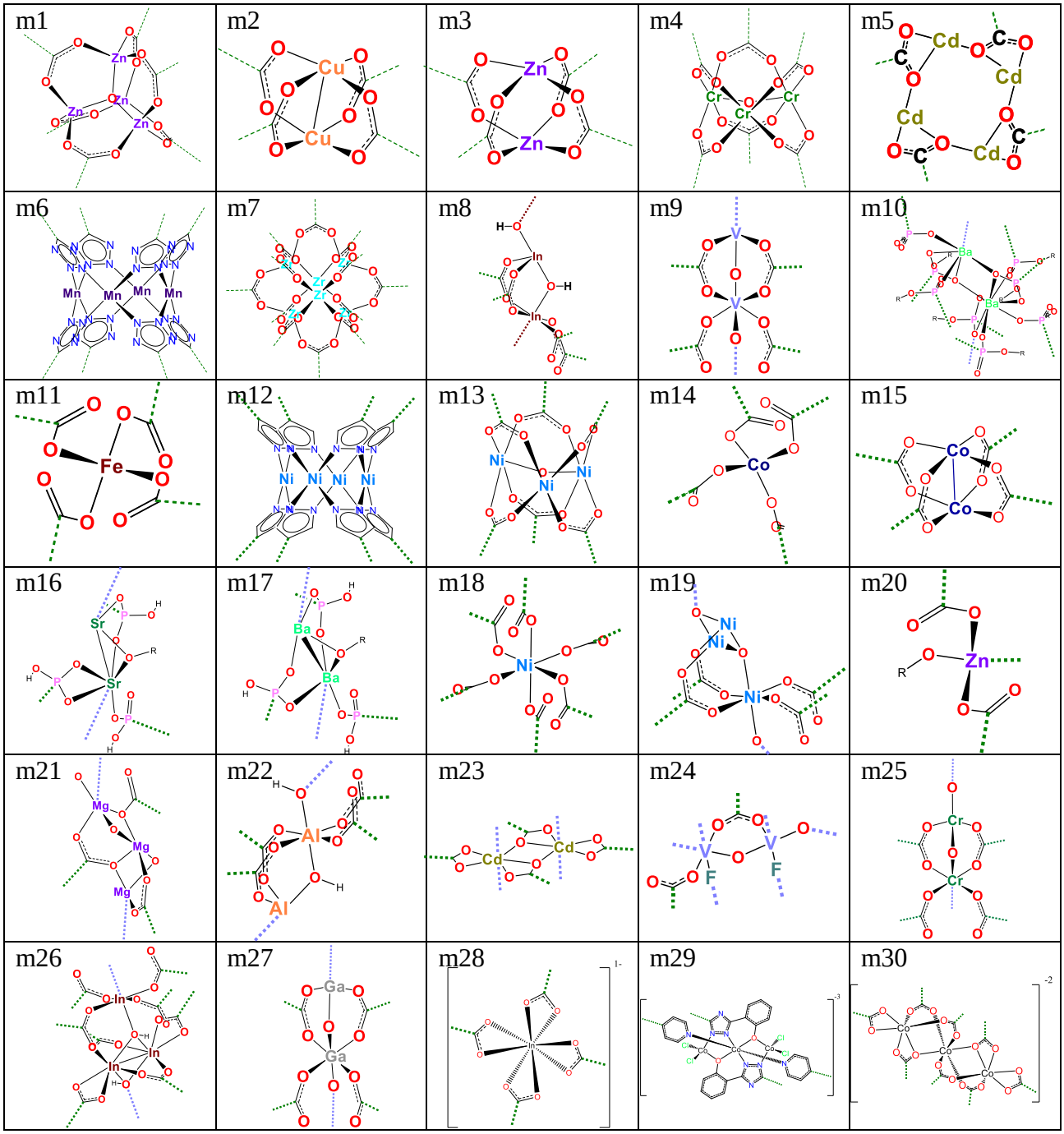

Figure 3-10. Inorganic SBUs used for structure generation (**m1** to **m30**).

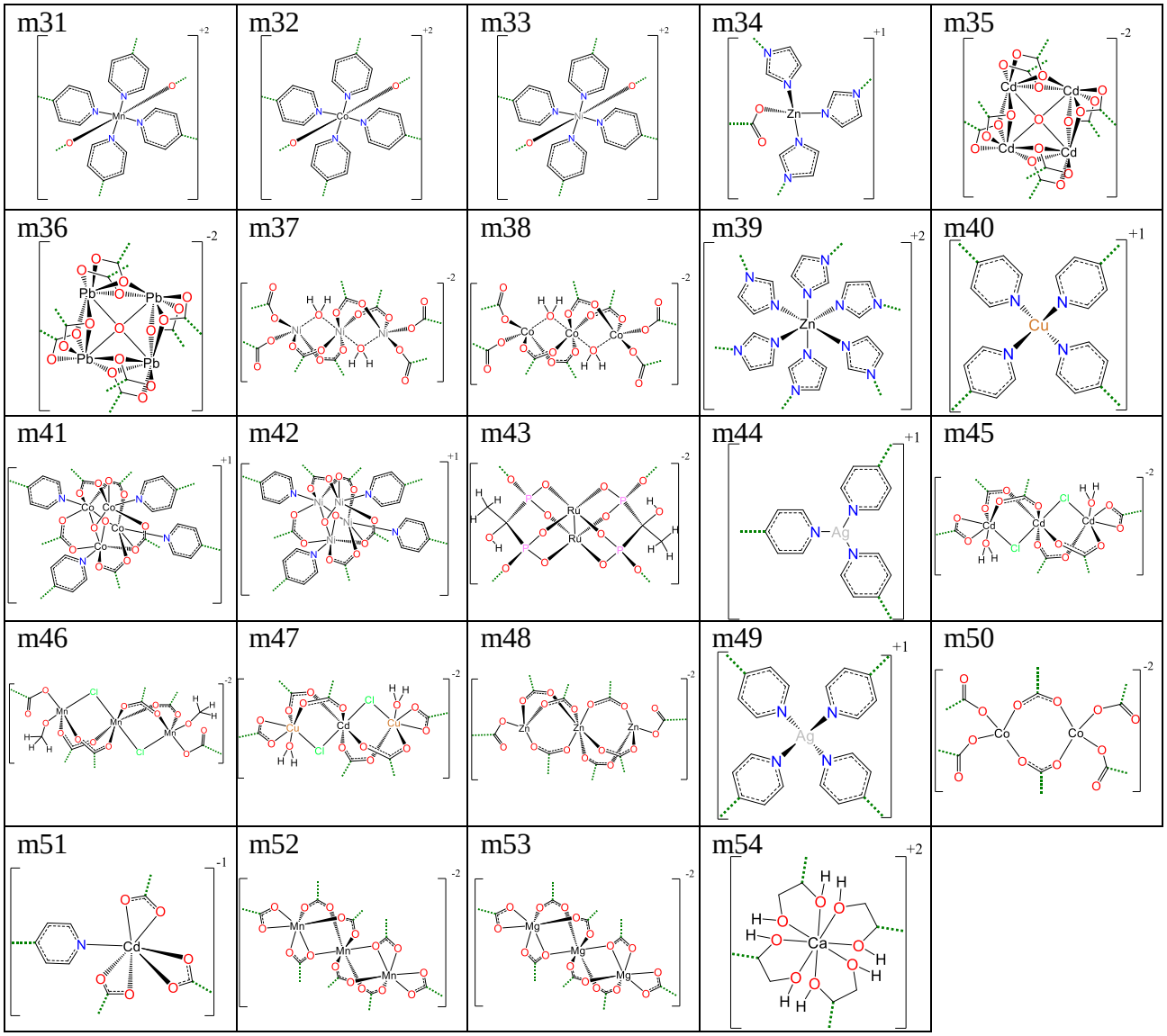

Figure 3-11. Inorganic SBUs used for structure generation (**m31** to **m54**).

3.3 Constructing Hypothetical Charged MOFs

The previously described SBUs were used to construct hypothetical charged MOFs. All of the SBUs shown above, including neutral, positively, and negatively charged SBUs, were used for structure generation. In addition, geometry optimization is employed to adjust unstable and unphysical structures constructed. Following the optimization, any neutral or unreasonable structures were excluded from this database. The details of structure generation and database constructions are described in the following subsections.

3.3.1 Generating MOFs Using TOBASCCO

TOBASCCO[2] is a program developed by members of the Woo Lab to construct MOFs using similar approach as the method by Martin and Haranczyk[20]. This method matches the SBUs to the underlying network topology to form periodic structures. As TOBASCCO was originally intended for generating neutral structures, modifications were necessary to generate charged structures.

First, the underlying network topologies[12] and combinations of organic and inorganic SBUs were chosen for the construction. Due to the infinite combinations, the types of organic SBUs were limited to 2 per structure and 1 inorganic SBU per structure. Then, according to the connectivity specified in the SBUs, they were connected to each other in attempts to reproduce the topology. While creating structures with SBUs carrying net charges, TOBASCCO was modified to account for the charges on individual SBU used. When a structure was successfully generated, the charges on the SBUs were summed up and recorded as the net charge on the

framework. The generated structures were described in a 'unit cell,' in which would be the minimum amount of atoms required to define the periodic structure.

The generated structures were labelled according to the SBUs incorporated within the MOF and its topology: str_m[**i**]_o[**j**](_o[**k**])_[**l**]. The indices of SBUs used were **i** for the inorganic SBU, **j** and **k** for the organic SBUs. If only 1 organic SBU was involved, the **k** term in the round brackets would not be included. Finally, **l** indicated the type of network topology for the MOF. As shown in Figure 3-13, the MOF **str_m31_o145_o141_fsg** with a FSG topology was generated with SBUs **m31**, **o145**, and **o141**.

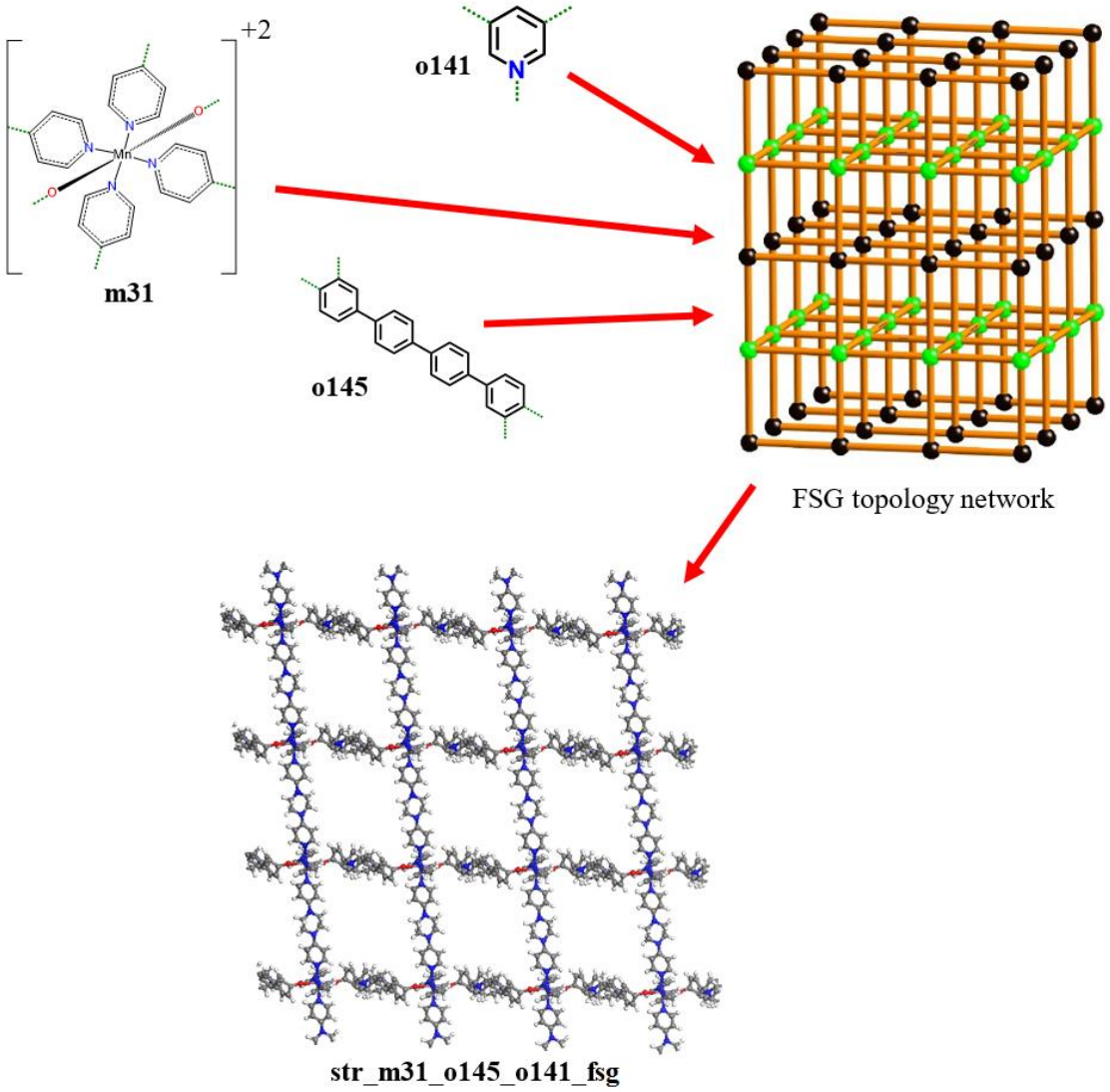

Figure 3-12. The construction of MOF **str_m31_o145_o141_fsg**.

To limit computational cost and the generation of an unlimited number of structures, the 'edge count' was another factor used in structure generating. The edge count specified the total number of SBUs allowed to be used in each structure; in this case, a maximum of 100 SBUs were used in each hypothetical MOF generation.

3.3.2 Selecting and Optimizing Hypothetical Charged MOFs Structures

Since the purpose of this study was to determine the effect of charges on MOFs, only charged MOFs were incorporated into the database. If a MOF generated was charge neutral, it was discarded.

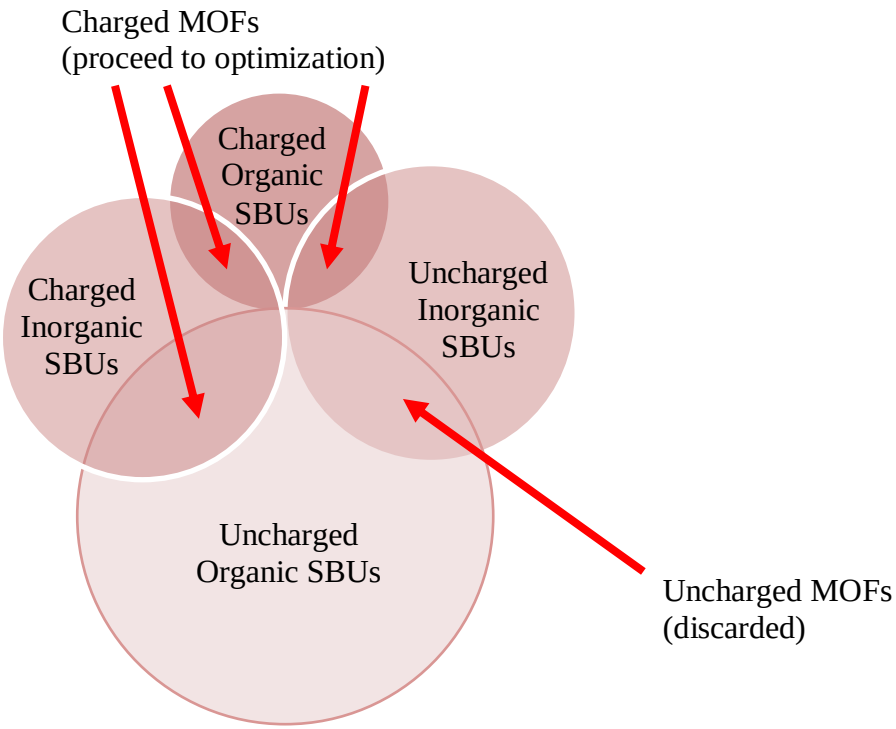

Figure 3-13. The SBUs used to construct the hypothetical MOFs could be charge positive, negatively, or neutral. Neutral MOFs generated were removed.

After the neutral MOFs were discarded, the geometries of the remaining hypothetical MOFs were optimized with the GROMACS package[3]. During optimization, universal force field (UFF) parameters[4] were assigned to the structures, molecular dynamics were performed, and all forces within the cells were minimized. To ensure the quality of the MOFs generated, the optimized structures were checked for unphysical features such as atom overlaps, abnormal bond

lengths or angles, as well as high maximum forces anywhere within the structure (6.5 kJ/mol/nm). If any of the aforementioned defects were found, the structure was discarded. As a result, only charged MOFs with reasonable structures were to enter the database. From the excess of 183,000 MOFs generated, over 47,000 MOFs were included in the database.

3.4 Validation of the Structure Generation Method

TOBASCCO has already been proven its ability, by members in the Woo Lab, to generate neutral MOF by successfully reproducing MIL-101. To validate TOBASCCO's ability in constructing charged hypothetical MOFs, a charged experimental structure was reproduced. A novel porous chiral In-MOF was first synthesized by Wang *et al.* in 2011[5], containing a -4 charge with SBUs **m28** and **o176** in a diamond topology. To reproduce the In-MOF, **str_m28_o176_dia** was generated with TOBASCCO and optimized with GROMACS[3]. The properties of the generated structure were evaluated with methods discussed in Chapter 2 and were compared with the experimental values.

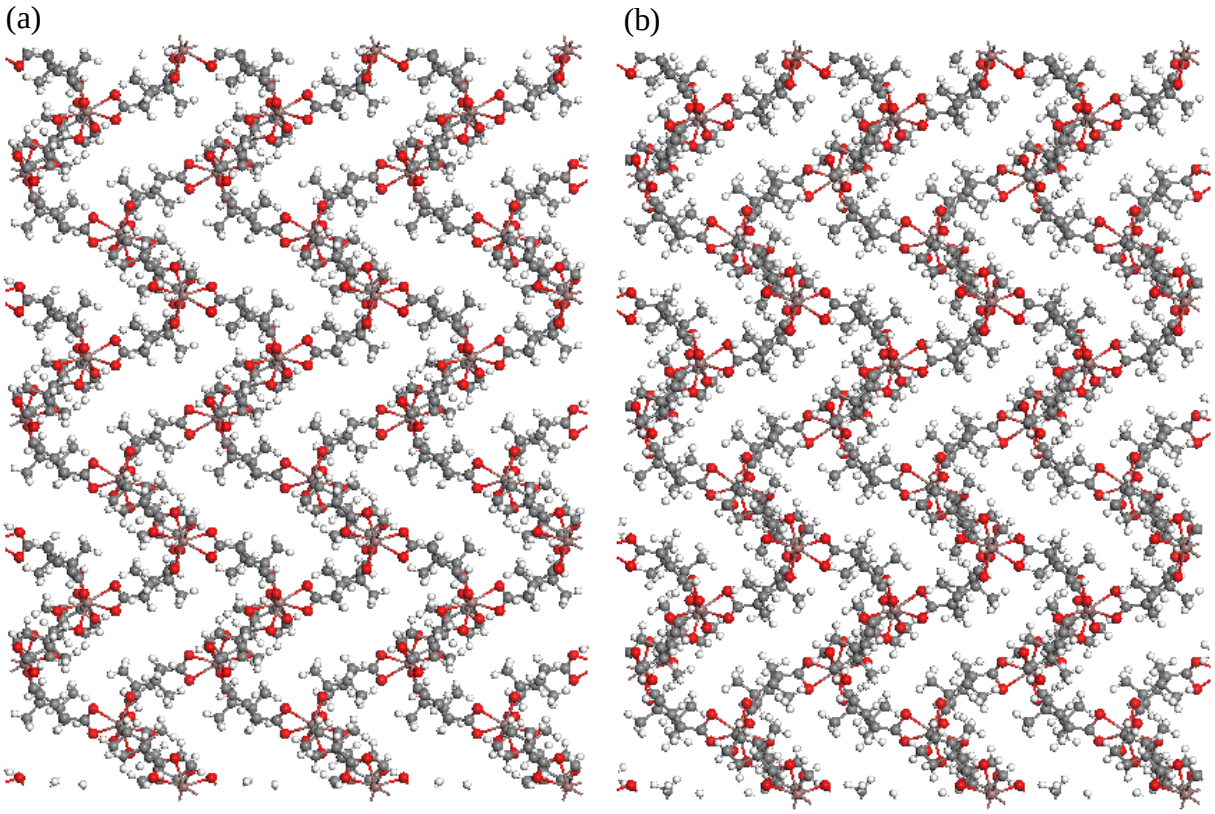

Figure 3-14. (a) MOF crystal structure obtained from the Cambridge Crystallographic Data Centre (CCDC)[5]. (b) MOF structure generated with TOBASCCO and optimized with GROMACS.

As shown in Figure 3-14, the pores and features of the two structures have no distinguishable differences upon visual inspection. The properties such as the cell dimensions, pore diameter, volume, and surface area, were calculated for the TOBASCCO structure. The pore volume and surface areas were calculated with a probe size of 1.82 Å. Listed in Table 3-1 are the calculated properties and the experimentally reported ones.

Table 3-1. Property comparisons between experimentally reported values by Wang *et al.*[5] and structure recreated by TOBASCCO.

Properties	Experimental Values	TOBASCCO Structure
Cell dimensions	a = 13.8954 Å b = 13.8954 Å c = 17.7870 Å	a = 13.9587 Å b = 13.9587 Å c = 17.7311 Å
Cell volume	3,434.4 $Å^3$	3,454.8 $Å^3$
Pore diameter	6.9 Å	7.06 Å
Pore volume	0.132 cm^3/g	0.178 cm^3/g
Surface area	607 m^2/g	780 m^2/g

As shown above in Table 3-1, the cell dimensions and pore diameter are in excellent agreement considering the computational structure and cell were optimized with a force field based method. The surface area and void volume of the recreated MOF differ slightly due to the sampling methods: the experimental setup cannot guarantee a complete evacuation of the MOF and the simulation does not discriminate whether a void space is accessible through the pores. The most definitive comparison was perhaps the differences in atomic positions between the two structures. The root-mean-square error of the fractional coordinates was calculated to be 0.323 Å and the maximum deviation was 0.702 Å. Considering the cell dimensions of 13.8954 Å x 13.8954 Å x 17.7870 Å, the 171 atomic positions in each of the two structures were nearly identical. In addition, the powder x-ray diffraction patterns between the two structures were generated using the "Reflex" module in Material Studio 6.0. Once again, the results from both structures were close to each other as shown in Figure 3-15.

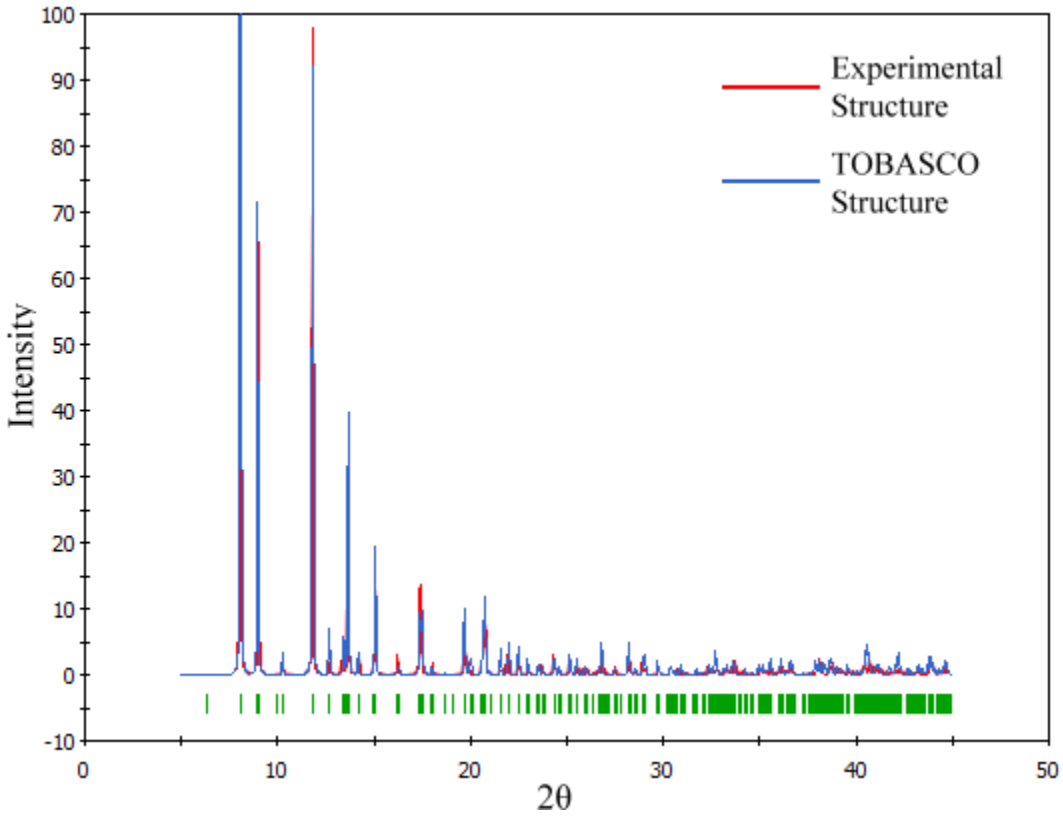

Figure 3-15. Simulated XRD patterns obtained from both the CCDC crystal structure and from the TOBASCCO generated and optimized structure.

The comparison between the generated and experimental charged MOFs shows that TOBASCCO can generate charged structures similar to the experimental structures. As **str_m28_o176_dia** was effectively the same as its experimental counterpart, it confirmed the validity of future hypothetical charged MOFs generated by TOBASCCO.

3.5 Database Contents

With all of the parameterized SBUs shown in Chapter 3.2, 47,244 unique structures were generated, resulting in a database of diverse charged hypothetical MOFs. This database contains 15,213 positively charged MOFs and 32,031 with negative charges, reflecting the ratio of positively and negatively charged SBUs used. The variety of properties not only includes the differences in structure and topology, but also the charge concentration, pore size, volume, and surface area.

The structures in the database encompass 1,050 topologies where the database made by Wilmer *et al.*[9,10] only included 6 topologies. The charges and volumes in the unit cell of each structure span a wide range of between -100e to +50e, and up to 1,022,823 $Å^3$, respectively. Due to the differences in cell volumes, the concentrations of charges are normalized to 10,000 $Å^3$ for easy comparisons. Figure 3-16 show the distribution of charge per volume for this work as well as the CoRE database by Chung *et al.*[1], the distribution data were normalized to the total number of MOFs in each database. The MOFs' charge per volume from this work has a fairly even spread as shown in Figure 3-16, whereas the majority of the MOFs in the Chung *et al.* database have low or no net charge. The databases by Wilmer *et al.*[9] was not shown in this figure since the MOFs in their database have no net charge on the framework.

The MOFs in the database from this work have charges per volume ranging from -56.75 to +20.44 e/10,000 $Å^3$. To put the charges into perspective, faujasite zeolites can have charge concentrations range from 0 to -60 e/10,000 $Å^3$ depending on their silica and alumina ratio; Zeolite 13X has a charge concentration of -53.75 e/10,000 $Å^3$ resulted from its 1.24 Si/Al ratio[21].

As zeolites consist of only aluminum and silicon oxides, this structural limitation results in only negatively charged frameworks whereas this MOF database has both[22].

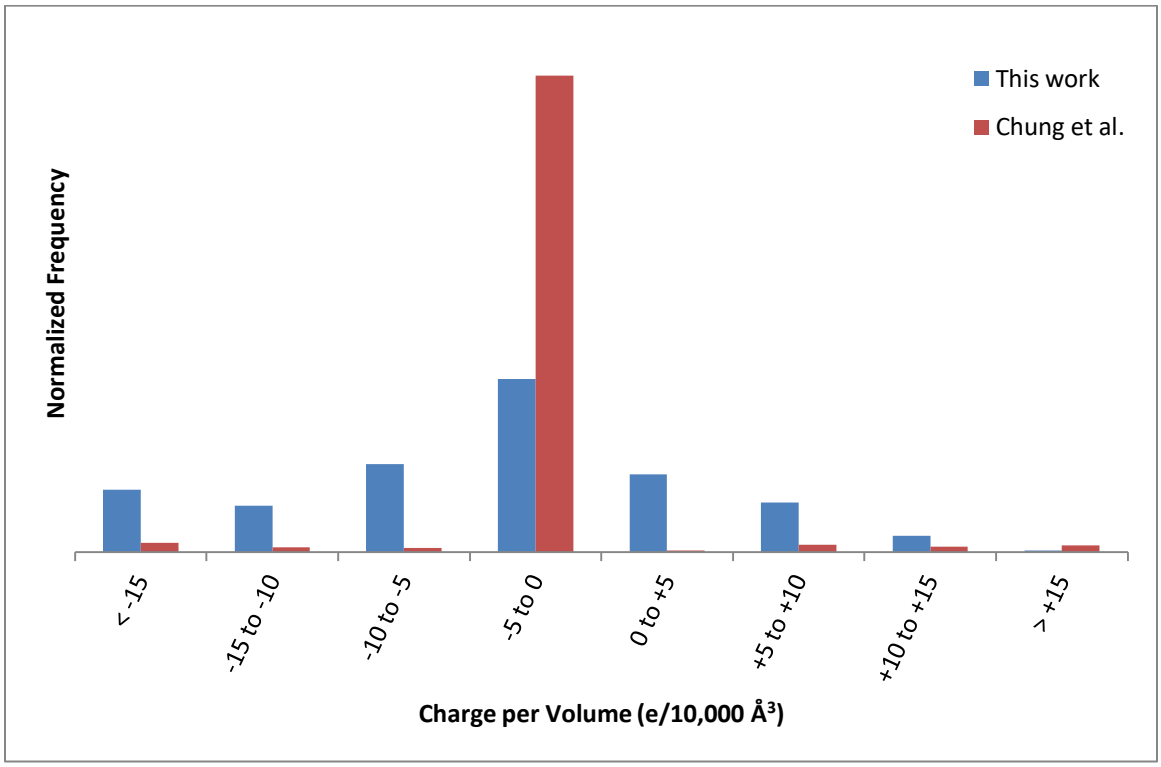

Figure 3-16. Normalized distribution of charge per volumes in charged MOFs databases.

In Figure 3-17, the normalized distribution of pore sizes are shown for the database built in this work as well as the existing databases. The pore sizes taken are the largest continuous channel where the sphere of a given diameter can fit through. The MOF with the largest continuous channel in this work has a diameter of 133.42 Å. The MOFs in this database have up to 3 channels when measured with a probe size of 1.82 Å, the radii of N_2 probes[23]. When comparing to the other two databases, the new database has a much wider distribution in pore

sizes. The pore size distributions for the new database are quite even up to 25 Å whereas very few MOFs in the other databases have pores larger than 15 Å.

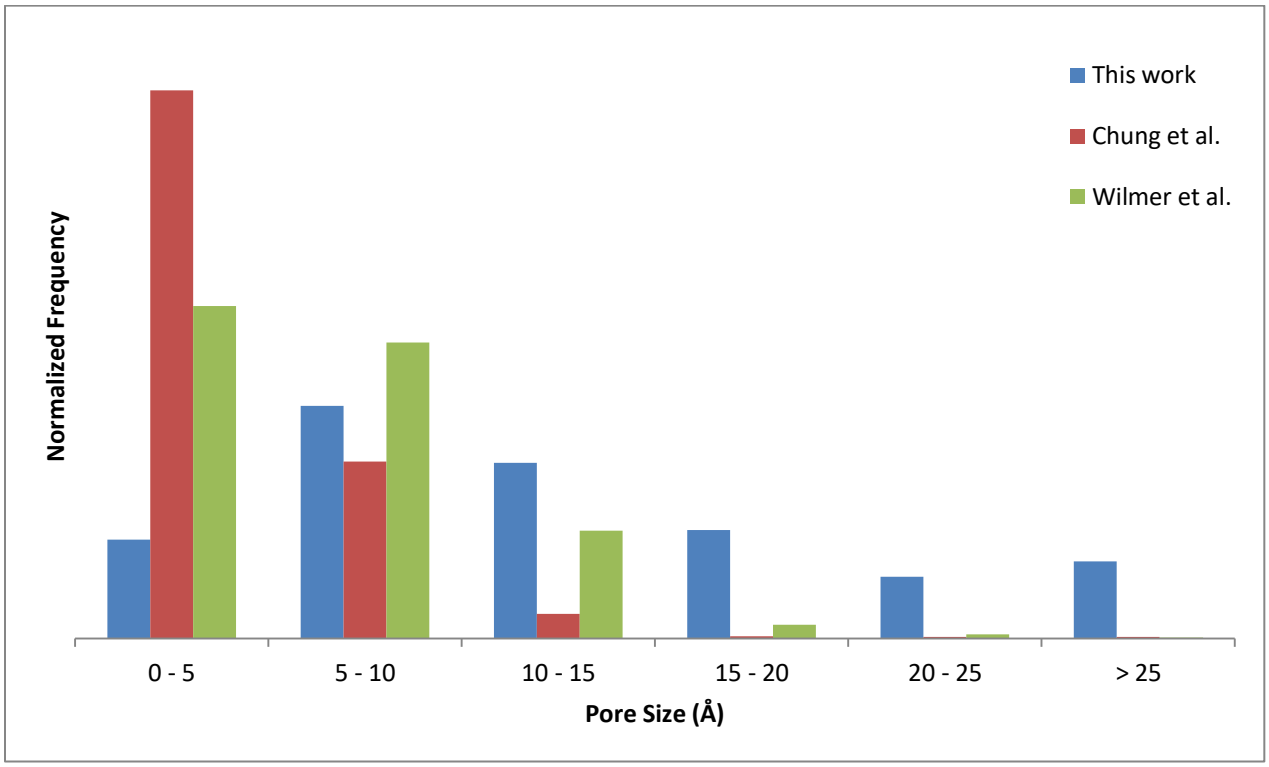

Figure 3-17. Normalized distribution of pore sizes of maximum continuous channel in MOF databases.

Figure 3-18 summarizes the normalized spread of void volumes measured with 1.82 Å probes, where the maximum volume is 33.31 cm^3/g. Yet again, the MOFs in the new database has a much wider range in void volume, which has a fairly even distribution up to 5 cm^3/g. Most MOFs in the CoRE database by Chung *et al.*[1] have void volumes below 1.0 cm^3/g and the MOFs in the Wilmer *et al.*[9] database have void volumes below 2.5 cm^3/g.

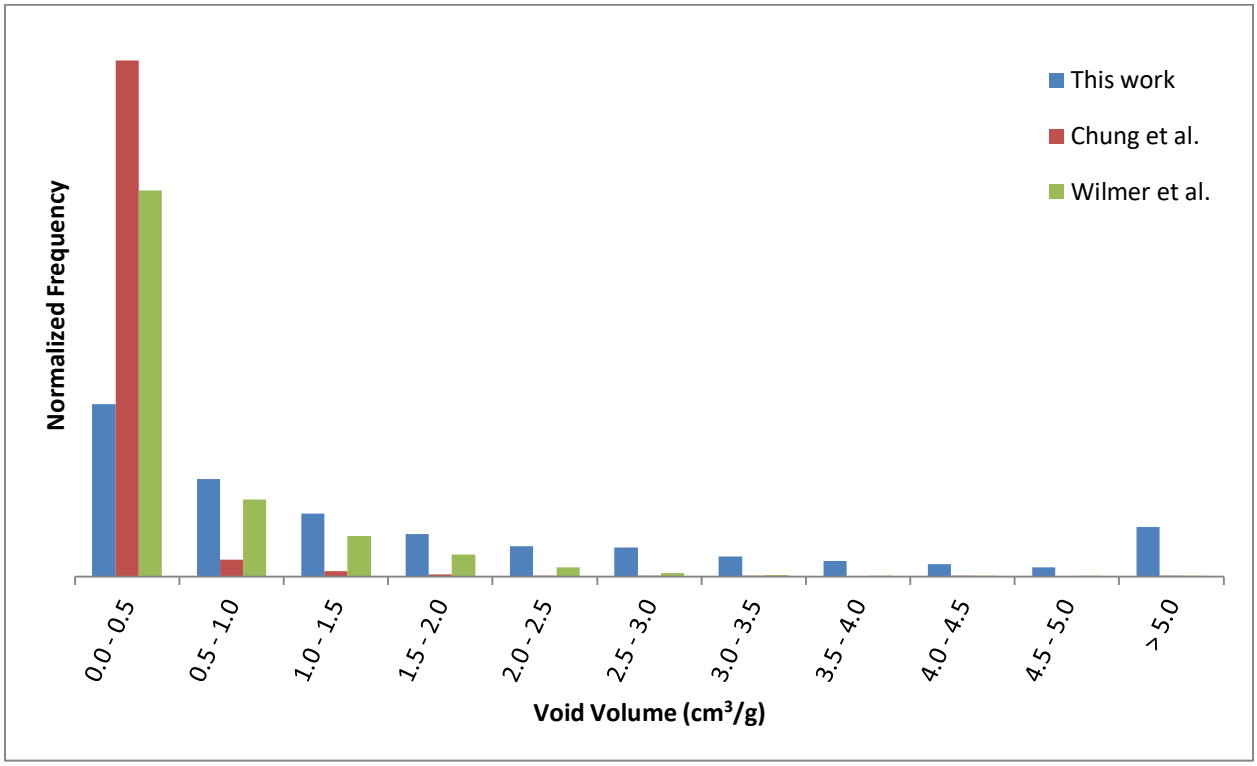

Figure 3-18. Normalized distribution of void volumes (probe size 1.82 Å) in MOF databases.

When comparing the range of gravimetric surface areas, Figure 3-19 shows a wide range of up to 9,756.24 m^2/g for this work. Once again, the range of surface areas from MOFs in this work span further than the other two. The databases by Chung *et al.*[1] and Wilmer *et al.*[9] include few MOFs above the surface area of above 6,000 m^2/g. The surface areas were also measured with a probe size of 1.82 Å. Another comparison can be made with these metrics to Yaghi and co-worker's MOF-5, which is known for its large void volume and high surface area[24]. The pore diameter of MOF-5 is 8.0 Å, its void volume is 1.04 cm^3/g and surface area is 2,900 m^2/g[24].

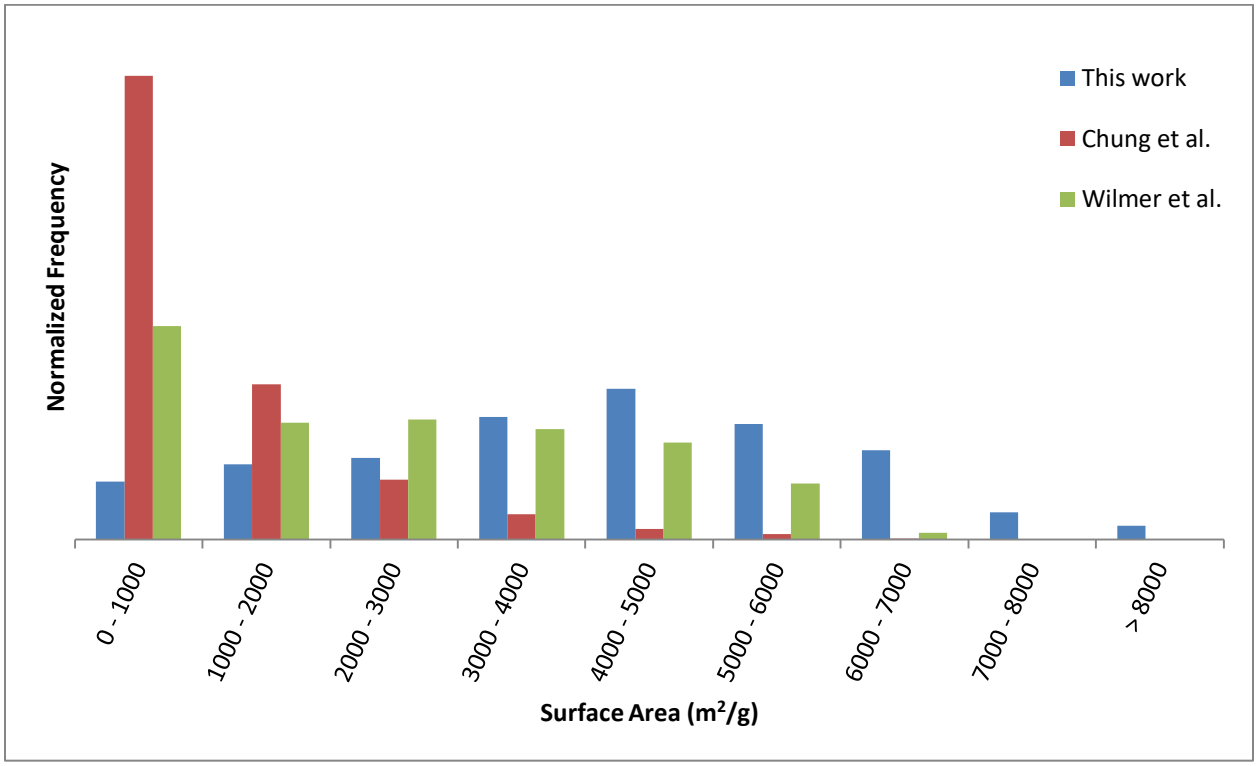

Figure 3-19. Normalized distribution of gravimetric surface areas (probe size 1.8 Å) in MOF databases.

As seen comparing with databases by Wilmer *et al.*[9] as well as Chung *et al.*[1], the database from this work has MOFs with a very wide range of pore and surface properties. In addition, these MOFs have a much higher range of net charges on their frameworks.

3.6 Summary

Using 254 SBUs obtained from existing MOFs, in excess of 183,000 hypothetical structures were generated. The geometries of these MOFs were optimized and over 47,000 of the reasonable structures with charges were selected for this database. More than 1,000 network topologies were used in the construction of the 47,000 MOFs in the database, much higher than other existing MOF databases[9–11]. In addition, the charged MOFs database also includes a

diverse range in a multitude of structural properties such as charges, pores, and surface areas. It is important to note that these charged frameworks generated were unfunctionalized. With the addition of 259 functional groups currently studied in the Woo Lab, it is estimated that well over a billion structures can potentially be generated from these frameworks[10].

TOBASCCO[2], the method of charged structure generation was adapted and validated by constructing a charged In-MOF synthesized experimentally[5]. It was found that the generated structure matches closely to the reported experimental crystal structure. Various structural properties such as atom positions, optimized cell dimensions, pores, and surface areas were in excellent agreement. The successful construction of the experimental In-MOF validated the method of structure generation. As valid structures, the hypothetical charged MOFs in the new database were evaluated for their performances in CCS which is discussed in the following chapter.

3.7 References

1. Chung, Y. G., Camp, J., Haranczyk, M., Sikora, B., Bury, W., Krungleviciute, V., Yildirim, T., Farha, O., Sholl, D., and Snurr, R. Computation-ready, Experimental Metal-organic Frameworks: A tool to Enable High-throughput Screening of Nanoporous Crystals. *Chem. Mater.* **26,** 6185–6192 (2014).

2. Boyd, P. G. and Woo, T. K. A Generalized Method for Constructing Hypothetical Nanoporous Materials of any net Topology from Graph Theory. *CrystEngComm* **18,** 3777–3792 (2016).

3. Hess, B., Kutzner, C., Van Der Spoel, D., and Lindahl, E. GRGMACS 4: Algorithms for Highly Efficient, Load-balanced, and Scalable Molecular Simulation. *J. Chem. Theory Comput.* **4,** 435–447 (2008).

4. Rappe, A. K., Casewit, C. J., Colwell, K. S., Goddard III, W. A., and Skiff, W. M. UFF, a full Periodic Table Force Field for Molecular Mechanics and Molecular Dynamics Simulations. *J. Am. Chem. Soc.* **114,** 10024–10035 (1992).

5. Wang, L., Song, T., Huang, L., Xu, J., Li, C., Ji, C., Shan, L., and Wang, L. A Porous Chiral In-MOF with Anionic-type Diamond Network: Synthesis, Structure and Nitrogen gas Adsorption. *CrystEngComm* **13,** 4005 (2011).

6. Furukawa, H., Cordova, K. E., O'Keeffe, M., and Yaghi, O. M. The Chemistry and Applications of Metal-organic Frameworks. *Science* **341,** 1230444 (2013).

7. Sumida, K., Rogow, D., Mason, J., McDonald, T., Bloch, E., Herm, Z., Bae, T., and Long J. Carbon Dioxide Capture in Metal-Organic Frameworks. *Chem. Rev. (Washington, DC, United States)* **112,** 724–781 (2012).

8. Zhou, H.-C., Long, J. R., and Yaghi, O. M. Introduction to Metal-organic Frameworks. *Chem. Rev.* **112,** 673–4 (2012).

9. Wilmer, C. E., Farha, O. K., Bae, Y.-S., Hupp, J. T., and Snurr, R. Q. Structure–property Relationships of Porous Materials for Carbon Dioxide Separation and Capture. *Energy Environ. Sci.* **5,** 9849 (2012).

10. Wilmer, C. E., Leaf, M., Lee, C. Y., Farha, O. K., Hauser, B. G., and Hupp, J. T. Large-

scale Screening of Hypothetical Metal-organic Frameworks. *Nat. Chem.* **4,** 83–9 (2012).

11. Martin, R. L., Simon, C. M., Smit, B., and Haranczyk, M. In Silico Design of Porous Polymer Networks: High-throughput Screening for Methane Storage Materials. *J. Am. Chem. Soc.* **136,** 5006–22 (2014).

12. O'Keeffe, M., Peskov, M. A., Ramsden, S. J., and Yaghi, O. M. The Reticular Chemistry Structure Resource (RCSR) database of, and symbols for, crystal nets. *Acc. Chem. Res.* **41,** 1782–9 (2008).

13. Allen, F. H. The Cambridge Structural Database: a Quarter of a Million Crystal Structures and Rising. *Acta Crystallogr. Sect. B Struct. Sci.* **58,** 380–388 (2002).

14. Mavrandonakis, A., Klontzas, E., Tylianakis, E., and Froudakis, G. E. Enhancement of Hydrogen Adsorption in Metal-organic Frameworks by the Incorporation of the Sulfonate Group and Li Cations. A Multiscale Computational Study. *J. Am. Chem. Soc.* **131,** 13410–4 (2009).

15. Goesten, M. G., Juan-Alcañiz, J., Ramos-Fernandez, E., Sai Sankar Gupta, K., Stavitski, E., van Bekkum, H., Gascon, J., and Kapteijn, F. Sulfation of Metal-organic Frameworks: Opportunities for acid Catalysis and Proton Conductivity. *J. Catal.* **281,** 177–187 (2011).

16. Seo, J., Whang, D., Lee, H., Jun, S. I., Oh, J., and Jeon, Y. J. A Homochiral Metal-organic Porous Material for Enantioselective Separation and Catalysis. *Nature* **404,** 982–6 (2000).

17. Huh, S., Kwon, T.-H., Park, N., Kim, S.-J., and Kim, Y. Nanoporous In-MOF with Multiple One-dimensional Pores. *Chem. Commun. (Camb).* 4953–5 (2009). doi:10.1039/b905138d

18. Chen, W.-X., Zhuang, G.-L., Zhao, H.-X., Long, L.-S., Huang, R.-B., and Zheng, L.-S. Magnetic and Thermal Properties of Three Ionothermally Synthesized Metal-carboxylate Frameworks of [M3(ip)4][EMIm]2 (M = Co, Ni, Mn, H2ip = Isophthalic acid, EMIm = 1-ethyl-3-methyl Imidazolium). *Dalton Trans.* **40,** 10237–41 (2011).

19. Kadantsev, E. S., Boyd, P. G., Daff, T. D., and Woo, T. K. Fast and Accurate Electrostatics in Metal Organic Frameworks with a Robust Charge Equilibration Parameterization for High-Throughput Virtual Screening of Gas Adsorption. *J. Phys. Chem. Lett.* **4,** 3056–3061 (2013).

20. Martin, R. L. and Haranczyk, M. Insights into Multi-Objective Design of Metal–Organic Frameworks. *Cryst. Growth Des.* **13,** 4208–4212 (2013).

21. Joos, L., Swisher, J. A., and Smit, B. Molecular Simulation Study of the Competitive Adsorption of H2O and CO2 in Zeolite 13X. *Langmuir* **29,** 15936–15942 (2013).

22. Van Speybroeck, V., Hemelsoet, K., Joos, L., Waroquier, M., Bell, R., and Catlow, C. Advances in Theory and Their Application Within the Field of Zeolite Chemistry. *Chem. Soc. Rev.* (2015). doi:10.1039/c5cs00029g

23. Walton, K. S. and Snurr, R. Q. Applicability of the BET Method for Determining Surface Areas of Microporous Metal−Organic Frameworks. *J. Am. Chem. Soc.* **129,** 8552–8556 (2007).

24. Eddaoudi, M., Li, H., and Yaghi, O. M. Highly Porous and Stable Metal-organic Frameworks: Structure Design and Sorption Properties. *J. Am. Chem. Soc.* **122,** 1391–1397 (2000).

4 High Throughput Screening of Charged MOF Database

Abstract

To explore the viability of using charged MOFs as post-combustion CCS materials, gas adsorption simulations were performed on the hypothetical charged MOFs database with the screening methods developed. As there were a large number of charged MOFs in the database, it was impractical to perform the screening process on all 47,000 charged MOFs. A representative group of 500 MOFs was chosen for the high throughput screening. As a baseline comparison, 500 hypothetical neutral MOFs from previous studies were used[1]. Under the same simulation conditions, the charged MOFs outperformed the neutral group in CO_2 uptakes, working capacities, and CO_2/N_2 selectivities. It was found that charges on the counter ions strongly affected the uptakes of CO_2. Also, specific structural features which resulted in the highest selectivity were identified. In the representative group of 500 charged MOFs, two probable candidates for post-combustion CCS applications were found. By the same ratio, the charged MOFs database should have around 289 MOFs with similar or higher performance in such application. The discovery of high performing candidates in hypothetical charged MOFs proved that charged MOFs may be a viable material in post-combustion CCS applications.

4.1 Introduction

In the previous two chapters, a database of hypothetical charged MOFs and methods to simulate the gas adsorption properties were developed. By simulating the gas adsorption properties of the hypothetical charged MOFs, the viability of using charged MOFs in post-combustion CCS applications was tested. To mimic the intermolecular interaction in gas adsorption simulations, partial atomic charges for each individual structure were required[2]. As outlined in Chapter 2.2, the derivations of such charges require computationally costly periodic DFT calculations. Many studies use charges parameterized for specific systems in order to reduce the time and computational resources required[1,3–8]. However, generic charges are not capable of adequately represent the intermolecular interactions in charged MOFs. For example, the generic charges developed by Fischer and Bell in 2013[9] underestimate the interaction between the framework and guest molecules by close to 30% in many cases. They concluded that it is important to use system-specific charges to produce the most accurate representation of electrostatic interactions[9]. Also, shown in Chapter 2.6, QEq charges[10] failed to mimic the electrostatics of a charged MOF and therefore cannot be used for the rapid screening. To effectively obtain the properties of the hypothetical charged MOFs in the database, while limiting the computational cost, a representative group of MOFs can be chosen from the database.

In gas adsorption simulations, temperature and pressure conditions affect the adsorption and desorption of gasses and they can be optimized to obtain the highest working capacity[11]. During adsorption, high pressure and low temperature conditions are ideal for high gas uptake. The opposite is true for desorption; low pressure and high temperature conditions allow the adsorbed gas to be driven from the sorbent[11,12]. One would instinctively use the most extreme

temperatures and pressures for the highest working capacity in post-combustion CCS processes. However, temperature and pressure changes made to flue gas would also require the input of energy; consequently, the process conditions of post-combustion CCS would also need to be optimized for the lowest energy requirement and cost[13].

In this work, gas adsorption properties such as CO_2 uptake, working capacity, and CO_2/N_2 selectivity were examined. Comparisons were made between the charged MOFs from the database to a group of hypothetical neutral MOFs from a previous study[1]. Structural properties between the two groups of MOFs were examined to ensure that the differences in adsorption properties were due to charges on the frameworks. In addition to comparing the adsorption properties between the charged and uncharged MOFs, specific structural features of high performing MOFs as well as the effects of extra-framework counter ions in charged MOFs were studied. Finally, the gas adsorption data were confirmed using structures of the high performing MOFs, where the geometries of those structures were re-optimized at the DFT level.

4.2 Computational Details

In this study, 500 charged MOFs were chosen from the charged MOFs database as a representative group. The group of MOFs selected are referred to as the Database Representative Group (DRG). The MOFs were selected to reflect the ratios of the SBUs present in the database. The resulting DRG contains 161 positively charged MOFs and 339 negatively charged MOFs, this reflected the ratio between the positively and negatively charged MOFs in the database. Comparisons were made between the 500 MOFs representing the hypothetical

charged MOFs database and 500 hypothetical neutral MOFs from a previous study[1]. Although the MOFs in the neutral group includes different types of functional groups, their overall net charge remains neutral. Also, the structural properties such as the surface areas, pore diameter, and pore volume of the two groups of MOFs were compared. Figure 4-1 to Figure 4-3 show that the distribution of the structural properties between the DRG and neutral MOFs were largely similar. Given the similar structural properties between the two groups of MOFs, the difference in gas adsorption properties would be attributed to the difference in framework net charge.

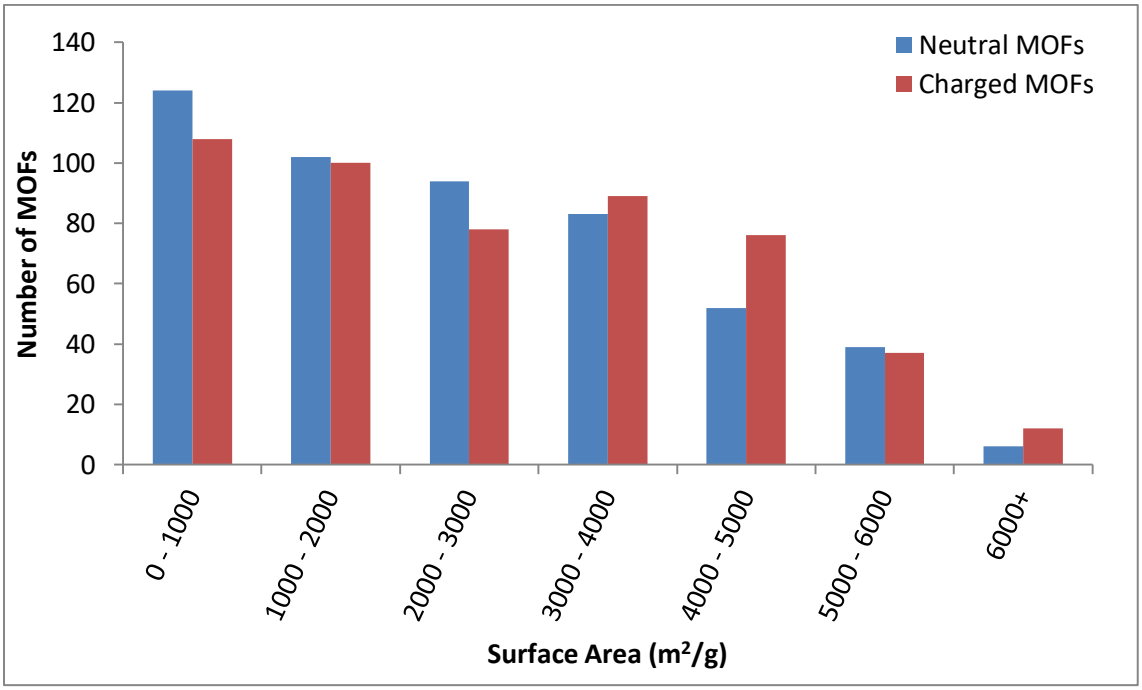

Figure 4-1. Surface areas histograms of DRG charged MOFs and neutral MOFs.

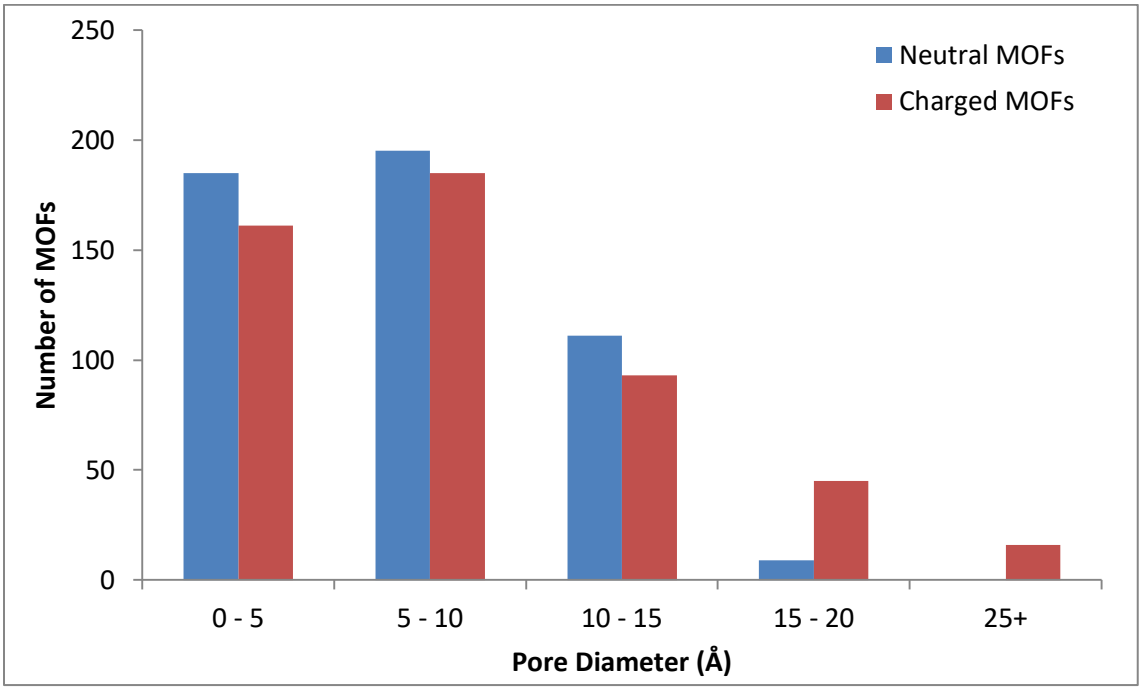

Figure 4-2. Pore diameters histograms of DRG charged MOFs and neutral MOFs.

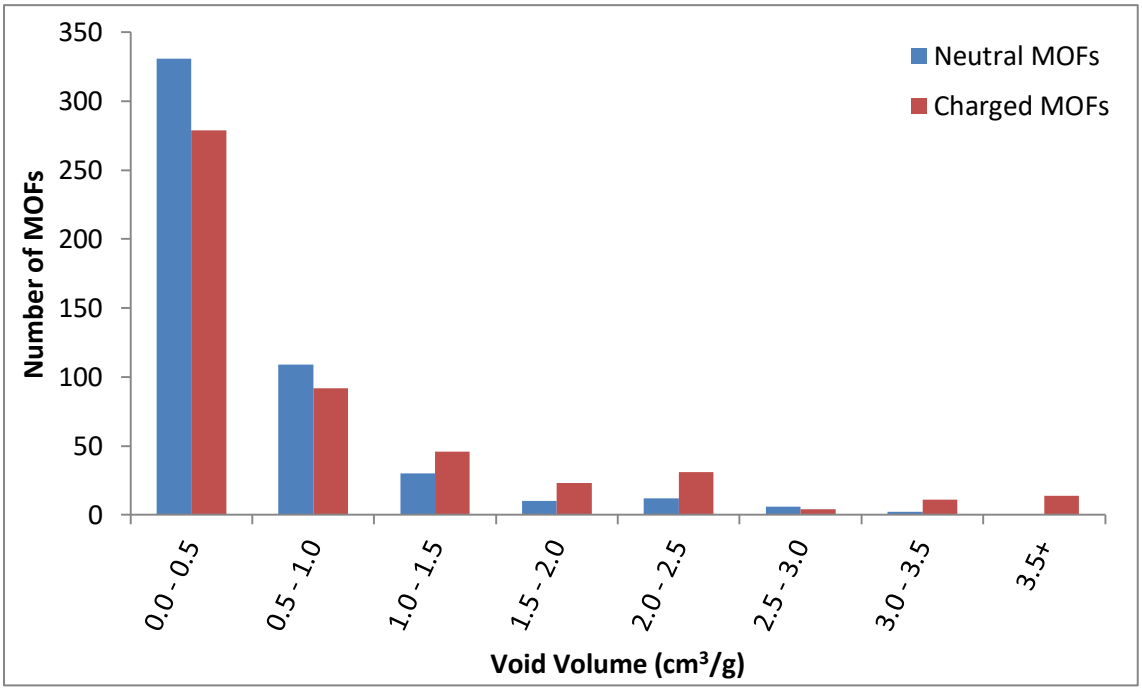

Figure 4-3. Void volumes histograms of DRG charged MOFs and neutral MOFs.

As discussed in Chapter 1.1, mild PSA conditions were used to minimize the cost of post-combustion CCS for implementation[13]. For a valid comparison, adsorption conditions of 298 K with a binary mixture of 0.15 bar CO_2 and 0.85 bar N_2 were used[13,14]. For desorption, CO_2 at 0.05 bar and the same temperature were used, 0.01 bar of N_2 was included to mimic the minute amount of N_2 adsorbed[13]. Since the amounts of N_2 adsorbed in each individual MOF differ, the pressure of N_2 during desorption is arbitrary. Four million equilibration steps and 32 million production steps were used in the charged MOFs' GCMC simulations to obtain the detailed results of adsorption and desorption. As for the neutral MOFs, 30,000 cycles were used for each equilibration and production steps since only the gas uptake quantity was needed. A cycle consists of N steps where N was the number of guest molecules within the simulations cell[15]. In charged MOFs, the framework net charges were neutralized with either Na^+ or Cl^- as counter ions. The locations of the counter ions were sampled with canonical MC ensemble during the simulations. In addition to the gas adsorption simulations, other property calculations were performed in order to correlate structural features with gas uptakes. Properties such as surface areas, pore sizes, and void volumes were calculated with a probe radius of 1.82 Å.

4.3 The Effects of Charges in MOFs on CO_2 Uptakes

To understand the effects of charges in MOFs on CO_2 uptakes, a comparison was made between the DRG MOFs with 500 hypothetical neutral MOFs used in a previous study[1]. As seen in Figure 4-4, the CO_2 uptakes by MOFs with net charges were generally higher than ones with neutral frameworks. At flue gas conditions, the averages of the CO_2 uptake of the two groups were 3.33 mmol/g for the charged MOFs and 1.17 mmol/g for the neutral MOFs. These averages reflected the charged MOFs' abilities in adsorbing more CO_2.

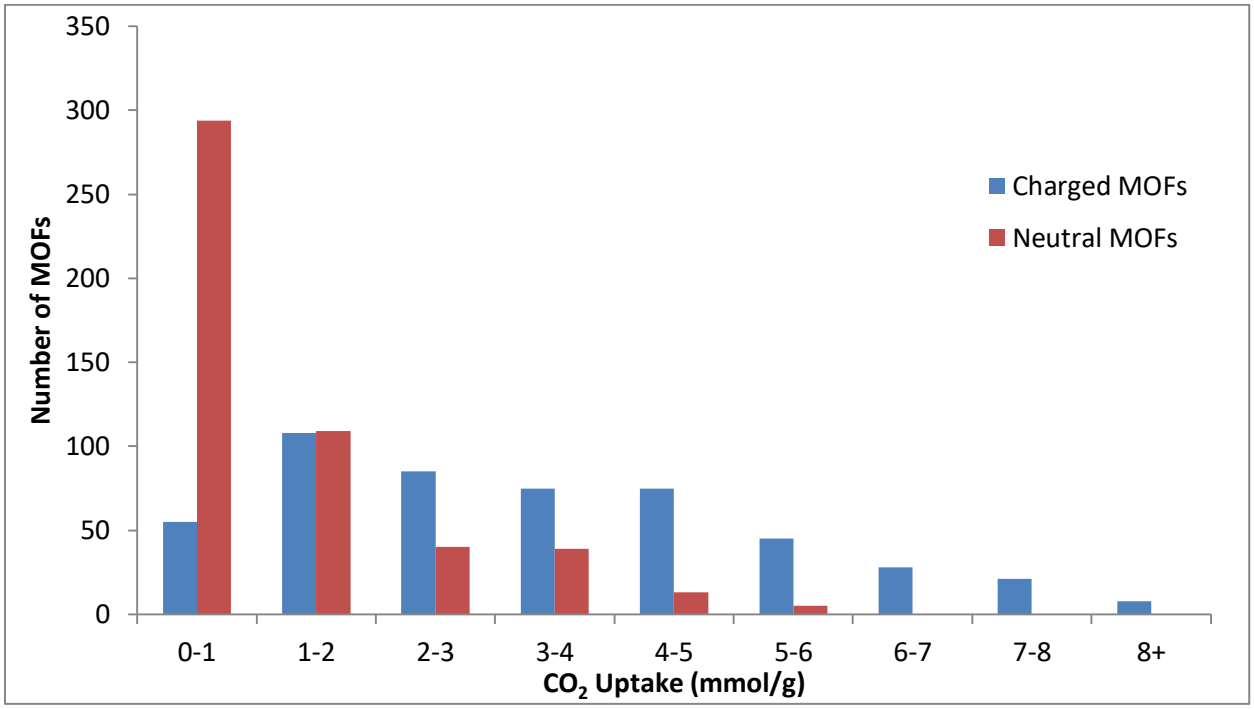

Figure 4-4. Histogram of CO_2 uptakes of the DRG charged MOFs and the neutral MOFs.

The uptakes of charged MOFs were then plotted against charges in the systems. As the unit cell of each MOF may have different sizes, the charges were normalized by volume. In Figure 4-5, a trend is seen that the higher the charge per volume, the higher the CO_2 uptake. Some outliers were present in the lower left and right hand corners of Figure 4-5; these charged MOFs with high charge per volume should be capable of adsorbing large quantity of CO_2. However, when the uptake of CO_2 was weighted against the pore volumes of the MOFs in Figure 4-6, the outliers became much smaller and a distinct V shape was formed. From Figure 4-6, it was clear that the lack of space in pores restricted the uptake of CO_2 in those previous outliers. The limited CO_2 uptake due to lack of available space was confirmed when the uptake was plotted against pore volume. In Figure 4-7, MOFs with pore volumes above 0.2 cm^3/g had an

even spread of CO_2 uptake, however, the CO_2 uptake in MOFs with less than 0.2 cm^3/g pore volumes were limited.

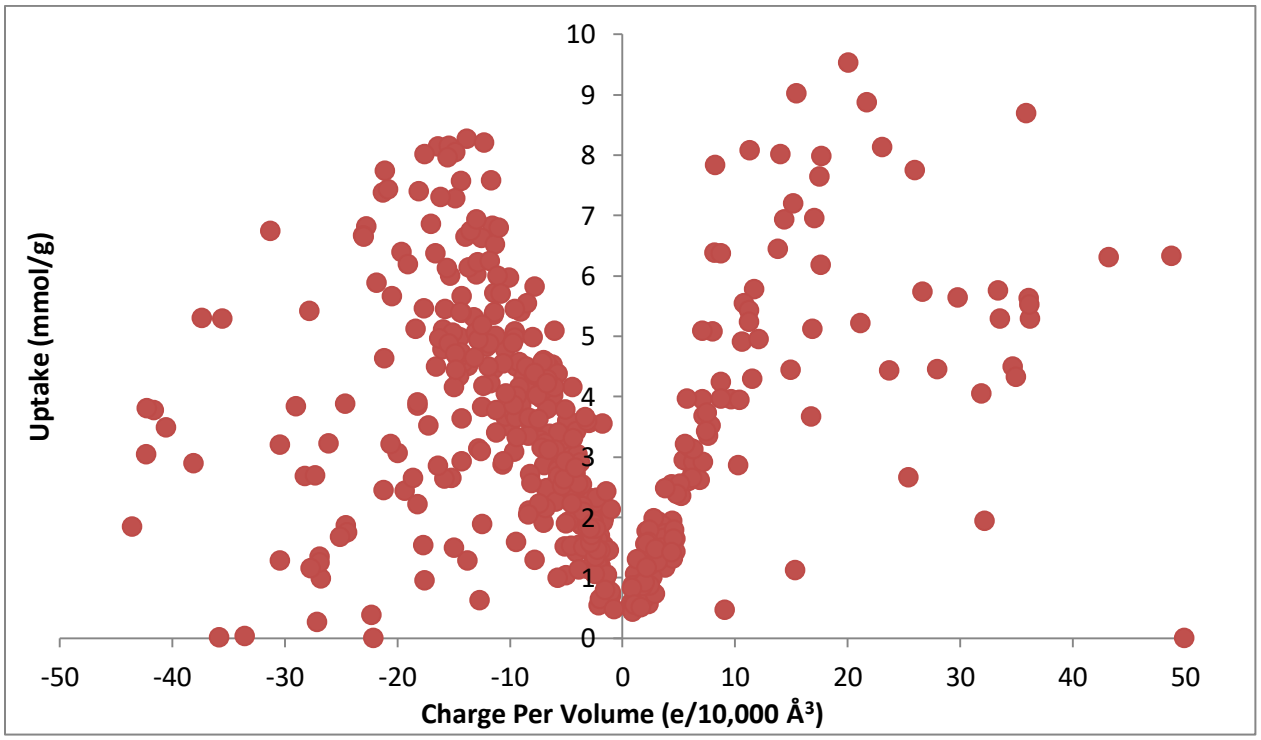

Figure 4-5. Uptakes of DRG MOFs plotted against their normalized charges.

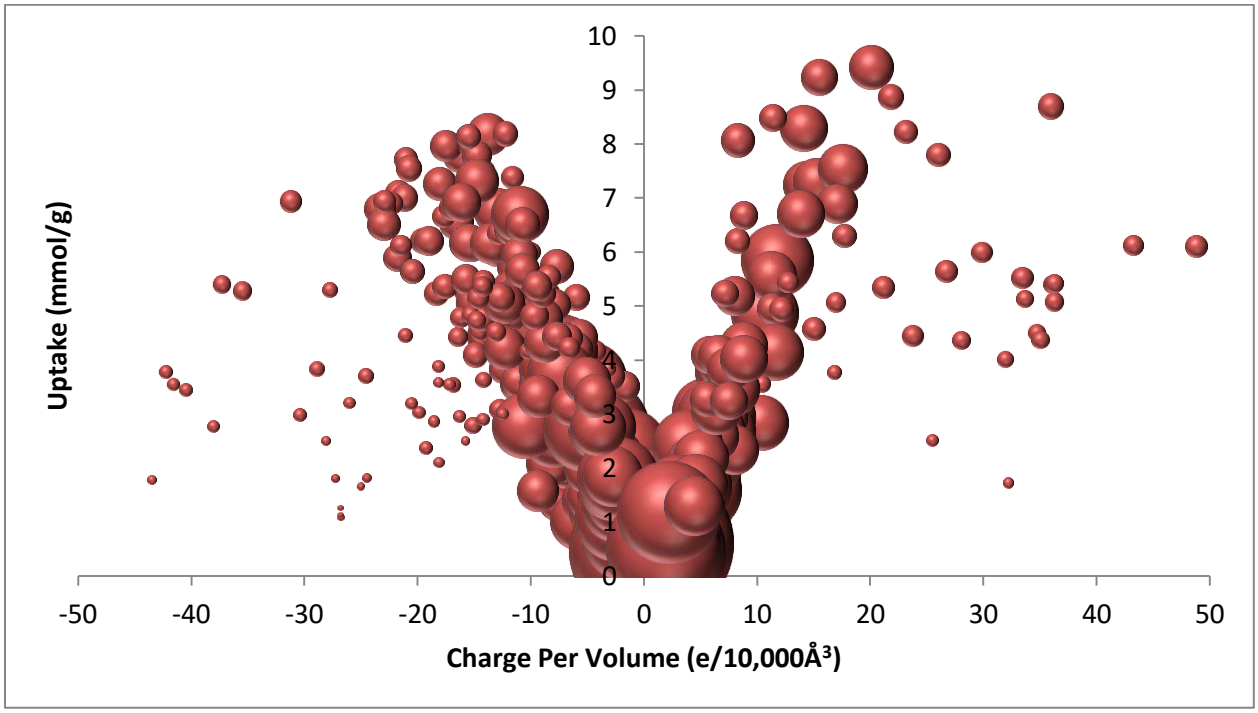

Figure 4-6. Uptakes of the DRG MOFs plotted against their normalized charges. The sizes of the data points were weighed by the pore volume of the MOF. The outliers from Figure 4-5 are no longer visible due to the lack of pore volume.

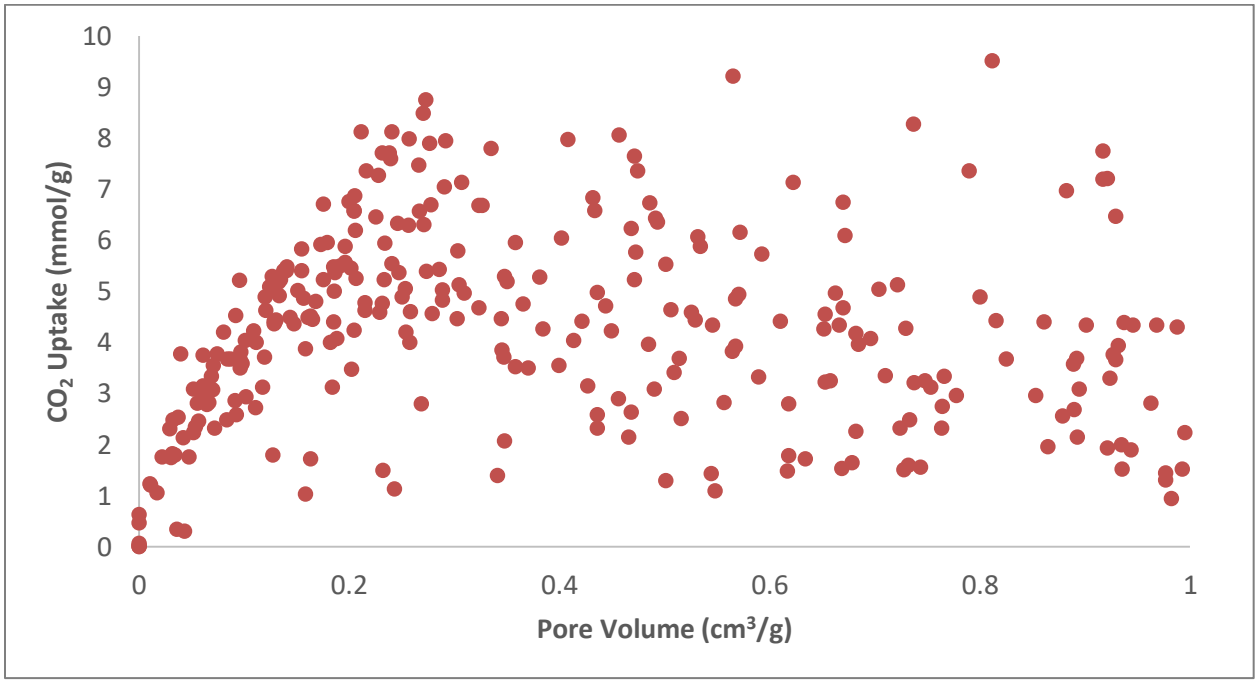

Figure 4-7. CO_2 Uptakes of the DRG MOFs plotted against pore volume. The uptakes were limited when MOFs have low pore volume.

To ensure that the high CO_2 uptakes in charged MOFs were the results of charges, gas adsorption simulations were performed without the attractive portion of the Lennard-Jones interactions. By using only the partial atomic charges to represent the attractive forces in intermolecular interactions, the CO_2 uptakes would be the results of electrostatic interactions. Six randomly selected hypothetical charged MOFs were used for these simulations, three positively charged and three negatively charged. Care was taken to ensure that the charge per volume of the MOFs were different, ranging from -12.95 to +11.74 e/10,000 $Å^3$. In Table 4-1, the CO_2 uptakes were obtained in two sets of simulations. In simulations not considering the attractive portion of the Lennard-Jones interaction, the CO_2 uptake observed was similar to the CO_2 uptake observed when all intermolecular interactions were taken into account. Thus, the high uptakes of charged MOFs were due to the electrostatic interactions from the charges in the MOFs. Given the non-negligible quadrupole moment of CO_2 molecules, electrostatic interactions occur between CO_2 and the charges on the MOFs' frameworks and counter ions[16,17]. Such interactions allowed for higher uptakes of CO_2 in charged MOFs than in neutral MOFs.

Table 4-1. CO_2 uptakes of six randomly chosen MOFs simulated with and without the attractive portion of the Lennard-Jones interaction.

MOF name	Charge per volume (e/10,000 $Å^3$)	Uptake with attractive Lennard-Jones interaction (mmol/g)	Uptake without attractive Lennard-Jones interaction (mmol/g)
str_m52_o67_dme	-12.95	6.07	5.94
str_m64_o88_xbv	-4.09	3.30	3.27
str_m66_o105_flu	-10.04	6.02	6.01
str_m56_o125_ant	+4.48	1.86	1.86
str_m57_o111_pha	+11.74	5.81	5.78
str_m75_o80_tbo	+2.48	0.87	0.85

4.4 The Effects of Counter Ions on CO_2 Uptakes

As seen in the previous section, 4.3, the long range electrostatic interactions allowed for the increase in CO_2 uptake in charged MOFs. The charges in these systems were localized on both the frameworks and the counter ions. As many different types of counter ions could be easily used in the same framework[18–20], the effects of counter ions on CO_2 uptakes were studied.

A study was conducted to compare the CO_2 uptakes of the charged MOFs when counter ions of different charges were used. In the original simulations, Na^+ and Cl^- were used to balance negatively and positively charged frameworks, respectively. As real ions with +2 or -2 charges may have significantly different properties than Na^+ and Cl^-, hypothetical counter ions Na^{+2} and Cl^{-2} were used. Aside from carrying double the net charge, the hypothetical counter ions have the same Lennard-Jones parameters as Na^+ and Cl^-. The differences in CO_2 uptake observed should be due to the differences in ion charges. Since doubly charged counter ions carry twice the charge, only half as many ions were required in each simulation cell to neutralize the net charge on the frameworks.

The average CO_2 uptakes of the original set and ones with doubly charged counter ions were 3.33 and 5.27 mmol/g, respectively, a 58.3% increase. Shown in Figure 4-8, as the charge of the counter ions doubled, the resulting CO_2 uptake increased, even though the number of counter ions were reduced by half. The average heats of adsorptions for the original set and the ones with hypothetical counter ions were 33.76 kJ/mol and 44.22 kJ/mol, respectively. The increase in heats of adsorptions in MOFs with doubly charged counter ions pointed to a rise in affinity of CO_2 guests. The change could be explained by the increase of electrostatic

interactions between the ions and the guest molecules due to a stronger charge on the ions. Also, as the guest molecules were allowed to freely rotate and orient themselves, the increased interactions could occur on both the carbon and the oxygens of the CO_2 molecules. Therefore, doubling the charges on both positively and negatively charged ions resulted in increased uptake.

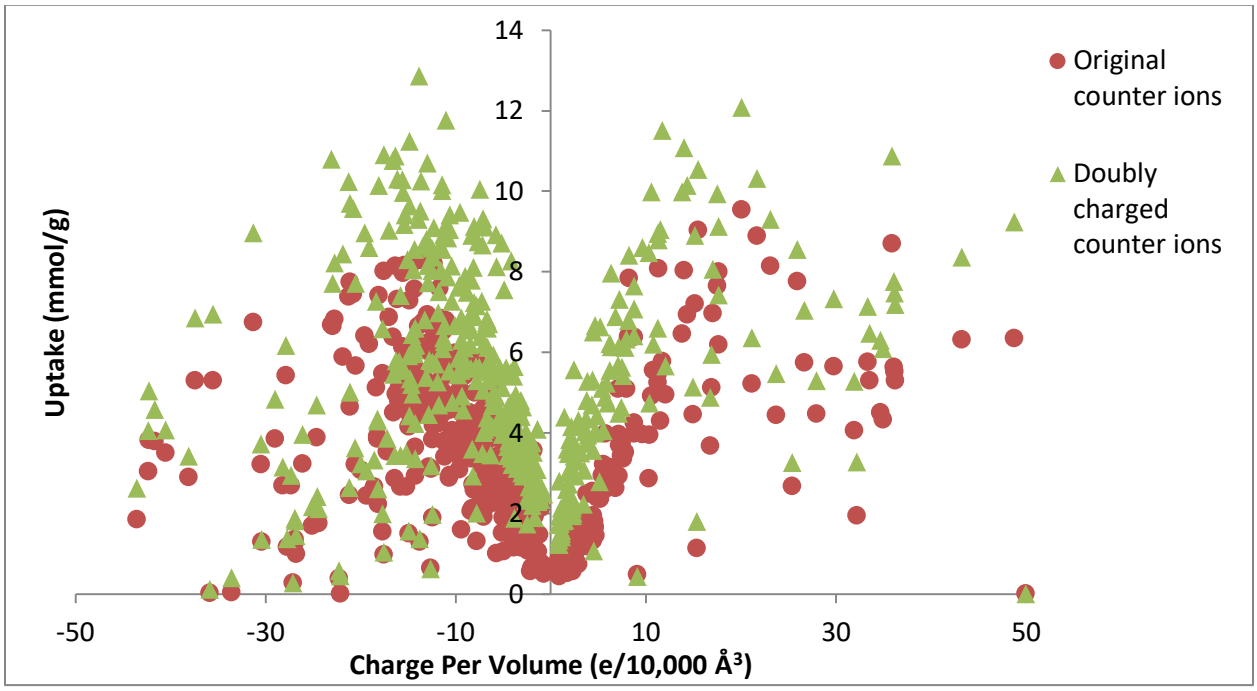

Figure 4-8. CO_2 uptakes of the DRG MOFs with original counter ions and with doubly charged hypothetical counter ions.

Unlike the metal atoms in inorganic SBUs, the counter ions were exposed in pores and were readily accessible by guest CO_2 molecules. The charges on the ions increased electrostatic interactions with the guest molecules, which lead to increased uptakes. To further understand the interactions between the counter ions and CO_2 guest molecules, the average distances between the ions and the carbon atom of the CO_2 molecules were taken from the DRG MOFs. RDFs were then plotted in Figure 4-9 and Figure 4-10. For systems with Cl^- counter ions, the RDF showed the guest CO_2 most commonly locate at a distance of 3.065 Å to the counter ion (Figure

4-9). For systems with Na^+ counter ions, the RDF plot shows a maximum peak at 3.549 Å for the distance between the CO_2 and Na^+ (Figure 4-10).

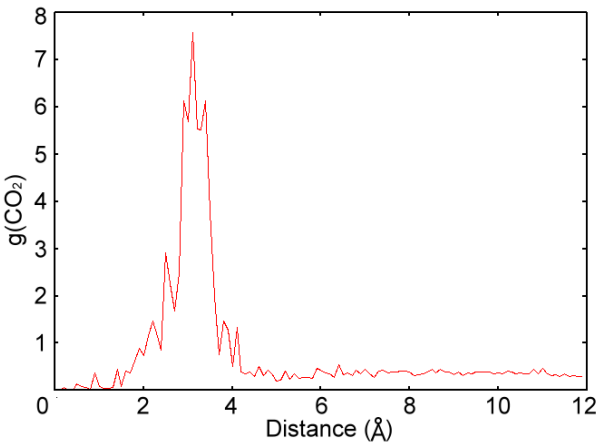

Figure 4-9. RDF plot of the average distances between Cl^- and the C of CO_2 guest molecules from all the DRG MOFs.

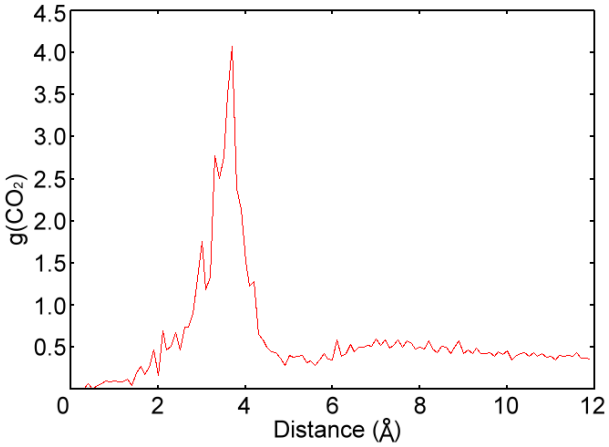

Figure 4-10. RDF plot of the distances between Na^+ and the C of CO_2 guest molecules from all the DRG MOFs.

Due to the partial positive charges on the C atoms and the partial negative charges on the O atoms, the CO_2 guest molecules would be oriented differently depending on the type of counter ions present. In the presence of the Cl^-, the partial positive charge on C atom would attract the Cl^- and the partial negative charge on the O atoms would repel the Cl^- ion. The opposite is true when Na^+ counter ions are present as they carry the opposite formal charge. Figure 4-11 and Figure 4-12 show the configurations of the CO_2 guest where the lowest possible energies were achieved when the two types of ions were present. In the presence of each ion, the minimum energy distance between the C atom and the ion was calculated numerically; while both the electrostatic and van der Waal interactions of all the atoms present are taken into consideration. The potential energy between the ions and the CO_2 were determined for the distances from 2 Å to 5 Å between the C atom and the ion, the distance with the lowest potential

energy is the numerical solution for the minimum energy distances. The force fields used here were the same as the ones used in the GCMC simulations: TraPPE force field designed for evaluating carbon dioxide adsorption in zeolites was used for CO_2 guest molecules[5]; the Universal Force Field and the formal charges were used for the counter ions[21]. Table 4-2 compares the values of the minimum energy distances and the observed values. The distances calculated numerically for the lowest energy was performed with both the Lennard-Jones and the electrostatic interactions taken into consideration. The observed values concur with the numerically calculated values with a difference of less than 1.64%.

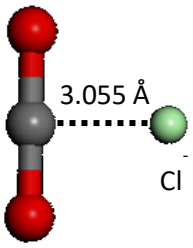

Figure 4-11. CO_2 and Cl^- configuration to result in the lowest energy.

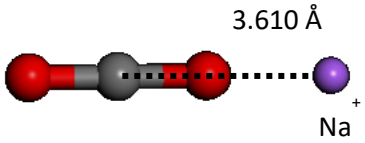

Figure 4-12. CO_2 and Na^+ configuration to result in the lowest energy.

Table 4-2. Calculated and observed distances between counter ions to C atoms of CO_2 guests.

	Calculated	RDF peak	Percent difference
Cl^- to C distances	3.055 Å	3.065 Å	0.34%
Na^+ to C distances	3.610 Å	3.549 Å	1.64%

Given the higher electronegativity of the oxygen atoms on the CO_2 molecules, they carry partial negative charges. Therefore, the oxygen atoms should be more attracted to the Na^+ counter ions

(Figure 4-12). The RDF of the distance between the oxygen atoms and the Na^+ ions was also plotted and illustrated in Figure 4-13. In this figure, two distinct peaks were shown for the two oxygen atoms, O(1) refers to the oxygen atom closer to the Na^+ ion and O(2) refers to the farther one. In Figure 4-13, the distances between the oxygen atoms and Na^+ were 2.463 Å and 4.613 Å, respectively. These two peaks were similar to the calculated distances for the lowest energy: 2.461 Å and 4.759 Å in Table 4-3. The distance from the Na^+ to the closer oxygen atom, O(1), was nearly identical to the calculated one (0.093%), whereas the second distance, O(2), had a higher difference (3.06%). The larger discrepancy for O(2) could be explained by a slightly rotated orientation of the CO_2 guest (Figure 4-14), where the O(2) is located closer to the Na^+ ion. The close proximity between counter ions and guest CO_2 molecules was also verified visually. When viewing the probability distributions of the counter ions and adsorbed CO_2 atoms in all 500 DRG MOFs, the CO_2 molecules were located close to a counter ion.

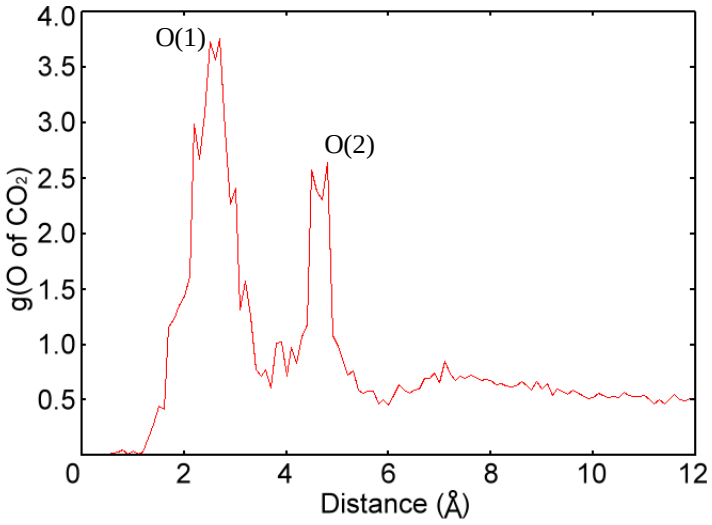

Figure 4-13. RDF plot of the average distances between Na^+ and the O atoms of CO_2 guest molecules from all of the DRG MOFs.

Table 4-3. Calculated and observed distances between Na^+ counter ions to O atoms of CO_2 guests.

	Calculated	RDF peak	Percent difference
Na^+ to O(1) distances	2.461 Å	2.463 Å	0.093%
Na^+ to O(2) distances	4.759 Å	4.613 Å	3.06%

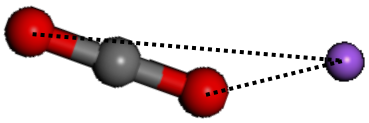

Figure 4-14. Alternative orientation of CO_2 and Na^+ where the CO_2 molecule is slightly rotated, resulting in the lowest energy.

As shown in chapter 4.2, CO_2 adsorption heavily depended on the charges present in the MOF. It was determined that the counter ion charges have the most effect on the uptake when counter ions with different charges were used. Since the counter ions resided in the pores of the MOFs, they were more accessible to the guest molecules than the framework atoms. As shown in the RDF graphs, the CO_2 guest molecules adsorbed were located close to the counter ions present. In addition, the distances between the CO_2 and the ions were ideal distances that allows for minimum potential energy. The interactions between CO_2 guests and counter ions, along with the changes in uptakes when different ions were used, showed that counter ions have significant effects on CO_2 gas adsorptions.

4.5 Working Capacity

To ensure economical implementation of CCS, MOFs with high working capacity are desired. As discussed in Chapter 1.1, new materials used for post-combustion CCS applications would require working capacities of 4 mmol/g or higher to be economically viable. The average working capacity of the DRG MOFs was 1.20 mmol/g, with the highest being 4.18 mmol/g. The working capacities of the 500 neutral MOFs had an average of 0.585 mmol/g and a maximum of 2.12 mmol/g. Between the two groups of MOFs, the charged MOFs outperformed the neutral ones by an average of over 200%. As shown in Figure 4-15, the working capacities of the charged MOFs were generally higher than those of the neutral MOFs.

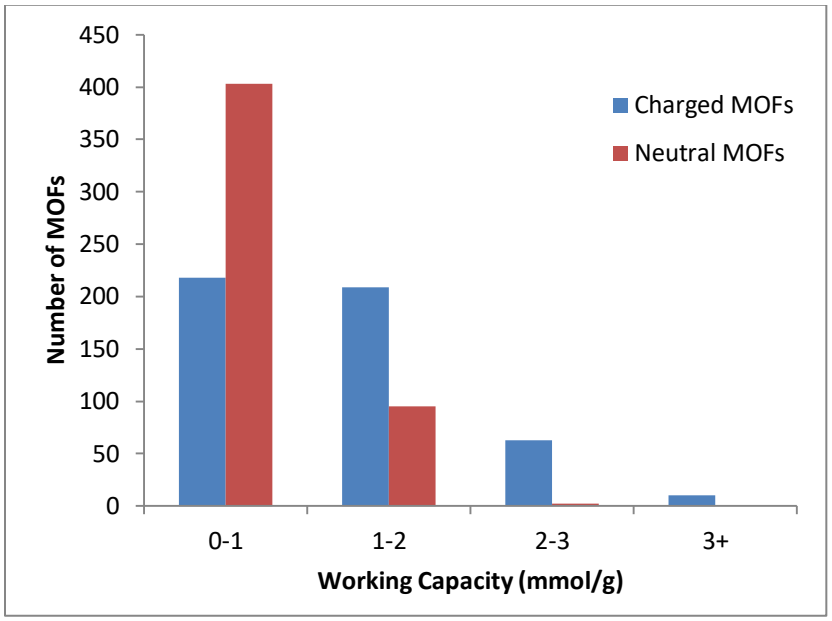

Figure 4-15. Histogram of CO_2 working capacities of the DRG charged MOFs and the neutral MOFs.

Similar to the observation in the previous section where charged MOFs have much higher uptakes than neutral ones, the working capacity of charged MOFs were also higher. From the DRG, two charged MOFs were identified with working capacities above 4 mmol/g. MOFs

str_m57_o80_fso and **str_m58_o160_o145_fsc** had working capacities of 4.18 and 4.05 mmol/g, respectively. The two high performers accounted for 0.4% of the 500 DRG MOFs. As the DRG was chosen for an accurate depiction of the whole database, theoretically around 189 hypothetical charged MOFs in the database of 47,000 should have working capacities higher than 4 mmol/g. These MOFs would be possible candidates for post-combustion CCS applications.

4.6 CO_2/N_2 Selectivity

As flue gas contains approximately 85% N_2, MOFs capable of selectively adsorbing CO_2 over N_2 are preferable for CCS applications. The CO_2/N_2 selectivity ratio required for efficient post-combustion CCS application should be 150 or higher[13]. While the average selectivity of the neutral group was 39.7, the average selectivity shown by the DRG MOFs was 593.5. The high selectivities exhibited by charged MOFs can be explained by their affinities towards CO_2 and N_2 molecules. Since neither CO_2 nor N_2 are formally charged or have a dipole moment, their interactions with the framework are dictated by their quadrupole moments and polarizability. In this study, the non-polarizable TraPPE force field[5] was used, therefore, only the quadrupole moment is considered. As CO_2 has a stronger quadrupole moment than N_2[17], the charges in MOFs would attract CO_2 guests more than N_2 guests. In charged MOFs, the average heat of adsorption for CO_2 was 33.76 kJ/mol, while it was only 12.26 kJ/mol for N_2 guests. The 21.50 kJ/mol difference in average heats of adsorption pointed to charged MOFs having much stronger affinities towards CO_2 than N_2. In neutral MOFs, the average heat of adsorption for CO_2 and N_2

were 24.52 kJ/mol and 13.14 kJ/mol, respectively. The difference in heats of adsorption was only 11.38 kJ/mol. While the average heats of adsorption for N_2 guests were similar between the two sets of MOFs, the charged MOFs had a higher average CO_2 heat of adsorption. As the heats of adsorption indicate the affinities toward a guest molecule, it showed that charged MOFs had higher affinities toward CO_2 than neutral MOFs, hence the higher CO_2/N_2 selectivities shown in Figure 4-16.

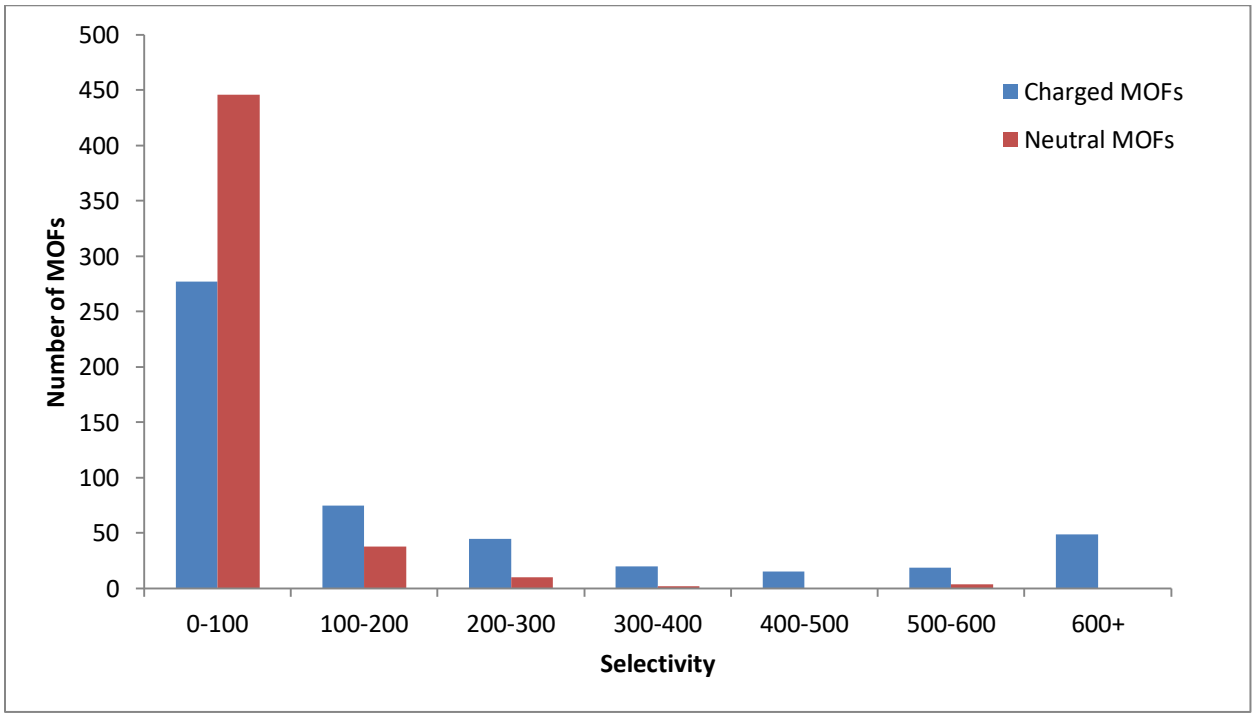

Figure 4-16. Histogram of selectivities in DRG charged MOFs and neutral MOFs.

Seeing that charged MOFs have higher selectivities than neutral MOFs, the correlation between selectivity and the magnitude of charge was examined. Figure 4-17 shows the

selectivities plotted against the normalized charges of the DRG MOFs. The distinct V shape present in Figure 4-17 was seen previously in Chapter 4.3, where MOFs with stronger charges had higher uptakes. This demonstrates that charge has a positive correlation with the CO_2/N_2 selectivity as it had with CO_2 uptake. The outliers in Figure 4-17 were insignificant once the selectivities were weighed by the pore volumes (Figure 4-18). This is similar to earlier observations that low pore volume resulted in low CO_2 uptake (Figure 4-6). As the outlier MOFs lack pore volume, it restricted the uptakes of both CO_2 and N_2 guests and rendered their selectivities irrelevant.

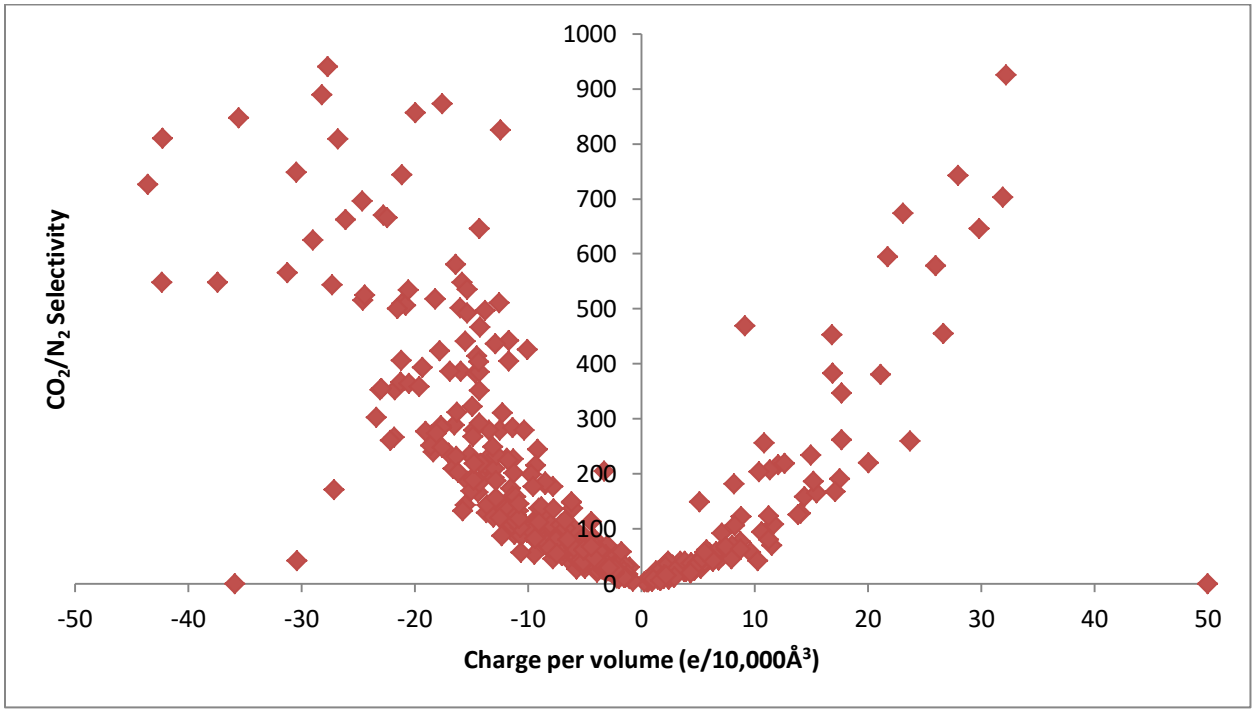

Figure 4-17. Selectivities of the DRG MOFs plotted against their normalized charges.

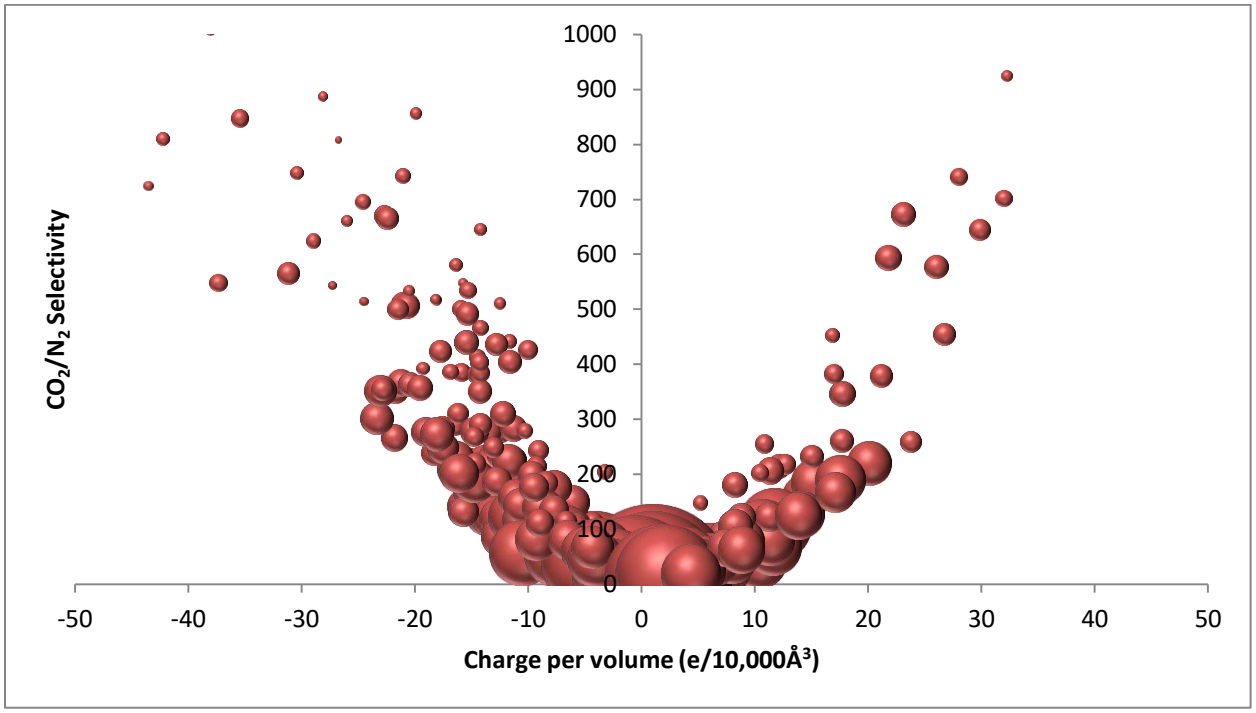

Figure 4-18. Selectivities of the DRG MOFs plotted against their normalized charges. The sizes of the data points were weighed by the pore volume of the MOF. The outliers from Figure 4-17 are no longer visible due to the lack of pore volume.

As discussed previously, flue gas may contain chemical species such as water, SOx, and NOx[13,22]. Even though these species would be removed prior to the post-combustion CCS process, trace water vapour may still be present in practice[13,23]. Due to its high polarity, water may interact with charges in the MOFs; it was feared that the MOF may be disrupted and selectivity may be reduced[24–26]. Simulations were performed on the DRG under flue gas condition with 0.01 bar of H_2O to simulate the presence of water at 33% relative humidity[22,27]. The average CO_2/N_2 selectivity with presence of water dropped from 593.5 to 233.7. However, despite the drop in average selectivity, 17 of the DRG MOFs still exhibited selectivities over 150 with the presence of water (Table 4-4). These 17 charged MOFs were examined to further understand the high selectivities with the presence of water. It should be noted that MOFs with

CO_2 uptakes less than 0.5 mmol/g were not considered, as these MOFs would not be suitable for post-combustion CCS applications. It was found that all 17 of the highly selective MOFs had minimal N_2 uptake, averaging at 0.129 mmol/g. The DRG and the neutral group had average N_2 uptakes of 0.232 mmol/g and 0.257 mmol/g, respectively. The higher ratio of CO_2/N_2 selectivity in the group of 17 highly selective MOFs was the result of the extremely low N_2 uptake. Since the high CO_2/N_2 selectivities observed in Table 4-4 were due to extremely low N_2 uptake, the actual selectivity may fluctuate and result in the high error within the ensemble.

Table 4-4. Highly selective MOFs with CO_2/N_2 selectivities above 150 with and without the presence of water.

MOF	Dry CO_2/N_2 Selectivity and Error	CO_2/N_2 Selectivity and Error With the Presence of Water
str_m57_o88_fsg	1435 ± 995	708 ± 3582
str_m52_o143_nab	670 ± 228	605 ± 533
str_m58_o158_o145_fsf	594 ± 229	1230 ± 2852
str_m81_o102_fsd	493 ± 204	525 ± 682
str_m66_o105_flu	426 ± 156	257 ± 155
str_m81_o102_fso	311 ± 78	169 ± 86
str_m81_o41_fsi	292 ± 72	333 ± 205
str_m79_o86_csq	284 ± 57	158 ± 78
str_m82_o100_ptt	280 ± 95	197 ± 103
str_m58_o117_fsh	256 ± 103	172 ± 121
str_m68_o107_fsg	207 ± 54	193 ± 121
str_m83_o106_o102_xbv	205 ± 71	183 ± 94
str_m68_o105_xat	182 ± 44	180 ± 99
str_m52_o153_o143_bal	174 ± 28	157 ± 78
str_m68_o76_sit	122 ± 25	162 ± 91
str_m83_o41_scu	112 ± 18	187 ± 89
str_m85_o109_uoc	106 ± 16	178 ± 100

Specific types of structural features were identified in the 17 highly selective MOFs. Figure 4-19 shows the histogram of pore diameters of the high selectivity MOFs compared

against the DRG, where the frequencies shown are normalized as percentages within each group. The pore diameters of the DRG MOFs were diverse, averaging 13.09 Å; however, the highly selective MOFs had a narrow range of pore diameters, averaging 6.59 Å.

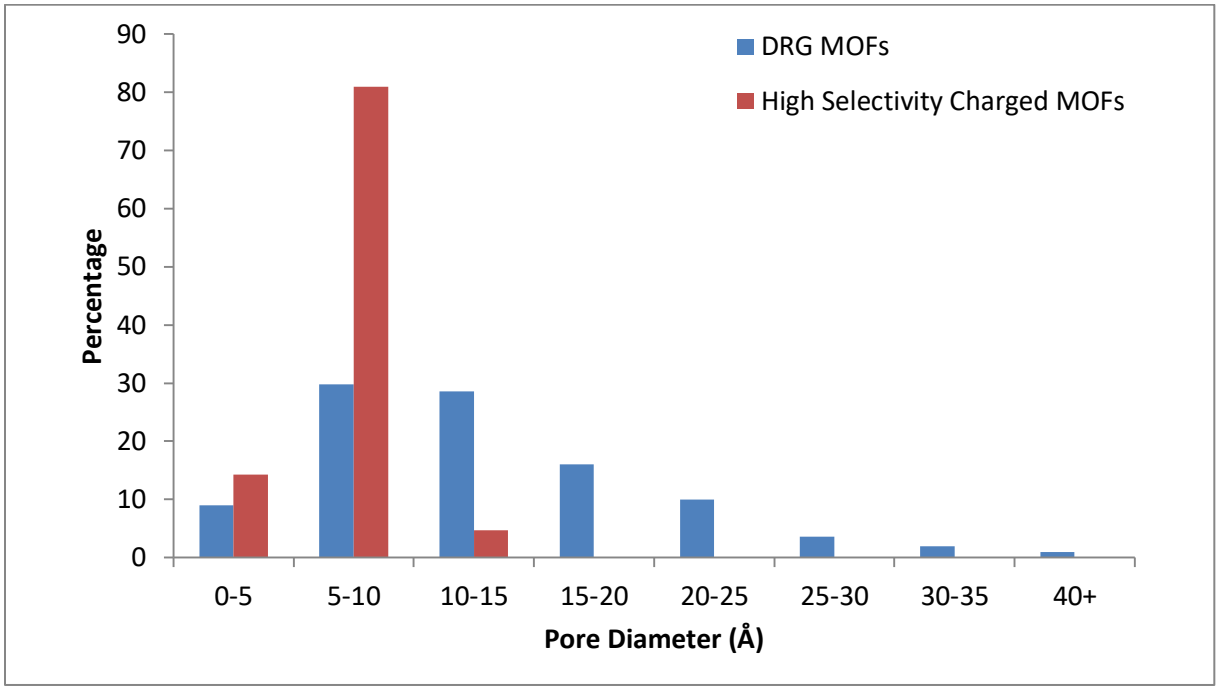

Figure 4-19. Pore diameter histograms of the DRG MOFs and high selectivity charged MOFs, where the frequencies were normalized to the bin with the highest frequency.

Similar to the pore diameters, the pore volumes of the highly selective MOFs also had a specific range. Figure 4-20 shows the pore volumes of the high selectivity MOFs and the DRG; once again the frequencies were normalized as percentages. The range of pore volumes of the 17 highly selective MOFs was very narrow compared to the DRG. More specifically, the high selectivity MOFs had a small average pore volume of 0.216 cm^3/g while the DRG had an average of 1.18 cm^3/g.

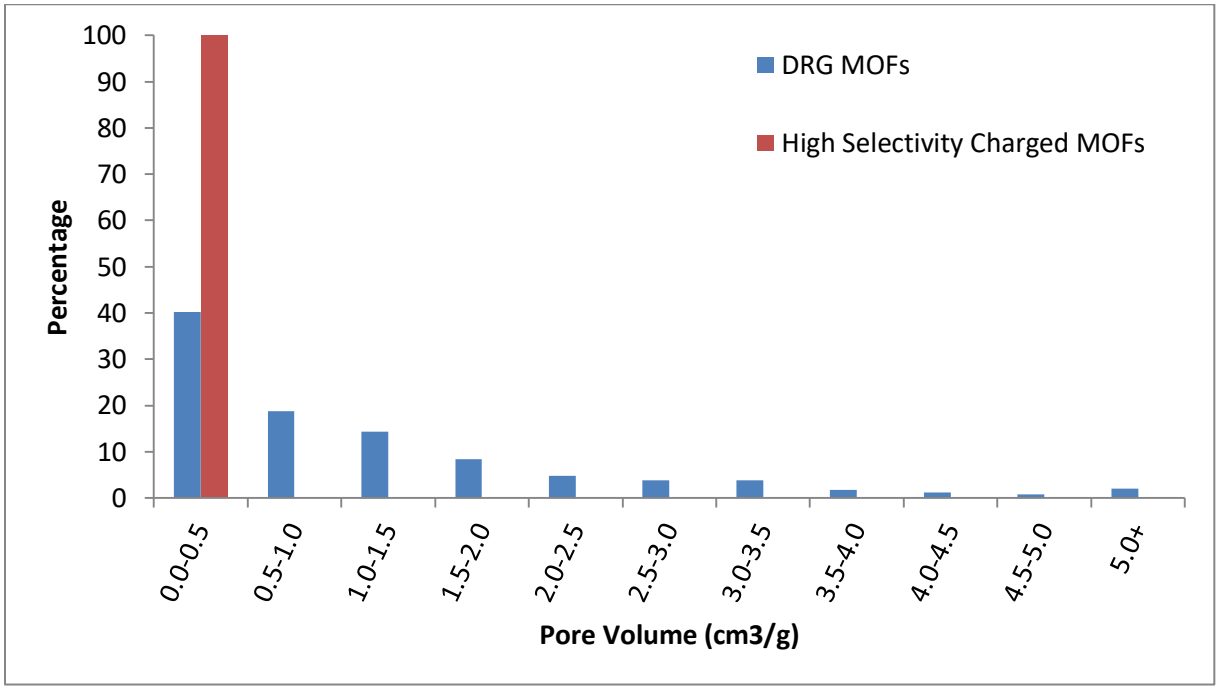

Figure 4-20. Pore volume histograms of the DRG MOFs and high selectivity charged MOFs, where the frequencies were normalized to the bin with the highest frequency.

The high selectivity resulting from the small pore diameters and volumes could be explained by the quadrupole moments of CO_2 and N_2. Since CO_2 has a higher quadrupole moment than N_2[17], CO_2 molecules introduced into the pores were more likely to have stronger interactions with the counter ion and bind favourably. A closer look at the heats of adsorptions for the guests revealed the differences in affinity towards CO_2 and N_2 guests. The average heats of adsorption for CO_2 and N_2 in the highly selective MOFs were 53.64 kJ/mol and 20.55 kJ/mol, respectively, a 33.09 kJ/mol difference. The CO_2 and N_2 averages for the entire DRG were 33.76 kJ/mol and 12.26 kJ/mol, respectively; the differences in heats of adsorption was only 11.50 kJ/mol. Between the two groups of charged MOFs, the group with small pore dimensions

had the higher difference in heats of adsorptions; therefore, their stronger affinity towards CO_2 than N_2 resulted in higher selectivities.

A hypothesis is put forward to explain the correlation between small pore volume and increased selectivity. Figure 4-21 and Figure 4-22 are hypothetical charged MOFs with two different pore sizes, the small pore size in Figure 4-21 limits the accessible pore volume to guests and counter ions. Consequently, most of the pore space is charged. Due to the higher quadrupole moment of CO_2, charges in MOFs have higher affinity towards CO_2 than N_2 molecules. As the CO_2 guests occupy space in the small pores, the lack of space results in a low N_2 uptake. In the larger pore shown in Figure 4-22, N_2 adsorptions are not restricted by the lack of space.

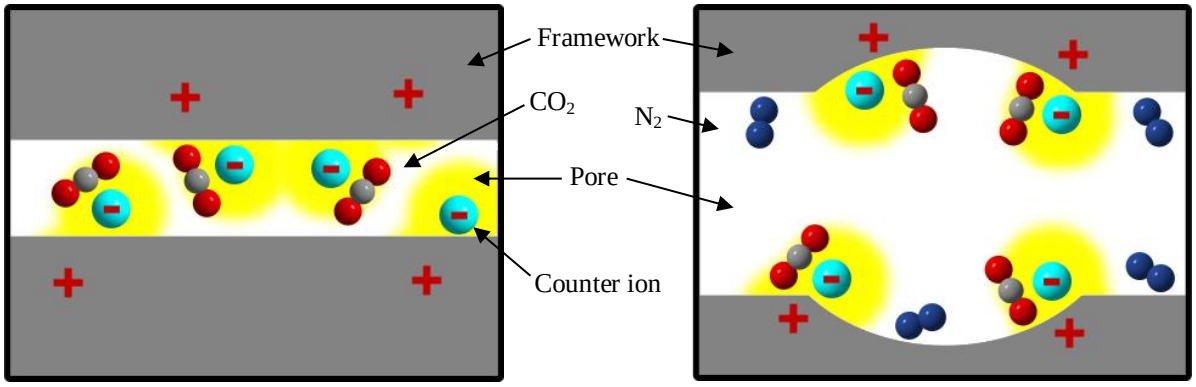

Figure 4-21. Hypothetical MOF with small pore diameter and volume where the charged area is highlighted. The lack of uncharged space reduces N_2 uptake.

Figure 4-22. Hypothetical MOF with large pore diameter and volume where the charged area is highlighted. The large pore allows for N_2 uptake, in addition to the CO_2 adsorbed.

In addition to finding specific structural features that resulted in high selectivity in MOFs, top performers were found. The 17 highly selective MOFs identified previously (Table 4-4) account for 4.2% of the DRG. By the same percentage, the hypothetical charged MOFs database

should contain approximately 1,984 MOFs capable of selectively adsorbing CO_2 over N_2 at a ratio above 150. These highly selective MOFs would be possible candidates for post-combustion CCS applications.

4.7 Studies on DFT Optimized Structures

In order to have the most accurate results, geometry optimization was performed at the DFT level on 19 top performing MOFs with fixed lattice parameters. The MOFs that were re-optimized included the two MOFs with working capacities above 4 mmol/g in Chapter 4.5, as well as the group of 17 charged MOFs with CO_2/N_2 selectivities above 150 in the presence of water from Chapter 4.6.

Table 4-5 lists the selectivities and working capacities of the selected MOFs with and without DFT optimization. With only the force field optimization, the selected MOFs had an average CO_2/N_2 selectivity of 339.1. The average selectivity of the DFT optimized structures was 354.7, a negligible difference when the associated error is taken into consideration. As the selectivities depend highly on the low uptake of the N_2 guests, they could easily fluctuate, hence the large error shown in Table 4-5. The average working capacities of the selected MOFs with and without DFT optimization were 1.893 mmol/g and 1.746 mmol/g respectively. As the gas adsorption uptakes are averages of the ensembles, the differences are also within the error range. In addition, the same top performers were identified as having the highest working capacities.

Table 4-5. Selectivities and working capacities of selected charged MOFs with and without DFT optimization. The table was sorted by the working capacity of the DFT optimized structure.

MOF Name	Original Selectivity and Error	DFT Optimized Structure Selectivity and Error	Original Working Capacity and Error (mmol/g)	DFT Optimized Structure Working Capacity and Error (mmol/g)
Average	339 ± 132	355 ± 102	1.9 ± 0.4	1.7 ± 0.4
str_m58_o160_o145_fsc	128 ± 16	152 ± 13	4.1 ± 0.6	4.3 ± 0.6
str_m57_o80_fso	166 ± 27	166 ± 18	4.2 ± 0.7	3.7 ± 0.5
str_m85_o109_uoc	106 ± 16	108 ± 12	3.5 ± 0.6	3.1 ± 0.5
str_m68_o76_sit	122 ± 25	111 ± 16	3.1 ± 0.6	2.9 ± 0.5
str_m68_o107_fsg	207 ± 54	236 ± 50	2.6 ± 0.6	2.4 ± 0.6
str_m68_o105_xat	182 ± 44	169 ± 29	2.3 ± 0.4	2.4 ± 0.4
str_m81_o102_fso	311 ± 78	307 ± 52	2.4 ± 0.4	2.1 ± 0.4
str_m52_o153_o143_bal	174 ± 28	171 ± 20	2.4 ± 0.6	2.0 ± 0.4
str_m83_o41_scu	112 ± 18	115 ± 13	1.5 ± 0.4	1.6 ± 0.3
str_m58_o158_o145_fsf	594 ± 229	608 ± 161	1.1 ± 0.4	1.2 ± 0.3
str_m81_o41_fsi	292 ± 72	293 ± 52	1.2 ± 0.2	1.1 ± 0.3
str_m79_o86_csq	284 ± 57	273 ± 45	0.8 ± 0.3	0.9 ± 0.3
str_m83_o106_o102_xbv	205 ± 71	228 ± 66	0.8 ± 0.2	0.8 ± 0.3
str_m58_o117_fsh	256 ± 103	266 ± 79	1.1 ± 0.3	0.8 ± 0.4
str_m66_o105_flu	426 ± 156	436 ± 114	1.3 ± 0.3	0.8 ± 0.3
str_m52_o143_nab	670 ± 228	722 ± 168	0.9 ± 0.3	0.8 ± 0.2
str_m82_o100_ptt	280 ± 95	302 ± 80	0.9 ± 0.2	0.8 ± 0.2
str_m81_o102_fsd	493 ± 204	588 ± 174	0.9 ± 0.4	0.8 ± 0.3
str_m57_o88_fsg	1435 ± 995	1490 ± 772	0.7 ± 0.3	0.6 ± 0.3

From the DFT optimized structures, the MOF **str_m58_o160_o145_fsc** was found to be the top performer. It had a CO_2/N_2 selectivity of 152.2 and working capacity of 4.317 mmol/g, both of which satisfy the criteria of post-combustion CCS applications. In addition, MOF **str_m57_o80_fso** was found to have high selectivity and working capacity close to the post-combustion CCS application requirement.

4.8 Summary

In order to explore whether charged MOFs are viable materials for post-combustion CCS applications, a database of 47,000 hypothetical charged MOFs was constructed and screened using methods outlined in the two previous chapters. Due to the high number of MOFs present in the database and the high computational cost of DFT calculations, a DRG of 500 hypothetical charged MOFs was chosen. The adsorption properties of the DRG were compared against 500 hypothetical neutral MOFs with similar structural properties. It was found that the average adsorption of CO_2 in charged MOFs was almost three times the amount of neutral MOFs. Also, the average working capacity of the DRG MOFs was more than double the average of the neutral group. It was found that the electrostatic interactions between the CO_2 guests and the charges in the MOFs resulted in the high uptake of CO_2; the higher charge per volume lead to more CO_2 adsorbed.

The charges on the MOFs' frameworks were neutralized by counter ions in the pores. As the counter ions were more exposed and easily accessible by guest molecules, interactions between the charged ions and the guests drastically affected the adsorption. With the low CO_2 partial pressure under flue gas conditions, RDF plots showed that CO_2 guests were absorbed close to the counter ions. This was observed regardless of the charge on the counter ion. In addition, the distances between the CO_2 guests and counter ions observed in the RDF plots matched the calculated distances where the lowest potential energy resulted. Therefore, interactions between counter ions and CO_2 guests had the most significant effect on the adsorption of the CO_2 guests.

As CO_2 molecules have higher quadrupole moments than N_2 molecules[17], charged MOFs have a stronger affinity towards CO_2 than N_2 guests. The average CO_2/N_2 selectivity of the DRG MOFs was 593.5, whereas the neutral group only had an average selectivity of 39.7. Similar to the CO_2 uptake, CO_2/N_2 selectivities also had a dependency on charge; stronger charges lead to higher selectivities of the MOFs. As the charges in MOFs may interact with water molecules, due to their dipole moments, the presence of water reduced the average selectivity. However, 17 of the DRG MOFs were capable of maintaining CO_2/N_2 selectivities of 150 or higher. All 17 highly selective MOFs were found to have small pore diameters and volumes. Due to the limited uncharged pore space and their higher affinity towards CO_2 than N_2, the uptake of N_2 in these MOFs were extremely low. As a result, the CO_2/N_2 selectivities were very high.

19 MOFs with the highest selectivities and working capacities were optimized with DFT to obtain the most accurate adsorption properties. Adsorption properties obtained from structures optimized with either force field or DFT were similar. Also, two of the same top performers were identified with adsorption properties similar to or higher than the requirement for post-combustion CCS applications.

By comparing groups of diverse charged MOFs and neutral MOFs, it was found that charged MOFs have much higher working capacities and CO_2/N_2 selectivities. Due to their superior performance, charged MOFs were proven to be viable materials for post-combustion CCS applications.

4.9 References

1. Kadantsev, E. S., Boyd, P. G., Daff, T. D., and Woo, T. K. Fast and Accurate Electrostatics in Metal Organic Frameworks with a Robust Charge Equilibration Parameterization for High-Throughput Virtual Screening of Gas Adsorption. *J. Phys. Chem. Lett.* **4,** 3056–3061 (2013).

2. Campañá, C., Mussard, B., and Woo, T. K. Electrostatic Potential Derived Atomic Charges for Periodic Systems Using a Modified Error Functional. *J. Chem. Theory Comput.* **5,** 2866–2878 (2009).

3. Lonsinger, S. R., Chakraborty, A. K., Theodorou, D. N., and Bell, A. T. The Effects of Local Structural Relaxation on Aluminum Siting Within H-ZSM-5. *Catal. Letters* **11,** 209–217 (1991).

4. Hirotani, A., Mizukami, K., Miura, R., Takaba, H., Miya, T., Fahmi, A., Stirling, A., Kubo, M., and Miyamoto, A. Grand Canonical Monte Carlo Simulation of the Adsorption of CO2 on Silicalite and NaZSM-5. *Appl. Surf. Sci.* **120,** 81–84 (1997).

5. García-Sánchez, A., Ania, C., Parra, J., Dubbeldam, D., Vlugt, T., Krishna, R., Calero, S. Transferable Force Field for Carbon Dioxide Adsorption in Zeolites. *J. Phys. Chem. C* **113,** 8814–8820 (2009).

6. Beerdsen, E., Dubbeldam, D., Smit, B., Vlugt, T. J. H., and Calero, S. Simulating the Effect of Nonframework Cations on the Adsorption of Alkanes in MFI-type Zeolites. *J. Phys. Chem. B* **107,** 12088–12096 (2003).

7. Beerdsen, E., Smit, B., and Calero, S. The Influence of Non-framework Sodium Cations on the Adsorption of Alkanes in MFI- and MOR-Type Zeolites. *J. Phys. Chem. B* **106,** 10659–10667 (2002).

8. Jaramillo, E. and Auerbach, S. M. New Force Field for Na Cations in Faujasite-Type Zeolites. *J. Phys. Chem. B* **103,** 9589–9594 (1999).

9. Fischer, M. and Bell, R. G. Modeling CO2 Adsorption in Zeolites Using DFT-derived Charges: Comparing System-specific and Generic Models. *J. Phys. Chem. C* **117,** 24446–24454 (2013).

10. Rappé, A. K. and Goddard III, W. A. Charge Equilibration for Molecular Dynamics Simulations. *J. Phys. Chem.* **95,** 3358–3363 (1991).

11. Mason, J. A., Sumida, K., Herm, Z. R., Krishna, R., and Long, J. R. Evaluating Metal–organic Frameworks for Post-combustion Carbon Dioxide Capture via Temperature Swing Adsorption. *Energy & Environmental Science* **4,** 3030 (2011).

12. Yu, C. H., Huang, C. H., and Tan, C. S. A Review of CO2 Capture by Absorption and Adsorption. *Aerosol and Air Quality Research* **12,** 745–769 (2012).

13. Ho, M. T., Allinson, G. W., and Wiley, D. E. Reducing the Cost of CO2 Capture from Flue Gases Using Pressure Swing Adsorption. *Ind. Eng. Chem. Res.* **47,** 4883–4890 (2008).

14. Sumida, K., Rogow, D., Mason, J., McDonald, T., Bloch, E., Herm, Z., Bae, T., and Long J. Carbon Dioxide Capture in Metal-Organic Frameworks. *Chem. Rev. (Washington, DC, United States)* **112,** 724–781 (2012).

15. Daff, T. D., Collins, S. P., Dureckova, H., Perim, E., Skaf, M. S., Galvão, D. S., and Woo, T. K. Evaluation of Carbon Nanoscroll Materials for Post-combustion CO2 Capture. *Carbon N. Y.* **101,** 218–225 (2016).

16. Leach, A. R. *Molecular Modelling: Principles and Applications*. *Prentice Hall Harlow UK* **2nd,** (2001).

17. Buckingham, A. D., Disch, R. L., and Dunmur, D. A. Quadrupole Moments of some Simple Molecules. *J. Am. Chem. Soc.* **90,** 3104–3107 (1968).

18. Yaghi, O. M., Li, G., and Li, H. Selective Binding and Removal of Guests in a Microporous Metal–organic Framework. *Nature* **378,** 703–706 (1995).

19. Zhao, X., Bu, X., Wu, T., Zheng, S., Wang, L., and Feng, P. Selective Anion Exchange with Nanogated Isoreticular Positive Metal-organic Frameworks. *Nat. Commun.* **4,** 2344 (2013).

20. James, S. L. Metal-organic Frameworks. *Chem. Soc. Rev.* **32,** 276 (2003).

21. Rappe, A. K., Casewit, C. J., Colwell, K. S., Goddard III, W. A., and Skiff, W. M. UFF, a full Periodic Table Force Field for Molecular Mechanics and Molecular Dynamics

Simulations. *J. Am. Chem. Soc.* **114,** 10024–10035 (1992).

22. Xiao, P., Zhang, J., Webley, P., Li, G., Singh, R., and Todd, R. Capture of CO2 from flue gas Streams with Zeolite 13X by Vacuum-pressure Swing Adsorption. *Adsorption* **14,** 575–582 (2008).

23. Gurjar, B., Ojha, C., Surampalli, R., Zhang, T., and Walvekar, P. in *Carbon Capture and Storage* 7–35 (2015).

24. Low, J. J., Benin, A. I., Jakubczak, P., Abrahamian, J. F., Faheem, S. A., and Willis, R. R.. Virtual high Throughput Screening Confirmed Experimentally: Porous Coordination Polymer Hydration. *J. Am. Chem. Soc.* **131,** 15834–42 (2009).

25. Schröck, K., Schröder, F., Heyden, M., Fischer, R. A., and Havenith, M. Characterization of Interfacial Water in MOF-5 (Zn4(O)(BDC)3)--a Combined Spectroscopic and Theoretical Study. *Phys. Chem. Chem. Phys.* **10,** 4732–9 (2008).

26. Li, G., Xiao, P., Webley, P. A., Zhang, J., and Singh, R. Competition of CO2/H2O in Adsorption Based CO2 Capture. in *Energy Procedia* **1,** 1123–1130 (2009).

27. David R Lide, E. CRC Handbook of Chemistry and Physics, Internet Version 2005. *CRC Press. Taylor Fr. Boca Rat. FL* 0 (2005). doi:10.1016/0165-9936(91)85111-4

5 Conclusions and Future Work

5.1 Summary of Results and Findings

Motivated by the need to reduce CO_2 emissions, the viability of using charged MOFs as a material for capturing CO_2 was examined in this work. To explore the capabilities of charged MOFs, a novel computational method for the determination of gas adsorption properties in charged periodic systems was developed. The automated series of programs, FA^{3}PS, overcame the challenge of simulating periodic systems with a net charge. In charged periodic systems, infinitely repeating periodic images, each with a net charge, represent an unphysical system with infinite energy. However, FA^{3}PS is capable of rendering the system neutral by applying a background charge or inserting counter ions when appropriate. To acquire gas adsorption properties, FA^{3}PS simulate the electrostatic interactions in the simulation cell using partial atomic charges derived using VASP and REPEAT[1,2]. A background charge is applied for neutralization charge derivation, while avoiding the possible polarization effects of the framework atoms by counter ions.

As the REPEAT method has been proven effective at representing the electronic structure in neutral systems[1,3,4], partial atomic charges derived in systems with a net charge was tested. The QM ESP was calculated with VASP in MOFs with large pores with and without ions for neutralization. Partial atomic charges were then fitted to reproduce the ESP using the REPEAT method. In the case when ions were included, the ions were inserted into the centre of the large pores to avoid possible polarization effects. Regardless of the overall net charge in the simulation cell, the partial atomic charges were in excellent agreement with the charges derived

from a neutral system. Therefore, REPEAT is capable of deriving partial atomic charges in systems with an overall net charge.

Using partial atomic charges to represent the ESP of the charged MOF frameworks, FastMC simulations were performed to obtain gas adsorption isotherms for the systems. In FastMC, counter ions are used to balance the charged systems in order to simulate the interactions between the ions and the rest of the system. The GCMC ensemble is used for guest molecules, as the number of those molecules fluctuates in order to simulate adsorption and desorption of the gas. The locations of the counter ions are also sampled with the canonical MC ensemble in the simulations.

To test the accuracy of the above methods, REPEAT charges were derived for a benzene-tris-tetrazolate MOF synthesized by Dincă *et al.*, which has a net charge of -3 in its unit cell and contains Mn^{+2} counter ions[5]. FastMC simulations were then performed to determine the positions of the Mn^{+2} counter ions. All of the experimentally determined counter ion locations were found using FastMC, showing that FA^{3}PS was capable of reproducing the electrostatic environments of charged MOFs. In addition, it was capable of mimicking the intermolecular interactions between the framework and guests, allowing for the evaluation of gas adsorption in charged periodic systems. FA^{3}PS also calculated the structural properties of the benzene-tris-tetrazolate MOF, such as pore dimensions and surface areas. The calculated values were in excellent agreement with the reported experimental values.

In order to adequately represent charged MOFs' gas adsorption capabilities, a diverse database of over 47,000 hypothetical charged MOFs was constructed. TOBASCCO, an

algorithm developed by the Woo Lab, was adapted to generate the charged MOFs. A total of over 183,000 structures were generated using 200 organic SBUs and 54 inorganic SBUs, where 33 of the SBUs were charged. Geometric optimizations using the GROMACS package[6] and universal force field parameters[7] were performed on the 183,000 charged structures generated. If the optimized structure presented any structural defects such as atomic overlaps, unphysical bond length, angle, or high internal force, the structure was excluded. The resulting database includes 47,244 hypothetical charged MOFs with diverse structural properties. When compared against other existing databases[8,9], the database constructed in this work is much more diverse in terms of charge concentration, pore size, volume, surface area, and topology.

To ensure that the structural generation and optimization methods were valid, an experimentally synthesized MOF was reproduced computationally. A porous chiral In-MOF reported by Wang *et al.* in 2011[10] was used for the validation. The generated structure successfully reproduced the 171 atomic positions of the experimentally reported structure. In addition, it also matched the reported cell dimensions, pore structures, and surface area. The successful reproduction of an experimentally synthesized MOF confirmed the legitimacy of the MOFs within the hypothetical charged MOFs database created in this work.

Using the methods developed to simulate the gas adsorption properties, as well as the hypothetical charged MOFs database, the feasibility of charged MOFs in post-combustion CCS application was explored. The simulation conditions were chosen for the most economical CCS implementation. The adsorption simulations were performed at 298 K with 0.15 bar of CO_2 and 0.85 bar of N_2. The desorption conditions were 0.05 bar of CO_2 with 0.01 bar of N_2 at 298 K.

To lower computational cost, a diverse group of 500 hypothetical charged MOFs was selected to represent the charged MOFs database, noted DRG MOFs. The adsorption properties of 500 hypothetical neutral MOFs[11] were also computed under the same simulation conditions for a baseline comparison. Although the neutral MOFs includes functional groups in their structures, the overall framework remains neutral. Also, it was found that the structural properties, such as the pore dimensions and surface areas, were similar between the two groups of MOFs. Therefore, the difference in gas adsorption properties between the neutral MOFs and the charged DRG MOFs would be attributed to the differences in framework net charge.

When comparing CO_2 uptake, working capacity, and CO_2/N_2 selectivity, charged MOFs outperformed neutral MOFs. Both the CO_2 uptake and working capacity were much higher in charged MOFs than in neutral ones. The average CO_2 uptake of the charged MOFs and neutral MOFs were 3.33 mmol/g and 1.17 mmol/g, respectively. The average working capacity of the charged MOFs was 1.20 mmol/g, while the average was only 0.585 mmol/g for the neutral group. When the same gas adsorption simulations were performed without the attractive portion of the Lennard-Jones interaction, the uptake in CO_2 barely diminished. Therefore, the higher CO_2 uptake and working capacities in charged MOFs were the result of the charges in MOFs. Due to the quadrupole moment of CO_2 molecules[12], charges on the counter ions were found to have the most effects on the adsorption of CO_2. In the presence of both positively and negatively charged ions, most of the adsorbed CO_2 guest molecules were located in regions where the lowest interaction energy between the CO_2 and counter ions was achieved. In addition, when using half as many counter ions with double the charge, the average CO_2 uptake increased by 58.3%. Once again, both positively and negatively charged ions with higher charges resulted in an increase in

uptake. The difference in uptake due to counter ions shows the significant effect of counter ions on the CO_2 adsorption.

Similar to CO_2 uptake, CO_2/N_2 selectivity also had a positive correlation with the magnitude of charges in MOFs. With both positive and negative charges, stronger charges lead to higher CO_2/N_2 selectivity. While the 500 neutral MOFs had an average selectivity of 39.7, the average selectivity was 593.5 for the charged MOFs. Due to the dipole moment of water molecules, they may interact with charges on MOFs' frameworks and reduce their selectivity. However, 17 charged MOFs were found to have CO_2/N_2 selectivities above 150 despite the presence of water vapour. Structural features common amongst the group of 17 highly selective MOFs were identified. The pore diameters and volumes of these MOFs were found to be much smaller than the average of the 500 DRG MOFs. The lack of uncharged pore volume resulted in extremely low N_2, as a result, the CO_2/N_2 selectivities of this group of MOFs remained high even in the presence of water.

To ensure the accuracy of the above findings, 19 of the top performing MOF structures were re-optimized at the DFT level before obtaining their gas adsorption properties. The adsorption data obtained were almost identical before and after the re-optimization; both the average selectivity and working capacity fell within 8% of the original data. Also, the same top performers were identified between the two sets of structures. As similar gas adsorption data were obtained from structures with either optimization method, it can be concluded that the earlier findings using force field optimized structures were valid. Therefore, for the purpose of

high throughput screening of these materials in the future, the force field optimization should provide adequate accuracy.

By examining the gas adsorption capabilities of charged MOFs, they were found to outperform their neutral counterparts. In order to implement post-combustion CCS economically, carbon capture materials are required to have working capacities above 4 mmol/g and selectivities above 150[13]. In the DRG of 500 hypothetical charged MOFs examined, two of them were probable candidates with working capacities and selectivities similar to or higher than the requirements. The discovery of high performing candidates in hypothetical charged MOFs proved that they may be a viable material in post-combustion CCS applications. In addition, charged MOFs are shown to be superior to neutral MOFs in post-combustion CCS applications.

5.2 Author's Contributions

In this project, the three major components are: (1) developing the novel computational methods to simulate the gas adsorption properties in charged materials, (2) constructing a diverse database of hypothetical charged MOFs to represent their capabilities, and (3) screening the database of hypothetical charged MOFs to determine high performers for carbon capture with the developed computational method. As neither the simulation method nor a diverse database of hypothetical charged MOFs have been reported in literature, the author was responsible for completing both. Since both the simulation method and database construction method in neutral materials have been previously developed in the Woo Lab, the author made adaptations to these computer programs to process charged MOFs.

The programs written by former members of the Woo Lab modified by the author include: FAPS, FastMC, and TOBASCCO[14]. FAPS is the group's code that fully automates the evaluation of gas adsorption properties of materials when given a structure. FAPS was modified to account for the MOF's net charge in determine the partial atomic charges of the system. In addition, FAPS was modified to calculate the appropriate number of counter ions, insert them into the simulation cells as mobile guests in the GCMC simulation. FastMC, which is the group's core GCMC code, was modified by the author to accept counter ions as mobile guests in order to balance the framework net charge. Additionally, with significant help from Peter Boyd (former Ph.D. student) the location sampling of FastMC was improved by introducing the multi-jump move into the GCMC algorithm. In order to construct a database of hypothetical charged MOFs, the author modified part of the TOBASCCO[14] code to account for the charges on the SBUs. The author performed necessary test calculations in order to validate the methods developed in this work.

For constructing the hypothetical charged MOFs database, the author was responsible for the generation, optimization, and selection of all the MOF structures. Following the database construction, the author validated the generated structures by comparing them to experimental structures. All of the calculations in this project were performed by the author, which includes the partial atomic charge derivations and gas adsorption simulations. Additional calculations to verify the effects of charges, counter ions, and DFT optimized structures were also performed by the author.

5.3 Future Work

As the objective of this project was to demonstrate the possibility of using charged MOFs as materials for post-combustion CCS applications, the discovery of additional high performing materials is an on-going process. The most direct approach is to screen the entire database of charged MOFs for their gas adsorption properties. To reduce the computational effort, partial atomic charge fitting methods with less computational cost may be used for a preliminary screening. The hypothetical charged MOFs database may also be expanded to increase the sample population. Firstly, MOFs may be constructed with additional SBUs such as those from other experimental MOFs. As the current database was only made up of SBUs from experimentally synthesized MOFs, constructing MOFs with hypothetical SBUs may greatly increase the size and diversity of the database. Secondly, charged MOFs generated in this work were limited to no more than 100 SBUs per structure due to computational cost; increasing the number of SBUs used can also generate additional structures. Thirdly, to ensure the quality of the charged MOFs generated, very stringent conditions were used to exclude approximately three quarters of the optimized structures. Less stringent constraints may be used while optimizing and eliminating generated structures to increase the diversity of the database. Finally and most importantly, the charged MOFs in this database can be functionalized to greatly increase the sample size of hypothetical charged MOFs. The 47,000 MOFs generated in the study were base structures without functionalization; by including the 259 functional groups currently studied by the Woo group, well over a billion structures may be generated. By increasing the size and diversity of the hypothetical charged MOFs database, additional sample populations can show

reliable trends to aid the design of post-combustion CCS material and may yield the ideal MOF structure for post-combustion CCS.

In this work, only Cl^- and Na^+ were used as extra-framework counter ions; another future direction may be to examine the gas adsorption properties with other types of counter ions. As seen in the results, counter ions have the most significant effect on gas adsorptions. Lastly, the high performing candidates discovered in this work can be passed onto experimentalists for synthesis and analysis. As the computational studies narrow down the search field and help guide experimental chemists in designing materials, collaborations with experimental chemists are required to confirm the validity and capability of the actual material.

5.4 References

1. Campañá, C., Mussard, B., and Woo, T. K. Electrostatic Potential Derived Atomic Charges for Periodic Systems Using a Modified Error Functional. *J. Chem. Theory Comput.* **5,** 2866–2878 (2009).

2. Kresse, G. and Furthmuller, J. VASP the Guide. *Comput. Physics, Fac. Physics, Univ. …* (2012).

3. Chen, D. L., Stern, A. C., Space, B., and Johnson, J. K. Atomic Charges Derived from Electrostatic Potentials for Molecular and Periodic Systems. *J. Phys. Chem. A* **114,** 10225–10233 (2010).

4. Manz, T. A. and Sholl, D. S. Chemically Meaningful Atomic Charges that Reproduce the Electrostatic Potential in Periodic and Nonperiodic Materials. *J. Chem. Theory Comput.* **6,** 2455–2468 (2010).

5. Dinča, M., Dailly, A., Liu, Y., Brown, C., Neumann, D., and Long, J. Hydrogen Storage in a Microporous Metal-organic Framework with Exposed Mn2+ Coordination Sites. *J. Am. Chem. Soc.* **128,** 16876–16883 (2006).

6. Hess, B., Kutzner, C., Van Der Spoel, D., and Lindahl, E. GRGMACS 4: Algorithms for Highly Efficient, Load-balanced, and Scalable Molecular Simulation. *J. Chem. Theory Comput.* **4,** 435–447 (2008).

7. Rappe, A. K., Casewit, C. J., Colwell, K. S., Goddard III, W. A., and Skiff, W. M. UFF, a full Periodic Table Force Field for Molecular Mechanics and Molecular Dynamics Simulations. *J. Am. Chem. Soc.* **114,** 10024–10035 (1992).

8. Chung, Y. G., Camp, J., Haranczyk, M., Sikora, B., Bury, W., Krungleviciute, V., Yildirim, T., Farha, O., Sholl, D., and Snurr, R. Computation-ready, Experimental Metal-organic Frameworks: A tool to Enable High-throughput Screening of Nanoporous Crystals. *Chem. Mater.* **26,** 6185–6192 (2014).

9. Wilmer, C. E., Farha, O. K., Bae, Y.-S., Hupp, J. T., and Snurr, R. Q. Structure–property Relationships of Porous Materials for Carbon Dioxide Separation and Capture. *Energy Environ. Sci.* **5,** 9849 (2012).

10. Wang, L., Song, T., Huang, L., Xu, J., Li, C., Ji, C., Shan, L., and Wang, L. A Porous Chiral In-MOF with Anionic-type Diamond Network: Synthesis, Structure and Nitrogen gas Adsorption. *CrystEngComm* **13,** 4005 (2011).

11. Kadantsev, E. S., Boyd, P. G., Daff, T. D., and Woo, T. K. Fast and Accurate Electrostatics in Metal Organic Frameworks with a Robust Charge Equilibration Parameterization for High-Throughput Virtual Screening of Gas Adsorption. *J. Phys. Chem. Lett.* **4,** 3056–3061 (2013).

12. Buckingham, A. D., Disch, R. L., and Dunmur, D. A. Quadrupole Moments of some Simple Molecules. *J. Am. Chem. Soc.* **90,** 3104–3107 (1968).

13. Ho, M. T., Allinson, G. W., and Wiley, D. E. Reducing the Cost of CO2 Capture from Flue Gases Using Pressure Swing Adsorption. *Ind. Eng. Chem. Res.* **47,** 4883–4890 (2008).

14. Boyd, P. G. and Woo, T. K. A Generalized Method for Constructing Hypothetical Nanoporous Materials of any net Topology from Graph Theory. *CrystEngComm* **18,** 3777–3792 (2016).